



Research Article

Bioavailability Enhancement and Food Effect Elimination of Abiraterone Acetate by Encapsulation in Surfactant-Enriched Oil Marbles

Tereza Boleslavská,^{1,2} Ondřej Rycheký,^{1,2} Martin Krov,² Pavel Žvátora,¹ Ondřej Dammer,¹ Josef Beránek,¹ Petr Kozlík,³ Tomáš Křížek,³ Jana Hořínková,⁴ Pavel Ryšánek,⁴ Jaroslava Roušarová,⁴ Nikolína Kutinová Canová,⁴ Martin Šíma,⁴ Ondřej Slanař,⁴ and František Štěpánek^{2,5}

Received 29 June 2020; accepted 27 August 2020

Abstract. Abiraterone acetate has limited bioavailability in the fasted state and exhibits a strong positive food effect. We present a novel formulation concept based on the so-called oil marbles (OMs) and show by *in vitro* and *in vivo* experiments that the food effect can be suppressed. OMs are spherical particles with a core-shell structure, formed by coating oil-based droplets that contain the dissolved drug by a layer of powder that prevents the cores from sticking and coalescence. OMs prepared in this work contained abiraterone acetate in the amorphous form and showed enhanced dissolution properties during *in vitro* experiments when compared with originally marketed formulation of abiraterone acetate (Zytiga[®]). Based on *in vitro* comparison of OMs containing different oil/surfactant combinations, the most promising formulation was chosen for *in vivo* studies. To ensure relevance, it was verified that the food effect previously reported for Zytiga[®] in humans was translated into the rat animal model. The bioavailability of abiraterone acetate formulated in OMs in the fasted state was then found to be enhanced by a factor of 2.7 in terms of AUC and by a factor of 4.0 in terms of C_{\max} . Crucially, the food effect reported in the literature for other abiraterone acetate formulations was successfully eliminated and OMs showed comparable extent of bioavailability in a fed-fasted study. Oil marbles therefore seem to be a promising formulation concept not only for abiraterone acetate but potentially also for other poorly soluble drugs that reveal a positive food effect.

KEY WORDS: bioavailability; bioequivalence; food effect; formulation; liquid marble.

Tereza Boleslavská and Ondřej Rycheký contributed equally to this work.

Electronic supplementary material The online version of this article (<https://doi.org/10.1208/s12248-020-00505-5>) contains supplementary material, which is available to authorized users.

¹ Zentiva, k.s., U Kabelovny 130, 102 37, Prague, Czech Republic.

² Department of Chemical Engineering, University of Chemistry and Technology, Prague, Technická 5, 166 28, Prague, Czech Republic.

³ Department of Analytical Chemistry, Faculty of Science, Charles University, Prague, Czech Republic.

⁴ Institute of Pharmacology, First Faculty of Medicine, Charles University and General University Hospital in Prague, Prague, Czech Republic.

⁵ To whom correspondence should be addressed. (e-mail: Frantisek.Stepanek@vscht.cz)

Abbreviations: API, active pharmaceutical ingredient; ASD, amorphous solid dispersions; AUC, area under the curve; ODP, original drug product; OM, oil marble; SEDDS, self-emulsifying drug delivery system; SMEEDS, self-microemulsifying drug delivery system;

INTRODUCTION

Poorly soluble drugs (i.e., drugs belonging to BCS groups II and IV) and their limited oral bioavailability currently present a major challenge to pharmaceutical scientists (1). An example of such a hard-to-formulate drug is abiraterone acetate, a prodrug of androgen biosynthesis inhibitor abiraterone, marketed under the original brand name Zytiga[®] and used as a medication for the treatment of metastatic castration-resistant prostate cancer (2). Abiraterone acetate has an extremely low bioavailability in the fasted state (estimated to be less than 10%) and exhibits a highly variable increase in bioavailability in the fed state (3–5). It has been reported that intake with high-fat meal leads to increase in overall exposures by approximately 17- and 10-fold, in terms C_{\max} and AUC, respectively. The original formulation must therefore be taken on a fasting stomach in high doses, 1000 mg daily (2). This not only is inconvenient for the patients, but also presents a risk of accidental overdose. Attempts have been made to establish safe dosing regimen for lower doses of Zytiga[®] administered with food—these attempts have however been unsuccessful so far

(3). This implies a need for the development of novel formulation strategies that would allow food effect elimination and thus safe dosing regimen for abiraterone acetate.

Therefore, it can be hypothesized that by using advanced formulation approaches to increase the bioavailability of abiraterone acetate on a fasting stomach, the dangerous food effect can be suppressed (6). Administration of the crystalline drug in the form of nanoparticles allowed dose reduction to 500 mg (7,8). Solymosi *et al.* reported a negligible food effect for a novel formulation based on continuous flow precipitation with Soluplus (9,10). Finally, we have shown in a recent study that amorphous solid dispersion (ASD) formulation based on precipitation inhibitor allowed 2.5-fold bioavailability enhancement in fasted rats (11).

Alternatively, lipid-based formulations of abiraterone acetate have been investigated recently (12). Complex lipid-based formulations can contain various oils, surfactants, and co-solvents. These systems can be categorized based on the Lipid Formulation Classification System (LFCS) into several groups among which the self-emulsifying drug delivery systems (SEDDS) and the self-microemulsifying drug delivery systems (SMEDDS) are of particular significance (13–15). These liquid formulations are usually filled into soft gelatin capsules. Even though these systems can be highly effective in bioavailability enhancement, they also have some drawbacks when compared with solid dosage forms.

As SEDDS and SMEDDS are essentially liquid formulations, it is not easily possible to alter their dissolution kinetics as such (16). Once the soft gelatin capsule is opened, it releases the whole content at once, forming a fine emulsion. The lipids are then available for enzymatic digestion (lipolysis), which is believed to be the critical step for drug absorption (15,17). Moreover, there are several challenges associated with soft gelatin capsules—e.g., cross-linking to the gelatin (which can result in poor dissolution) or the necessity to employ a special production line (18). Due to these aspects of liquid oil-based drug delivery systems, there have been efforts towards the solidification of these types of formulations (15). SEDDS solidification techniques have been reviewed recently by Joyce *et al.* (19). In the present work, we are introducing a novel approach towards the preparation of solidified oil-based formulations of abiraterone acetate based on the so-called oil marbles.

The general term “liquid marble” refers to a droplet covered by a layer of non-wetting solid particles that stabilize the interface and cause the droplet to behave and roll as if it were a rigid sphere. (20,21) Most of the existing literature on pharmaceutical applications of liquid marbles is concerned with water-based systems covered by hydrophobic powders (22). Such marbles typically contain about 90% w/w of the liquid core, depending on the interfacial tension, the droplet diameter, and the particle size. Solid particles on the surface prevent the encapsulated liquid from evaporation or leakage and protect the marbles from agglomeration, thus improving their handling properties (20,21). Although oil-based liquid marbles can be prepared as well, they are not so well documented in the literature and their practical application has so far been hindered by a limited choice of sufficiently oleophobic powders for coating (23). A fully liquid oil core combined with an insufficiently oleophobic powder leads to an unfavorable ratio between the oily core and the shell

material, which ultimately limits the achievable drug load in the formulation.

Therefore, the aim of the present work was to overcome this limitation by formulating the oil-based core in such way that it can be combined even with wettable powders without their excessive absorption into the core. The resulting oil marbles (OMs) combine the advantages of oil-based formulations in terms of bioavailability enhancement and those of solid dosage forms in terms of handling the product. It will be shown that OMs can be filled into hard gelatin capsules and handled similarly as a solid material once they are prepared. We will demonstrate that unlike fully liquid formulations, OMs can provide a range of dissolution profiles depending on the matrix composition and OM size. Crucially, it will be shown that OM formulation of abiraterone acetate leads not only to improved dissolution *in vitro* but also to significant bioavailability enhancement *in vivo* and ultimately successful elimination of the food effect.

MATERIALS AND METHODS

Materials

Abiraterone acetate was provided by Zentiva, k.s. (Prague, Czech Republic). Capmul oil MCM NF was purchased from Abitec (Columbus, USA); Capryol PGMC was kindly donated by Gattefossé (Saint-Priest, France). Surfactants (summarized in Supplementary Material, Table S1) were purchased from Sigma-Aldrich. Natural oils (olive oil, rapeseed oil, and castor oil) were purchased from Merck (Germany). Hydroxypropyl methylcellulose (HPMCAS-LF) was bought from Shin-Etsu Chemical. Powders for biorelevant media were purchased from Biorelevant.com Ltd. (London, UK). The biorelevant dissolution media were prepared according to the manufacturer's protocol. All solvents used were at least of HPLC grade.

Solubility Measurements

In order to select the most appropriate oil for the OMs, the solubility of abiraterone acetate in several candidate oils was determined using the shake flask method. Briefly, an excess of abiraterone acetate was added to an Eppendorf vial containing 1 mL of the oil and the resulting suspension was shaken at 37°C for 24 h. At the end of the experiment, the vials were centrifuged at 10,000 RPM for 10 min, the supernatant was diluted ten times into isopropyl alcohol, and the concentration of abiraterone acetate in the resulting solution was determined by HPLC (method adapted from our previous study) (11).

As an additional component of the OM formulation, surfactants were screened for their ability to enhance the solubility of abiraterone acetate in aqueous media. The solubility was determined using the shake flask method described above. Surfactants with relatively higher melting point (around 50°C) were selected along with several commonly used non-ionic surfactants such as Tween. The full list of surfactants is provided in Supplementary Material, Table S1. Phosphate buffer pH 6.8 supplemented with these surfactants at different concentrations (namely 1.0, 0.5, 0.25,

and 0.125 mg/L) was used as the dissolution media in the shake flask method.

Preparation of Oil Marbles

All components of the oil core (abiraterone acetate, oil, surfactant) were weighted and placed into a flask. The mixture was heated in a bath at 56°C and stirred for 20 min at 250 RPM to allow complete dissolution and homogenization of the mixture. Oil Marbles were created by dripping the liquid at a rate of 2 Hz using a 30G needle connected to a precise syringe pump, into a powder bed placed in Petri dish that moved underneath the needle tip at a velocity of approximately 10 mm/s in order to allow sufficient distance between the individual OMs. The powder bed was maintained at room temperature (approximately 20°C); HPMCAS-LF was used as the covering powder material. After 3 min (time necessary for the droplets to cool down and partially solidify), the Petri dish was shaken to fully cover the droplets by the powder. Thanks to the surface cooling of the droplets, the HPMCAS powder remained just on the surface even though it is not fully oleophobic. The final product—the oil marble—therefore behaves as a non-sticking solid sphere regardless of the physical consistency of the oily core.

Physicochemical Characterization

Sieve Analysis

After preparation, the OMs were separated by sieving to obtain size classes with a defined diameter. To assess the effect of OM size on *in vitro* dissolution properties of the formulation, the following size fractions were collected: 1.4–2 mm, 2–3 mm, 3–4 mm, 4–5 mm, 5–6 mm, and > 6 mm. Since the rat capsules intended for an *in vivo* study have an inner diameter of 2 mm, only the smallest fraction (1.4 to 2 mm) of OMs was used for the *in vivo* study.

X-ray Powder Diffraction Analysis

X-ray powder diffraction (XRPD) patterns were obtained with the laboratory X-ray diffractometer X'PERT PRO MPD PANalytical with copper radiation $\text{CuK}\alpha$ ($\lambda = 1.542 \text{ \AA}$, 45 kV/40 mA), 2-theta range 2–40°, with step size 0.02° 2 θ and time per step 300 s. Primary optics setting is as follows: Soller slits 0.02 rad, automatic PDS, 10 mm mask, 1/4° anti-scatter slit, irradiated sample area 10 mm. Secondary optics setting is as follows: 5.0 mm anti-scatter slit, Soller slits 0.02 rad, detector X'Celerator with maximal active length. Silicon zero background holders were used for measurement. A few OMs were placed on the holder and gently pressed by a Petri dish to obtain a flat surface. All samples of OM were measured on XRPD to confirm if abiraterone acetate inside the marbles was present in the crystalline or amorphous form.

Drug Load Analysis

The actual drug load in the oil marbles was determined by extraction into methanol. Approximately 80 mg of OMs was weighted into a 20-mL volumetric flask and extracted into methanol. The resulting solution was diluted 10 times,

and the concentration of abiraterone acetate was determined on HPLC using a method adapted from our previous study (11).

In Vitro Dissolution Testing

Dissolution experiments were conducted using standard USP 2 dissolution bath equipped with a mini-paddle apparatus (Sotax, Switzerland). The dissolution media were preheated to 37°C and the stirrer speed was set to 125 RPM; these conditions were kept constant throughout the experiment. OMs were placed into a weighing boat and administered directly into the dissolution vessel. The weight of abiraterone acetate corresponded to 20 mg in all dissolution experiments. Liquid samples (500 μL) were collected in predefined time points, filtered through a 0.45- μm filter, immediately diluted with 500 μL of MeOH, and analyzed on HPLC. Unlike the dissolution medium, the filtrate was clear, suggesting the absence of any particles or droplets that would scatter light.

As dissolution media simulating fasted and fed conditions, biorelevant buffers were used—FeSSIF v2 pH 5.8, FaSSIF pH 6.5, and FaSSIF pH 6.5 supplemented with pancreatin (10 mg/mL) (24). Furthermore, pH shift experiment was designed. Briefly, 130 mL of 10 mM HCl pH 2 was used to simulate gastric conditions. After 30 min, concentrated FaSSIF buffer was added to the dissolution vessel to obtain 195 mL of FaSSIF buffer pH 6.5.

In Vivo Bioequivalence Study

Chemicals

Ketamine (Narkamon 100 mg/mL inj. sol.; Bioveta, Ivanovice na Hané, Czech Republic), xylazine (Rometar 20 mg/mL inj. sol.; Bioveta, Ivanovice na Hané, Czech Republic), and isoflurane (IsoFlo 250 mL; Zoetis/Pfizer, Czech Republic) were used for anesthetization. Enoxaparin (Clexane inj. 4000 IU/0.4 mL; Sanofi-Aventis, Czech Republic), heparin (Heparin Léčiva inj. 1 \times 10 mL/50KU; Zentiva, Czech Republic), amoxicillin with clavulanic acid (Synulox RTU inj. 100 mL; Zoetis/Pfizer, Czech Republic), and ketoprofen (Ketodolor inj. 100 mL; LeVet Pharma b.v., Netherlands) were used for peri-operative anti-coagulant, antibiotic, and analgesic treatments, respectively. Surgical Skin Glue was purchased from Henry Schein (Brno, Czech Republic). For dosing, mini gelatin drug delivery capsules, size 9el (Harvard Apparatus, USA), were used.

Animals

Male Wistar rats purchased from Velaz (Prague, Czech Republic) were housed under standard conditions (12-h light-dark cycle, 22 \pm 2°C temperature and 50 \pm 10% relative humidity) and fed on water and standard granulated diet *ad libitum*. All experiments were performed in accordance with the Guiding Principles for the Use of Animals in Charles University, First Faculty of Medicine, and every effort was made to minimize animal suffering. The experimental animal project was approved by the Ministry of

Education, Youth and Sports, Czech Republic (MSMT-9445/2018-8).

Preparation of Capsules for *In Vivo* Dosing

The mini capsules containing reference formulation were filled with the crushed original drug product Zytiga® to contain approximately 4.2 mg of abiraterone acetate. For the test formulation, two capsules were filled with OM formulation pre-selected on the basis of previous *in vitro* studies. Each capsule contained approximately 2.1 mg of abiraterone acetate—two capsules containing the test formulation were given to each animal by oral gavage.

Experimental Design and Procedure

A randomized, single-dose, laboratory-blinded, 2-period, 2-sequence, crossover bioequivalence study was conducted under fasting conditions in rats to compare the bioavailability of abiraterone after oral administration of test and reference (Zytiga®, Janssen-Cilag SpA, Latina, Italy) formulations (Table I part A). Another randomized, single-dose, laboratory-blinded, 2-period, 4-sequence, crossover comparative bioavailability study was conducted in rats to compare the effect of food on bioavailability of abiraterone after oral administration of test and reference formulations (Table I part B).

All rats underwent cannulation of *a. carotis* with catheters made from medical-grade polyurethane (1.9-3Fr, Instech Laboratories, Plymouth Meeting, USA). Prior to the surgery, 2.5–5% isoflurane was used to anesthetize the rats, continued with ketamine (100 mg/kg, i.m.) and xylazine (5 mg/kg, i.m.). Prophylactic amoxicillin with clavulanic acid (1 mL/kg, s.c.) was administered prior to the surgery to minimize the risk of an infection. After the cannulation, ketoprofen (5 mg/kg, s.c.) was applied. Catheters were flushed with 200 µL of physiological saline and 50 µL of heparin and sealed by 20 µL of glycerol with heparin every day. Peri-procedural thromboembolism prophylaxis with enoxaparin (10 mg/kg, s.c. q.d.) was applied from 12 h prior to surgery until the end of study. The third day after the cannulation, rats were randomly assigned into study groups and dosing of abiraterone acetate containing formulation was performed.

For dosing under fasted state, the access of the animals to food was restricted between 4 h prior to dosing and 4 h after that, and capsule was administered by X-9el dosing syringe (Torpac Inc., Fairfield, USA) followed by 1 mL of

water via oral gavage. For dosing under fed state, administered capsule was immediately followed by 1 mL of homogenized mixture (1:1) of olive oil with Nutridrink (Nutricia, Danone, Amsterdam, Netherlands) via oral gavage and the access of the animals to food was not restricted. Total dose of abiraterone acetate was measured in each capsule and ranged between 4.18–4.53 mg and 4.00–4.27 mg for reference and test formulations, respectively. Therefore, all concentration data has been normalized to body weight of each animal. Blood samples (100 µL) were then collected for 7 h (0, 0.5, 1, 1.5, 2, 2.5, 3, 4, 5, and 7 h) after the dosing. Volume replacement with 100 µL of saline was provided after each sampling and 50 µL of heparinized saline flush (1250 IU/mL) of the catheter together with sealing by heparinized glycerol used to secure the catheter patency. Blood samples were centrifuged for 10 min (4500×g, 4°C) and serum aliquots were stored at –80°C until analyses. A wash-out period of 48 h between consecutive doses was applied.

Analytical Methods

Determination of abiraterone in plasma samples was carried out on the Shimadzu UHPLC Nexera X3 coupled with a Triple Quad 8045 tandem mass spectrometer (Shimadzu, Kyoto, Japan). Kinetex EVO C18 column (100 mm × 2.1 mm, 1.7 µm particle size) from Phenomenex (Torrance, USA), thermostatted at 40°C, was used for the analysis. The mobile phase consisted of 0.1% formic acid in deionized water (solvent A) and acetonitrile (solvent B). The flow rate of the mobile phase was maintained at 0.35 mL/min. The optimized gradient program (min/% B) was 0/30, 1.5/90, 3.0/90, 3.5/30, and 6.0/30. The injection volume was 2 µL, and samples were kept at 10°C. To reduce the cleaning time of the ion source, we switched the MS six-port valve to waste for the first 2.6 min and for the last 2.2 min of analysis. The tandem mass spectrometry measurement was performed in multiple reaction monitoring (MRM) mode using positive electrospray ionization. MRM transitions of 350.3 > 156.1 (Q1 pre-bias –17 V, Q3 pre-bias –27 V, and collision energy –57 V) and 354.3 > 160.1 (Q1 pre-bias –17 V, Q3 pre-bias –30 V, and collision energy –57 V) were monitored for abiraterone and abiraterone-d4 (internal standard), respectively. The ion source was set as follows: nebulizing gas flow: 3 L/min, heating gas flow: 10 L/min, interface temperature: 300°C, desolvation line temperature: 250°C, heat block temperature: 400°C, and drying gas flow: 10 L/min. A total of 100 µL of 100% acetonitrile (containing abiraterone-d4; *c* = 32 ng/mL) was added to 25 µL of plasma, shaken (vortex), and centrifuged (10 min/9800×g). A total of 70 µL of supernatant was transferred into a chromatographic vial.

The method was validated in terms of linearity, LOD, accuracy, precision, selectivity, recovery, and matrix effects. The calibration curve was constructed in the blank plasma with seven concentrations by plotting the ratio of the peak area of the analyte to that of deuterium-labeled IS against analyte concentration. The calibration curve was statistically analyzed by $1/x^2$ weighted linear regression analysis using the least squares regression method, which improved the accuracy in low concentrations. The developed method was linear (coefficients of determination (R^2) higher than 0.9996) in the concentration range of 0.5–600 ng/mL with the

Table I. Experimental Design of *In Vivo* Studies

A	Group no.	Formulation sequence
	1	R–T
	2	T–R
B	Group no.	Formulation/condition sequence
	1	R (fasted)–R (fed)
	2	T (fasted)–T (fed)
	3	R (fed)–R (fasted)
	4	T (fed)–T (fasted)

R reference, T tested formulation

accuracy (relative error %) within $\pm 7.1\%$, and the interday and intraday precisions (RSD %) ranged from 2.4 to 5.2%. LOD value was determined as $3.3 \times \sigma/S$ ratio, where σ is the baseline noise obtained from the blank matrix and S is the slope of the regression line (based on peak heights) obtained from the linearity data. The mean of LOD value was 0.03 ng/mL, which showed satisfactory sensitivity for abiraterone determination in plasma samples. Recovery was evaluated by comparing concentration of abiraterone found in the pre-protein-precipitation spiked plasma sample with the concentration found in the corresponding post-protein-precipitation spiked sample at three concentrations (1, 50, and 250 ng/mL). Method selectivity was monitored by injecting six plasma samples (mass spectrometer was set in scan mode). These chromatograms showed no interfering compound within the retention time window of abiraterone. Moreover, the developed method uses a tandem mass spectrometer in specific SRM mode, which ensures high selectivity. Matrix effect was evaluated at two concentration levels (1 and 100 ng/mL) of six plasma samples. It was determined by comparing the concentration of abiraterone found in the post-protein-precipitation spiked plasma sample with that found in the 80% acetonitrile spiked with abiraterone (without matrix effect). The matrix effect ranged from 80 to 108%. To assess the validity of the analytical method, calibration was performed every day before measuring samples and quality control samples were injected after each 7th sample.

Data Analysis and Statistics

Statistical and pharmacokinetic analysis was performed using Phoenix WinNonlin[®] (Certara, Princeton, USA). C_{\max} , T_{\max} , and AUC were evaluated. The natural logarithmic transformation of C_{\max} and AUC was used for all statistical inference. AUC was calculated using the trapezoidal rule, and C_{\max} and T_{\max} were taken directly from the observed data. The pharmacokinetic parameters were analyzed using an ANOVA model. The fixed factors included in this model were the effects of subject, treatment, period, and sequence. The 90% confidence interval for the ratio of geometric least squares means between the test and reference products was calculated. Actual sampling times were used for all pharmacokinetic calculations, while scheduled sampling times were used only for plotting of mean pharmacokinetic profiles. The maximum difference between actual and per-protocol sampling times was 5 min. GraphPad Prism version 8.00 for Windows (GraphPad Software, La Jolla, USA) was used to plot mean pharmacokinetic profiles.

RESULTS

Selection of Formulation Components Based on Solubility

Based on recently published SMEDDS formulations of abiraterone acetate that contained mixtures of castor oil and artificial oils (12), it was decided to explore the solubility of abiraterone acetate in other natural oils (rapeseed oil and olive oil) compared with castor oil, as well as in several artificial oils (Capmul MCM NF and Capryol PGMC). The results are summarized in Fig. 1a (the underlying values can be found in Supplementary Material, Table S2). From the

natural oils, castor oil with solubility of abiraterone acetate 137.7 mg/L was chosen for the preparation of oil marbles due to its highest solubility. For the artificial oils (Capmul MCM NF dissolved 53.3 mg/L and Capryol PGMC 735.1 mg/L), both were used in combination with different surfactants as described in “Preparation of Oil Marbles and Their Physicochemical Characterization.” Surfactants for the formulation were selected based on their solubilization effect for abiraterone acetate and their physical consistency. The preparation of OMs coated by HPMCAS powder requires the usage of solid or semi-solid excipients. Thus, surfactants with a melting point around 50°C (based on manufacturer and literature data) (25–30) were included in the list of possible surfactants (Supplementary Material, Table S1). Along with these, the solubilization capacity of some commonly used non-ionic surfactants (such as Tweens) was tested. The ability of selected surfactants to enhance the solubility of abiraterone acetate was assessed in a phosphate buffer pH 6.8. The solubility of abiraterone acetate alone was under the detection limit of the UPLC method. The highest enhancements were occurred for Kolliphor RH40, Tween 80, Tween 20, and Pluronic F127 (see Fig. 1b).

Preparation of Oil Marbles and Their Physicochemical Characterization

Based on the solubility data, we prepared four types of OMs with a different composition of the inner core, as summarized in Table II. We focused mainly on the manufacturability of the marbles while using surfactants that provided the highest solubility for abiraterone acetate. Some of the surfactants that provided good solubility were found to be unsuitable for the preparation of oil marbles, namely Tween 20 and Tween 80. Both are liquid at room temperature, and we were not able to prepare a mixture that would allow the formation of stable OMs coated by a thin layer of HPMCAS powder. Butylated hydroxyanisole (BHA) was added to all formulations in order to decrease undesired oxidation processes.

For mixture A, solid surfactant Pluronic F-127 was used as the main solubilizing agent (this surfactant showed good solubility for abiraterone acetate in phosphate buffer). Tween 65 was used as a solidifying agent. The resulting mixture thus formed a rather solid core. For mixture B, both used surfactants (solid Pluronic F-127 and liquid Kolliphor RH40) showed the ability to solubilize abiraterone acetate. Their mixture also allowed formation of a solid oil core at room temperature although softer than when using mixture A. Mixture C was prepared using surfactants that have a high melting point, but they did not perform well in the solubility measurements. We therefore assumed that this mixture would not perform well in the dissolution studies although the solid core could still contain molecularly dispersed abiraterone acetate (see Fig. 3). For mixture D, both used surfactants (Pluronic F-127 and Span 40) are solid materials but only Pluronic F-127 showed solubility enhancement.

As a covering material, HPMCAS-LF, a polymeric excipient with pH-dependent solubility, was used. This covering material was chosen for two main reasons: (i) pH-dependent solubility of this polymer allows pH-controlled

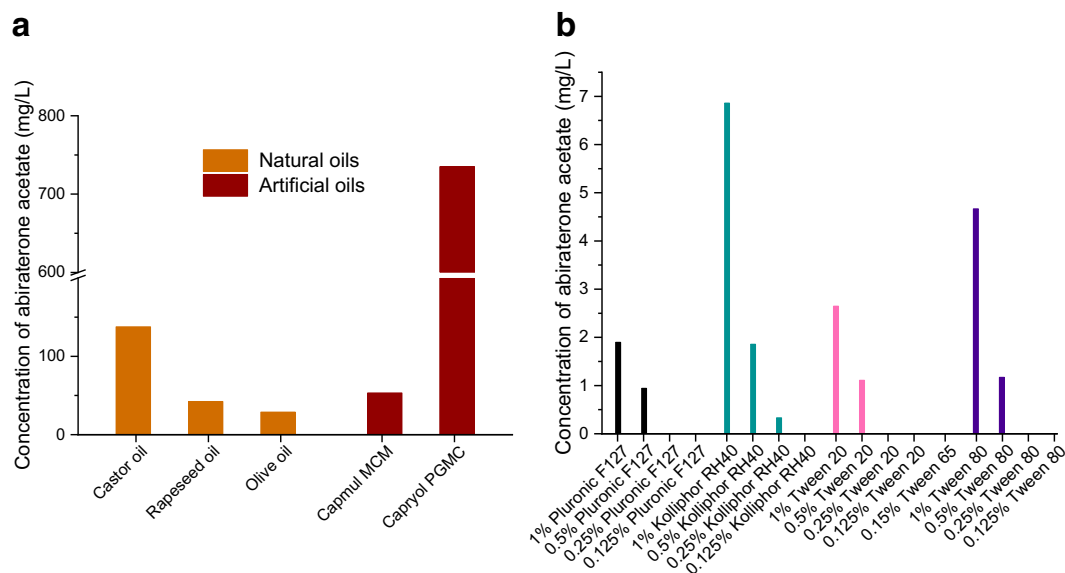


Fig. 1. **a** Solubility of abiraterone acetate in various natural and artificial oils. **b** The solubility enhancement of abiraterone acetate due to various surfactants in phosphate buffer pH 6.8

release since we believe that tuning the release of abiraterone acetate based on pH is crucial for food effect elimination; (ii) in our previous study (11), HPMCAS-LF was identified as a potent precipitation inhibitor—this might allow drug absorption even when supersaturated state is reached in a given environment (this phenomenon is usually referred to as parachute effect) (31). We were able to prepare marbles smaller than 2 mm in diameter that could be filled into capsules for rodents (capsule size 9el) as shown in Fig. 2. Larger size fractions were also prepared and used for studying the impact of OM size on the dissolution properties (see “*In Vitro* Dissolution Testing”).

Figure 3 shows XRPD diffractograms of OM samples. Crystalline abiraterone acetate was not detected in any of the samples. It can be concluded that abiraterone acetate is probably molecularly dispersed in all four formulations. The detected diffraction peaks correspond to excipients, namely to triblock copolymers (Poloxamer 188, Pluronic F-127, Kolliphor) and solid co-surfactants (Span 65, Span 40). The XRPD diffractograms of these excipients are summarized in Supplementary Material, Fig. S1. The drug load as determined by methanol extraction corresponded with theoretical drug load in the melt. As anticipated, the actual drug load is decreased by addition of a thin layer of HPMCAS. The actual drug content determined for OM sample B (intended for the *in vivo* study) was found to be 6.2%.

In Vitro Dissolution Testing

As bioavailability of abiraterone acetate is reported to be limited in fasting conditions, special attention should be paid to dissolution in media closely mimicking these conditions. For this purpose, a pH shift experiment that represents a transfer of API from a fasting stomach to a fasting intestine was designed. The results for OM formulation B are shown in Fig. 4a. Less than 10% of abiraterone acetate was released under acidic condition—this is due to poor solubility of the coating material (HPMCAS-LF) in acidic pH. Coverage of the oil marbles by this polymeric excipient therefore seems to be very efficient. Interestingly, when OMs were administered to the dissolution test in the rodent capsules, there was a slight increase in the release rate in acidic pH (and a subsequent shift of dissolution curve in the FaSSIF stage). This is most probably due to mechanical damage of the covering powder layer of the marbles when they are placed into the capsules. Although the damage of the powder layer apparently translates into dissolution behavior, the overall effect on dissolution properties was considered negligible and hence all subsequent studies were performed without the capsules.

Having established that the HPMCAS-LF coating on the OMs effectively prevents dissolution under acidic conditions, all four OM formulations were then compared in a dissolu-

Table II. Oil Marbles—Different Samples and Their Composition (Weight Percent)

Sample	Abiraterone acetate (%)	Capmul MCM NF (%)	oil PGMC (%)	Capryol oil (%)	Castor oil (%)	Pluronics F-127 (%)	Kolliphor RH40 (%)	Tween 65 (%)	Span 40 (%)	Span 65 (%)	Poloxamer 188 (%)	BHA (%)
OM A	6.9	23.1	-	23.1	23.2	-	23.6	-	-	-	-	0.1
OM B	7.0	23.1	-	23.3	23.5	23.0	-	-	-	-	-	0.1
OM C	8.1	-	23.0	22.8	-	-	-	-	22.9	23.1	-	0.1
OM D	7.8	-	22.6	22.1	24.5	-	-	22.8	-	-	-	0.1

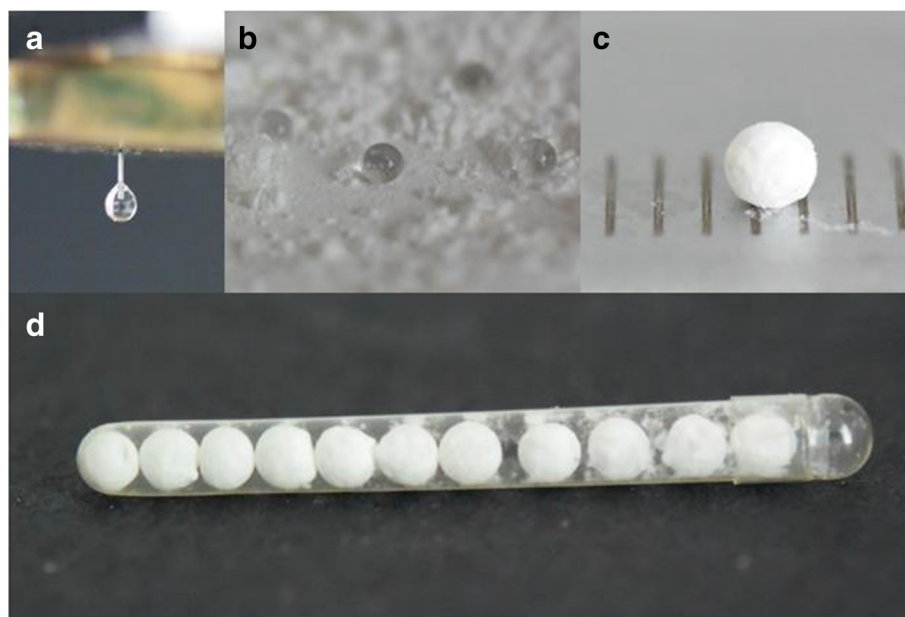


Fig. 2. Formation of oil marbles. **a** Initial droplet of the core material. **b** Droplets after deposition on a powder bed. **c** Finished oil marble coated by HPMCAS-LF. **d** Sub-2-mm OMs filled into rodent capsules size 9el

tion experiment in FaSSIF media (Fig. 4b). As a reference, the dissolution of a crushed Zytiga[®] tablet (original drug product containing abiraterone acetate) (2) under the same conditions is shown as reported in our previous study (11). The fraction dissolved for most OM formulations except formulation C is considerably higher. Also, no precipitation was observed throughout the experiment suggesting maintained supersaturation of abiraterone acetate when compared with crystalline API present in the original drug product.

OM formulation C contained only surfactants that did not show significant solubility enhancing properties (Span 65 and Poloxamer 188). On the other hand, significant improvement in dissolution rate was seen for both OM formulations A and D. Both of these formulations contained one surfactant that showed solubility enhancing properties (Pluronic F-127) and one that either showed only minor or no effect (Span 40 or Tween 65). Finally, the fastest dissolution rate was

observed for OM formulation B; both surfactants used in this formulation increase the solubility of abiraterone acetate. As the release rate in FaSSIF buffer was the highest for OM formulation B and no precipitation was observed, this formulation was retained for further studies.

The effect of OM size on the release kinetics was assessed next. Although the size needed for *in vivo* study in the rat animal model was determined by the inner diameter of the rodent capsules, understanding the effect of OM is useful for further formulation development. The results of dissolution experiment plotted in Fig. 4c clearly show that marble size has a direct effect on the release rate from the oil marble. It is therefore possible to control the release rate from OMs just by changing their diameter. This might be especially useful when targeting certain dissolution profile. It is also a major distinguishing feature of OMs compared with liquid SMEDDS formulations.

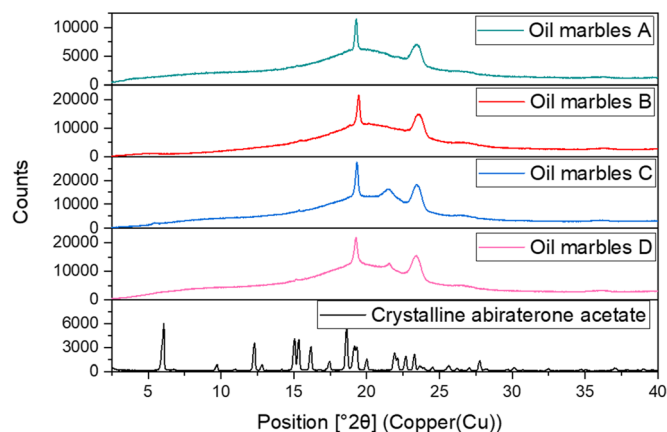


Fig. 3. XRPD diffractograms of OM formulations A–D compared with crystalline abiraterone acetate—the XRPD diffractograms of individual formulation components can be found in Supplementary Material, Fig. S1

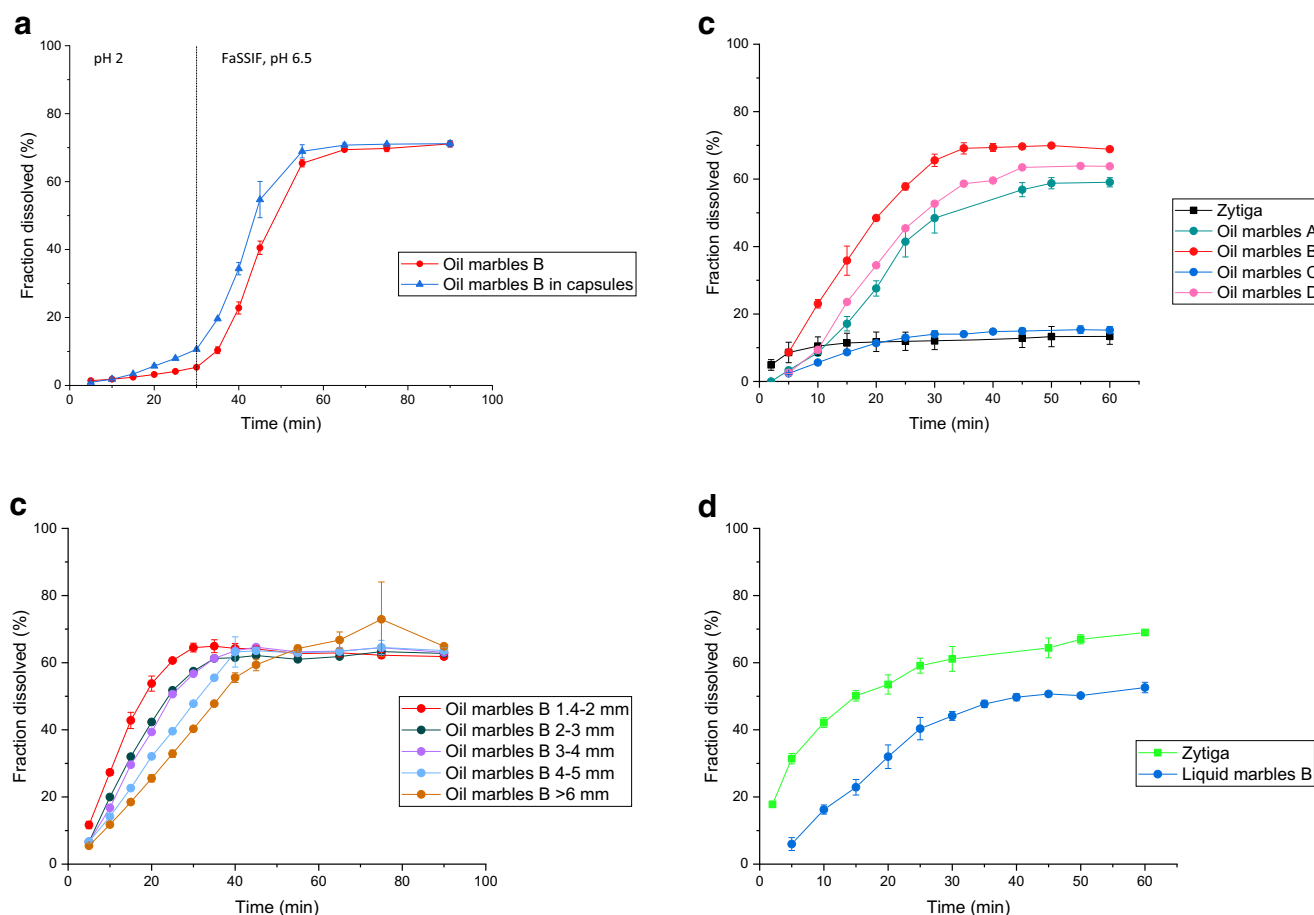


Fig. 4. Mean (\pm SD, $n = 3$) *in vitro* dissolution profiles of **a** OM formulation B in pH shift dissolution experiment. 0–30 min 10 mM HCl pH 2, 130 mL; 30–90 min FaSSIF pH 6.5, 195 mL; mini-paddles at 125RPM; **b** oil marbles A–D compared with Zytiga[®] in FaSSIF media, pH 6.5, 200 mL, mini-paddles at 125RPM; **c** different marble sizes of OM formulation B in FaSSIF media, pH 6.5, 200 mL, mini-paddles at 125RPM; **d** OM formulation B compared with Zytiga[®] in FeSSIF v2 media, pH 5.8, 200 mL, mini-paddles at 125RPM. Fraction dissolved corresponds to abiraterone acetate—abiraterone (product of hydrolysis of abiraterone acetate) was not detected in neither of the experiments. Fraction dissolved corresponds to abiraterone acetate—abiraterone (product of hydrolysis of abiraterone acetate) was not detected in neither of the experiments

As abiraterone acetate is prone to enzymatic hydrolysis upon oral administration (24,32), a dissolution experiment in biorelevant media supplemented with pancreatic enzymes was designed. Also, the effect of lipolysis is assessed when pancreatic enzymes are present in the dissolution media (17). The digestion of lipidic excipients present in the OM formulation might play an important role in the absorption of the drug even though the mixtures prepared in this study fall into group III according to LFCS—drugs can be reportedly absorbed from type III formulations even without digestion (13,14). Three different formulations were tested in the presence of pancreatic enzymes: (i) original drug product Zytiga[®]; (ii) amorphous solid dispersion with HPMCAS-LF as a carrier (11); (iii) formulation in oil marbles (OM B). The concentration of abiraterone acetate, its hydrolysis product abiraterone, and the total concentration of both compounds are plotted over time in Fig. 5. The area under the curve was calculated for total concentration as a measure of the overall quantity of the API theoretically available for absorption.

It is believed that both abiraterone acetate and abiraterone can permeate through the intestinal wall (32).

These results therefore imply that highest bioavailability should be reached for the OM formulation. Moreover, the dissolution curves in pancreatin-enriched media provide an insight into the lipolysis of lipids. The release rate of the drug (when plotted as the combined concentration of abiraterone and abiraterone acetate) is slightly higher when compared with dissolution experiment in FaSSIF (see Fig. 4). This might be caused by the degradation of lipids thus releasing the drug. Also, last time point (90 min) indicates some precipitation of the drug. However, the time window in which the drug is solubilized should be wide enough to allow drug absorption before the precipitation starts.

Finally, since our goal is to suppress food effect reported for abiraterone acetate, also *in vitro* experiments simulating fed conditions were evaluated. For this purpose, dissolution in FeSSIF v2 was conducted. The results are plotted in Fig. 4d.

FeSSIF v2 media have pH 5.8, which is close to the borderline where HPMCAS-LF dissolves (pH 5.5–6). That explains why less API is released from the oil marbles in the fed state simulated fluid (approximately 53% of the administered dose) than in the fasted state simulated fluid (68% of the administered dose). For Zytiga[®], only 13% of the

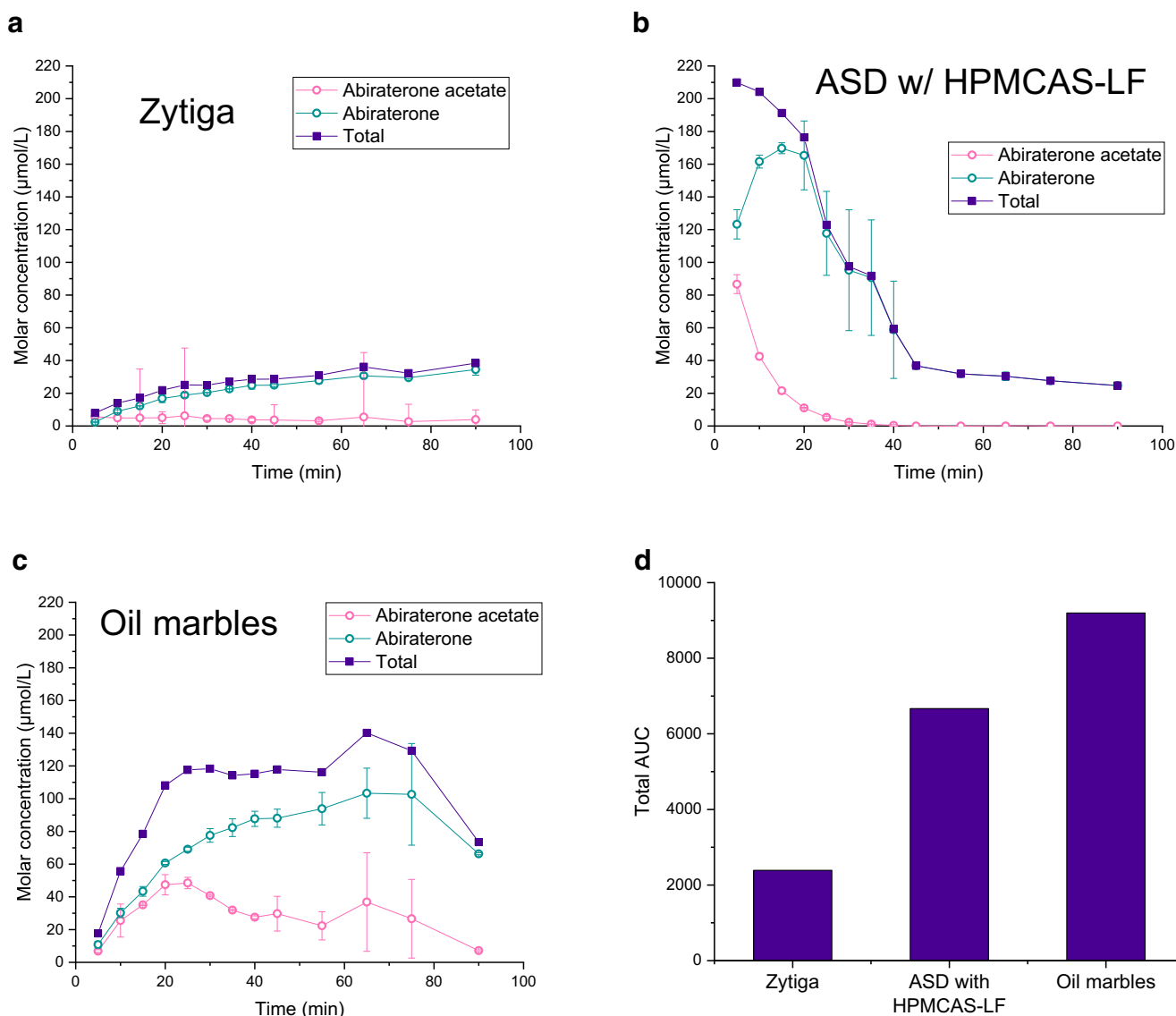


Fig. 5. *In vitro* dissolution in FaSSiF buffer supplemented with pancreatin. Abiraterone acetate (in pink), abiraterone (in green), and total concentration of both compounds (in blue) are plotted. **a** Original drug product Zytiga[®]. **b** Amorphous solid dispersion with HPMCAS-LF as carrier. **c** Oil marbles B. **d** Total API available for absorption plotted as area under the curve of all three formulations

administered dose is dissolved under simulated fasted conditions compared with 69% of the administered dose dissolved under simulated fed conditions. Moreover, Zytiga[®] apparently dissolves faster in the fed state simulated intestinal fluids than the OM formulation. If this behavior translates into *in vivo* scenario, the positive food effect reported for original drug product Zytiga[®] that can lead to toxic exposures of abiraterone acetate could be suppressed.

In Vivo Study

In crossover bioavailability study design, 8 rats completed both periods as planned. The weight of enrolled rats ranged between 309 and 428 g, while administered weight-normalized doses ranged from 10.30 to 13.78 mg/kg.

Abiraterone pharmacokinetic parameters after administration of test (oil marbles B) and reference (Zytiga[®]) formulations to fasted rats are summarized in Table III. The

rate of drug absorption was substantially higher after administration of test formulation in comparison to reference product as documented by approximately 4-fold C_{max} and shorter T_{max} , although the difference in T_{max} values between test and reference formulations did not reach statistical significance. The extent of abiraterone absorption was approximately 2.7-fold higher after the test formulation in comparison to the reference product. Figure 6a shows the mean abiraterone pharmacokinetic profiles after both products.

Concentrations of pre-dose blood samples were all below the limit of quantification (1 ng/mL) indicating that the wash-out period (48 h) was sufficient. However, the sampling interval, although derived from our previous experience (11), was rather short as the β elimination phase has not been covered in 3 and 2 pharmacokinetic profiles after administration of reference and test formulations, respectively. The AUC_{last}/AUC_{inf} ratio in the rest of animals ranged from 0.71

Table III. Abiraterone PK Parameters After Administration of Test (OM B) and Reference (Zytiga®) Formulations to Rats ($n = 8$) in the Fasted State. T_{\max} Values Are Given as Median (interquartile range). C_{\max} , AUC_{last} , and Test/Reference Ratios Are Given as Geometric Mean (90% Confidence Intervals)

Formulation	C_{\max} (ng/mL g)	$T/R C_{\max}$ (%)	AUC_{last} (mg/mL min g)	$T/R AUC_{\text{last}}$ (%)	T_{\max} (min)
Reference	0.143 (0.073–0.281)	N/A	30.3 (14.3–64.2)	N/A	244 (228–420)
Test	0.569 (0.206–1.566)	397.8 (213.8–740.1)	81.0 (32.1–204.4)	267.4 (165.7–431.6)	168 (114–252)

to 0.99 for the reference formulation and 0.58 to 0.95 for the test formulation, which indicates that the difference in total exposure between formulations is underestimated and would be probably even higher, if the sampling interval covered the whole PK profile thoroughly.

A total of 12 rats were enrolled into the food effect study to get complete pharmacokinetic profiles from 11 subjects. One of the rats had to be excluded due to difficulties with sample collection. Thus, pharmacokinetic profiles under fasted and fed conditions were compared after administration of reference and test formulations in 5 and 6 subjects, respectively. The weight of rats ranged between 355 and 432 g. Weight-normalized doses of abiraterone ranged from 10.75 to 13.33 mg/kg. Table IV shows summarized pharmacokinetic parameters after administration of test (OM B) and reference (Zytiga®) products under fasted or fed state. The reference formulation resulted in approximately twice as high as AUC_{last} in the fed state compared with fasted rats, which corresponds to significantly increased exposure of abiraterone observed with food in humans (2).

There was, however, no food effect on abiraterone absorption from test formulation evidenced by similar C_{\max} and AUC_{last} values under the fasted and fed states. For both formulations, absorption was prolonged in the fed state. The test formulation required less time to reach the maximum plasma concentration than the reference. Mean (SD) abiraterone pharmacokinetic profiles are showed in Fig. 6b and c.

Concentrations of pre-dose blood samples were all below the limit of quantification (1 ng/mL), suggesting that the wash-out period between dosing (48 h) was sufficient. Although this food effect study was not powered to compare

differences between formulations in fasting conditions, the results correspond with observations from the first part of the study. Zytiga® is standardly administrated in the fasted state. When comparing abiraterone exposure of both formulations, administration of oil marbles led to twice as high AUC_{last} as Zytiga® in the same dose. If we consider the advantage of eliminated food effect, oil marbles seem to be a promising drug formulation for abiraterone acetate.

DISCUSSION

The main goal of this work was to prepare and test a new formulation concept for abiraterone acetate based on the so-called oil marbles (OMs). We have successfully prepared OMs from different mixtures of oils and surfactants that showed an ability to solubilize abiraterone acetate. Although the design space for the preparation of oil marbles was not covered exhaustively, we have shown several manufacturable OM formulations using surfactants of different chemical structures and physical properties.

All prepared samples of OMs exhibited an amorphous character which shows that abiraterone acetate remains molecularly dispersed in the oil-based matrix even after it cools down to room temperature. This implies that the dissolution rate from the OM formulation will depend only on the rate at which the matrix components are being dispersed in the dissolution media. The marble size hence turned out to be the crucial parameter for the *in vitro* performance of the oil marbles. While keeping in mind that the performance of lipid-based formulations does not rely solely on the dissolution profiles, the results showed that

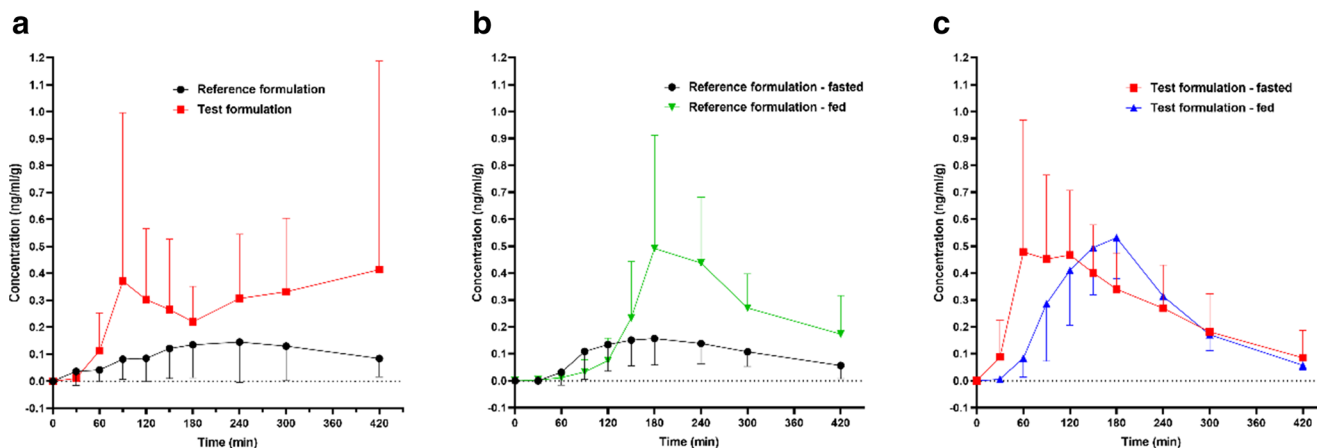


Fig. 6. Mean (\pm SD) abiraterone pharmacokinetic profiles in rats: **a** after administration of reference and test formulations in fasted condition; **b** after administration of reference formulation in fasted and fed conditions; **c** after administration of test formulation in fasted and fed conditions

Table IV. Abiraterone PK Parameters After Administration of Test and Reference Formulations to Rats ($n=11$) in Fasted and Fed Conditions. T_{\max} Values Are Given as Median (Interquartile Range). C_{\max} , AUC_{last} , and Fed/Fasted Ratios Are Given as Geometric Mean (90% Confidence Intervals)

Formulation	C_{\max} (ng/mL g)	Fed/fasted C_{\max} (%)	AUC_{last} (mg/mL min g)	Fed/fasted AUC_{last} (%)	T_{\max} (min)
Reference fasted	0.231 (0.176–0.302)	N/A	40.0 (31.3–51.1)	N/A	179 (157–226)
Reference fed	0.550 (0.318–0.950)	238.5 (131.1–433.9)	80.7 (40.6–160.4)	201.8 (86.7–469.4)	218 (185–288)
Test fasted	0.546 (0.199–1.480)	N/A	94.7 (43.2–207.4)	N/A	125 (68–178)
Test fed	0.530 (0.351–0.801)	103.8 (58.3–184.9)	93.6 (62.6–140.1)	105.1 (76.4–144.5)	152 (148–178)

release profiles can be controlled simply by adjusting the size of OMs. This can be crucial when targeting certain dissolution/absorption profile.

To further understand the behavior of OM formulation, *in vitro* experiment with pancreatic enzymes was designed. Overall, all conducted *in vitro* tests showed a tendency towards higher fraction dissolved under fasting conditions for OM formulation when compared with the original drug formulation Zytiga[®]. These results provided a solid base for subsequent *in vivo* testing, where a significantly higher relative bioavailability of OMs was indeed observed.

In order to address the effect of food on the bioavailability of different abiraterone acetate formulations, a fasted-fed *in vivo* study was designed and conducted. It had been shown before that a high fat content in meal has a significant impact on the bioavailability of abiraterone acetate (5). Limited bioavailability of the original drug product Zytiga[®] under fasting conditions resulted in a significant positive food effect in the rat animal model, which is consistent with previously conducted human studies.

A 1:1 mixture of olive oil and Nutridrink was dosed to rats to create the fed state. The use of this mixture was based not only on previous experience but also on conditions described in the literature. The administration of 1–2 mL of oil is a standard approach to introduce fed conditions in rat PK studies (33,34). However, since the formulation was dosed in hard gelatin capsules, we had to ensure that the rat stomach also contains some aqueous phase in which the capsules could dissolve.

The fasted state comparative bioavailability study has shown a rather unexpected double C_{\max} pattern for abiraterone after OM (Fig. 6a). This finding was mainly driven by a single animal outlying with exceptionally high abiraterone serum concentrations at the sampling points between 240 and 420 min. In the food effect study, the C_{\max} and AUC values demonstrated limited effect of food for OM formulation, but the T_{\max} was substantially prolonged at the fed state, which could be a result of a non-formulation-dependent effect of the presence of food in the gastrointestinal tract that increased secretion, delayed gastric emptying, influenced intestinal peristaltic movement, or competed with drugs on absorption transporters (35). Furthermore, a large variability in the serum drug concentrations has been observed in the OM group at the fasted state. This observation was caused by the fact that always one of the animals achieved C_{\max} was at 60, 90, and 120 min, while in the rest of the group, a “plateau” was seen between 90 and 300 min with no clear T_{\max} . These findings point out to the main limitation of our studies, which is limited study

population. Another limitation is that the pharmacokinetic performance of OM has been studied *in vivo* in a rat model, which is known to have different gastrointestinal physiologies and conditions that may make direct extrapolation of the findings to man difficult. However, the food effect, which is known from human studies, has been well captured in our food effect study, which suggests sufficient study sensitivity. Furthermore, we applied a crossover comparative study design, which allows to limit the study population as it is the most robust study design to limit intersubject variability for the comparison of performance of two (or more) formulations. The limitation of the small study sample is that we could not reliably describe the T_{\max} and some other pharmacokinetic variables but the between-formulation comparison, which was the aim of the study, has been well demonstrated. The relatively higher bioavailability of oil marbles under fasting conditions resulted in a significantly suppressed food effect in rats.

CONCLUSION

Overall, it can be concluded that oil marbles represent a promising formulation approach that combines the advantages of liquid-state lipidic formulations such as SEDDS/SMEDDS, namely rapid dissolution, with advantages of solid dosage form such as handling, ability to be filled into hard gelatin capsules, and the possibility to adjust release rate by size. In the specific case of abiraterone acetate, the oil marble formulation made it possible to suppress differences in the oral bioavailability under fed and fasted conditions in rats, and therefore help to eliminate the strong positive food effect for which this molecule has been known. Due to natural differences in rat and human gastrointestinal physiology, these results should be confirmed in human studies as the next step.

AUTHOR CONTRIBUTIONS

The manuscript was written through contributions of all authors. All authors have given approval to the final version of the manuscript.

FUNDING

T.B. received support from the Specific University Research (project MŠMT no. 21-SVV/2019). F.Š. received support from the Czech Science Foundation (project GAČR no. 19-26127X). O.R. received support from the Technology Agency of the Czech Republic (project no. TJ02000143). T.K.

received support from Charles University Research Centre program no. UNCE/SCI/014. O.S. received support from the Charles University project PROGRES Q25/LF1. This work received support from Zentiva, k.s.

COMPLIANCE WITH ETHICAL STANDARDS

All experiments were performed in accordance with the Guiding Principles for the Use of Animals in Charles University, First Faculty of Medicine, and every effort was made to minimize animal suffering. The experimental animal project was approved by the Ministry of Education, Youth and Sports, Czech Republic (MSMT-9445/2018-8).

Conflict of Interest The authors declare that they have no competing interests.



REFERENCES

- Boyd BJ, Bergstrom CAS, Vinarov Z, Kuentz M, Brouwers J, Augustijns P, et al. Successful oral delivery of poorly water-soluble drugs both depends on the intraluminal behavior of drugs and of appropriate advanced drug delivery systems. *Eur J Pharm Sci.* 2019;137:104967.
- Zytiga, EMA/CHMP/542871 – Assessment report for Zytiga, EMA (European Medicines Agency). 2011.
- Lubberman FJE, Benoist GE, Gerritsen W, Burger DM, Mehra N, Hamberg P, et al. A prospective phase I multicentre randomized cross-over pharmacokinetic study to determine the effect of food on abiraterone pharmacokinetics. *Cancer Chemother Pharmacol.* 2019;84(6):1179–85.
- Chi KN, Spratlin J, Kollmannsberger C, North S, Pankras C, Gonzalez M, et al. Food effects on abiraterone pharmacokinetics in healthy subjects and patients with metastatic castration-resistant prostate cancer. *J Clin Pharmacol.* 2015;55(12):1406–14.
- Chien C, Smith M, Porre P. Effect of food on abiraterone pharmacokinetics: a review. *Int J Pharm.* 2017;2.
- Schultz HB, Meola TR, Thomas N, Prestidge CA. Oral formulation strategies to improve the bioavailability and mitigate the food effect of abiraterone acetate. *Int J Pharm.* 2020;577:119069.
- Yonsa, Drug Approval Package: YONSA (abiraterone acetate), FDA (U.S. Food and Drug Administration). Food and Drug Administration (FDA). 2018.
- Goldwater R, Hussaini A, Bosch B, Nemeth P. Comparison of a novel formulation of abiraterone acetate vs. the originator formulation in healthy male subjects: two randomized, open-label, crossover studies. *Clin Pharmacokinet.* 2017;56(7):803–13.
- Solyosi T, Ötvös Z, Angi R, Ordasi B, Jordán T, Molnár L, et al. Novel formulation of abiraterone acetate might allow significant dose reduction and eliminates substantial positive food effect. *Cancer Chemother Pharmacol.* 2017;80(4):723–8.
- Solyosi T, Ötvös Z, Angi R, Ordasi B, Jordán T, Semsey S, et al. Development of an abiraterone acetate formulation with improved oral bioavailability guided by absorption modeling based on in vitro dissolution and permeability measurements. *Int J Pharm.* 2017;532(1):427–34.
- Boleslavská T, Světlík S, Žvátora P, Bosák J, Dammer O, Beránek J, et al. Preclinical evaluation of new formulation concepts for abiraterone acetate bioavailability enhancement based on the inhibition of pH-induced precipitation. *Eur J Pharm Biopharm.* 2020;151:81–90.
- Legen I, Peternel L, Novak Stagoj M, Homar M, Rozman Peterka T, Klancar U. Self-microemulsifying drug delivery system of abiraterone or abiraterone acetate, WO 2014/009434 A1 2014.
- Pouton CW, Porter CJ. Formulation of lipid-based delivery systems for oral administration: materials, methods and strategies. *Adv Drug Deliv Rev.* 2008;60(6):625–37.
- Mullertz A, Ogbonna A, Ren S, Rades T. New perspectives on lipid and surfactant based drug delivery systems for oral delivery of poorly soluble drugs. *J Pharm Pharmacol.* 2010;62(11):1622–36.
- Mu H, Holm R, Müllertz A. Lipid-based formulations for oral administration of poorly water-soluble drugs. *Int J Pharm.* 2013;453(1):215–24.
- Bernkop-Schnurch A, Jalil A. Do drug release studies from SEDDS make any sense? *J Control Release.* 2018;271:55–9.
- Carriere F. Impact of gastrointestinal lipolysis on oral lipid-based formulations and bioavailability of lipophilic drugs. *Biochimie.* 2016;125:297–305.
- Sonali BH, Sushmita SC, Sonali SK, Suchita LS, Sugave RV. A review on: soft gelatine capsule. *Int J Innov Pharm Sci Res.* 2018;6(6):59–71.
- Joyce P, Dening TJ, Meola TR, Schultz HB, Holm R, Thomas N, et al. Solidification to improve the biopharmaceutical performance of SEDDS: opportunities and challenges. *Adv Drug Deliv Rev.* 2019;142:102–17.
- Aussillous P, Quéré D. Liquid marbles. *Nature.* 2001;411(6840):924–7.
- McHale G, Newton MI. Liquid marbles: principles and applications. *Soft Matter.* 2011;7(12):5473.
- Hapgood KP, Khanmohammadi B. Granulation of hydrophobic powders. *Powder Technol.* 2009;189(2):253–62.
- Janská P, Rychecký O, Zdražil A, Štěpánek F, Čejková J. Liquid oil marbles: increasing the bioavailability of poorly water-soluble drugs. *J Pharm Sci.* 2019;108(6):2136–42.
- Geboers S, Stappaerts J, Mols R, Snoeys J, Tack J, Annaert P, et al. The effect of food on the intraluminal behavior of abiraterone acetate in man. *J Pharm Sci.* 2016;105(9):2974–81.
- Rowe RC, Sheskey PJ, Quinn ME. Handbook of pharmaceutical excipients. 6th ed. USA: Pharmaceutical Press and American Pharmacists Association; 2009.
- Kabanov AV, Batrakova EV, Alakhov VY. Pluronic® block copolymers as novel polymer therapeutics for drug and gene delivery. *J Control Release.* 2002;82(2):189–212.
- Kolliphor RH40, BASF Technical information no. 03_111141e-01.
- Tween 20, Sigma Aldrich Product information no. 1379.
- Tween 80, Sigma Aldrich Product information no. 1754.
- Kolliphor EL, BASF Technical information no. 03_111139e-02.
- Brouwers J, Brewster ME, Augustijns P. Supersaturating drug delivery systems: the answer to solubility-limited oral bioavailability? *J Pharm Sci.* 2009;98(8):2549–72.
- Stappaerts J, Geboers S, Snoeys J, Brouwers J, Tack J, Annaert P, et al. Rapid conversion of the ester prodrug abiraterone acetate results in intestinal supersaturation and enhanced absorption of abiraterone: in vitro, rat in situ and human in vivo studies. *Eur J Pharm Biopharm.* 2015;90:1–7.
- Brocks DR, Wasan KM. The influence of lipids on stereoselective pharmacokinetics of halofantrine: important implications in food-effect studies involving drugs that bind to lipoproteins. *J Pharm Sci.* 2002;91(8):1817–26.
- Shayeganpour A, Jun AS, Brocks DR. Pharmacokinetics of Amiodarone in hyperlipidemic and simulated high fat-meal rat models. *Biopharm Drug Dispos.* 2005;26(6):249–57.
- Welling PG. Effects of food on drug absorption. *Annu Rev Nutr.* 1996;16:383–415.

Publisher's Note Springer Nature remains neutral with regard to jurisdictional claims in published maps and institutional affiliations.

RESEARCH ARTICLE

Validity of cycloheximide chylomicron flow blocking method for the evaluation of lymphatic transport of drugs

Pavel Ryšánek¹  | Tomáš Grus² | Peter Lukáč² | Petr Kozlík³ |
 Tomáš Křížek³ | Jiří Pozniak⁴ | Jaroslava Roušarová¹ | Jana Královičová¹ |
 Nikolína Kutinová Canová¹ | Tereza Boleslavská^{5,6} | Jan Bosák⁵ |
 František Štěpánek⁶ | Martin Šíma¹  | Ondřej Slanař¹

¹Institute of Pharmacology, First Faculty of Medicine, General University Hospital in Prague, Charles University, Prague, Czech Republic

²Department of Cardiovascular Surgery, First Faculty of Medicine, General University Hospital in Prague, Charles University, Prague, Czech Republic

³Department of Analytical Chemistry, Faculty of Science, Charles University, Prague, Czech Republic

⁴Third Department of Surgery, First Faculty of Medicine, Motol University Hospital, Charles University, Prague, Czech Republic

⁵Preformulation and Biopharmacy Department/Clinical Development Department, Zentiva, k.s, Prague, Czech Republic

⁶Department of Chemical Engineering, University of Chemistry and Technology, Prague, Czech Republic

Correspondence

Pavel Ryšánek, Institute of Pharmacology, Albertov 4, 128 00 Praha 2, Czech Republic.
 Email: pavel.rysanek@lf1.cuni.cz

Martin Šíma, Institute of Pharmacology, Albertov 4, 128 00 Praha 2, Czech Republic.
 Email: martin.sima@lf1.cuni.cz

Funding information

Charles University Research Centre, Grant/Award Number: UNCE/SCI/014; Univerzita Karlova v Praze, Grant/Award Number: SVV 260 523

Background and purpose: Lymphatic transport of drugs after oral administration is an important mechanism for absorption of highly lipophilic compounds. Direct measurement in lymph duct cannulated animals is the gold standard method, but non-invasive cycloheximide chylomicron flow blocking method has gained popularity recently. However, concerns about its reliability have been raised. The aim of this work was to investigate the validity of cycloheximide chylomicron flow blocking method for the evaluation of lymphatic transport using model compounds with high to very high lipophilicity, that is, abiraterone and cinacalcet.

Experimental approach: Series of pharmacokinetic studies were conducted with abiraterone acetate and cinacalcet hydrochloride after enteral/intravenous administration to intact, lymph duct cannulated and/or cycloheximide pre-treated rats.

Key results: Mean total absolute oral bioavailability of abiraterone and cinacalcet was 7.0% and 28.7%, respectively. There was a large and significant overestimation of the lymphatic transport extent by the cycloheximide method. Mean relative lymphatic bioavailability of abiraterone and cinacalcet in cycloheximide method was 28-fold and 3-fold higher than in cannulation method, respectively.

Conclusion and implications: Cycloheximide chylomicron flow blocking method did not provide reliable results on lymphatic absorption and substantially overestimated lymphatic transport for both molecules, that is, abiraterone and cinacalcet. This non-invasive method should not be used for the assessment of lymphatic transport and previously obtained data should be critically revised.

KEYWORDS

abiraterone, bioavailability, biodistribution, cinacalcet, lymph duct cannulation, pharmacokinetics

1 | INTRODUCTION

Lymphatic transport is a potential way of drug transfer into systemic circulation after oral dosing. Upon absorption into intestinal mucosa,

highly lipophilic compounds are typically incorporated into chylomicrons and secreted into mesenteric lymph, which is drained into systemic circulation by a system of lymphatic vessels (Charman & Stella, 1986; Porter et al., 2007). Lymphatic transport has been

studied for several compounds in the last few decades. It has been shown as a potential way of increasing oral bioavailability, evading the liver first-pass effect and enhancing pharmacodynamic effects in compounds targeting immune cells physiologically present in the lymph (Han, Hu, Quach, Simpson, Edwards, et al., 2016a; Shackelford et al., 2003).

There are several animal models currently used for the investigation of lymphatic transport of drugs. The gold standard methodology relies on direct measurement of drug concentration in the lymph in various animal species, whereas rat is the most common one (Trevaskis et al., 2015). However, a non-invasive chylomicron flow blocking approach in rats has also been used gaining substantial popularity in recent years (Dahan & Hoffman, 2005). This method is based on the assumption that cycloheximide administered intraperitoneally shortly before oral dosing of the investigated compound blocks its lymphatic transport without affecting other ways of intestinal absorption.

Yet there are no robust validation data with only one direct comparative study for **cholecalciferol**, **vitamin D₃**, (Dahan & Hoffman, 2005) and one indirect comparison for **halofantrine** (Caliph et al., 2000; Lind et al., 2008). In a recently published systematic review, we observed a general trend towards higher relative bioavailability via lymph in **cycloheximide** studies (Rysanek et al., 2020). The median relative bioavailability via lymph was 47.3% and 25.7% in cycloheximide and lymph duct cannulation studies, respectively. Furthermore, a significant difference was reported for compounds with $\log P < 5$, where the respective parameters were 47.3% and 2.26%. We therefore suspected a vast overestimation by the cycloheximide method especially for drugs with lower lipophilicity.

Abiraterone acetate is a highly lipophilic compound ($\log P \sim 4.5$) used in the treatment of castration resistant prostate cancer. It has a pronounced food effect in men, with up to 17-fold increase in C_{\max} and tenfold increase in AUC when administered with high-fat meal (Chi et al., 2015). For safety reasons, this led to posology restriction to fasted state only.

Cinacalcet hydrochloride is another highly lipophilic molecule ($\log P \sim 6.5$) used in the treatment of hyperparathyroidism. Similarly to abiraterone, there is a significant food effect after oral administration in humans, albeit not that high. Its bioavailability increases by 50–70% depending on the fat content in the meal (Padhi et al., 2007).

As shown for other lipophilic compounds, significantly increased bioavailability after high-fat food intake may be caused by enhanced lymphatic transport (Khoo et al., 2001; Trevaskis et al., 2010). Therefore, we hypothesized that intestinal lymphatic transport could be involved in the processes of abiraterone and cinacalcet absorption after oral administration.

The aim of this study was to investigate the validity of the non-invasive cycloheximide chylomicron flow blocking method for the evaluation of lymphatic transport by a comparison with invasive lymph duct cannulation method using two model compounds with high to very high lipophilicity, that is, abiraterone and cinacalcet.

What is already known?

- Lymphatic transport of drugs plays an important role in intestinal absorption of many highly lipophilic compounds
- Cinacalcet and abiraterone are highly lipophilic drugs used to treat hyperparathyroidism and prostate cancer, respectively.

What does this study add?

- Non-invasive cycloheximide chylomicron flow blocking method is not reliable in estimating intestinal lymphatic transport of drugs.
- Oral cinacalcet is absorbed by a high proportion through the lymph, whereas abiraterone is not.

What is the clinical significance?

- Lymphatic transport may be involved in cinacalcet pronounced positive food effect.

2 | METHODS

2.1 | Abiraterone dosing forms preparation

Zytiga tablets were crushed and filled into mini gelatine capsules, size 9el (Harvard Apparatus, USA). Abiraterone acetate content in one capsule was 4.1 mg.

Abiraterone oil solution was prepared by abiraterone acetate powder dissolution in DMSO to achieve a concentration of 40 mg ml^{-1} . Abiraterone DMSO solution $100 \mu\text{l}$ was then added to 1 ml olive oil and vortexed (Vortex mixer, Labnet international, Inc.) for 1 min to produce a homogenous emulsion. The dosing form was prepared freshly not more than 30 min before dosing.

Abiraterone solution for intravenous administration (1 mg ml^{-1}) was prepared according to Kumar et al. (2013). Briefly, abiraterone was dissolved in solution containing 10% DMSO, 10% mixture of Kolliphor HS 15 and ethanol (1:1, V/V), 10% Cremophor EL and 70% Captisol (20% Captisol in water). The concentration of abiraterone was determined using HPLC analysis.

2.2 | Cinacalcet dosing forms preparation

Cinacalcet hydrochloride powder was dissolved in DMSO to achieve a concentration of 30 mg ml^{-1} . Cinacalcet DMSO solution $100 \mu\text{l}$ was then added to 1 ml olive oil and shaken to mix the DMSO and oil fractions. The dosing form was prepared freshly not more than 30 min before dosing.

Cinacalcet intravenous formulation was prepared by cinacalcet hydrochloride powder dissolution in DMSO in concentration 3 mg ml^{-1} . This solution was further diluted with distilled water to achieve a concentration of 0.3 mg ml^{-1} .

2.3 | Animals

All animal experiments were performed under approval from the Ministry of Education, Youth and Sports, Czech Republic (MSMT-9445/2018-8) and are reported in compliance with the ARRIVE guidelines (Percie du Sert et al., 2020) and with the recommendations made by the *British Journal of Pharmacology* (Lilley et al., 2020). All efforts were made to minimize animal suffering. Male Wistar rats (weight 300–450 g, age 3–5 months) were purchased from Velaz s. r. o., Prague, Czech Republic. They were housed under standard conditions (12-h light/dark cycle, 22°C temperature and 50% humidity) in cages with wood shavings bedding (two rats per cage during acclimation and one rat per cage during experiment) and fed on water and granulated diet ad libitum. The acclimation period took at least 1 week. The animals were randomly assigned to experimental arms.

2.4 | Lymphatic transport studies in cannulated rats

Mesenteric lymph duct cannulated anaesthetized rat model was used as previously described with slight modifications (Trevaskis et al., 2015). Rats were left on normal diet and given 1 ml olive oil 1 h prior to surgery to facilitate the mesenteric lymph duct visualization. They were anaesthetized with an i.m. combination of xylazine (5 mg kg^{-1}) and ketamine (100 mg kg^{-1}) after a rapid isoflurane induction maintaining spontaneous breathing throughout the whole experiment. Transverse laparotomy was performed. Mesenteric duct was identified cranially to superior mesenteric artery and cannulated with heparin prefilled 0.97 mm O.D., 0.58 mm I.D. polyethylene catheter (Instech Laboratories, Plymouth Meeting, USA). The catheter was fixed in place with two to three drops of tissue adhesive (Surgibond[®], SMI AG, Belgium). A duodenal catheter was also placed (same parameters as for lymphatic catheter) via a small duodenotomy and fixed with a purse string suture or tissue adhesive. The abdominal wall was sutured in two layers with both catheters leaving the abdominal cavity on the right side of the animal. At the end of the procedure, right jugular vein was cannulated for blood sampling (3 Fr polyurethane catheter, Instech Laboratories, Plymouth Meeting, USA).

The rats were then placed on heated pads and covered with blanket to prevent heat loss. Cinacalcet (3 mg) oil solution and abiraterone (4 mg) oil solution were dosed slowly via duodenal catheter over 30 min. The mass of olive oil administered in each dosage form was 1 ml. Abiraterone (4 mg) capsule was dosed deeply intraduodenally via small incision during the surgery before

the wound closure. Whole lymph was collected in regularly changed Eppendorf tubes from the time when oil solution dosing started, or capsule was inserted into duodenum. The rats were continuously hydrated with normal saline at a rate of 3 ml h^{-1} intraduodenally using infusion pump (Perfusor[®] compact^{plus}, B. Braun Melsungen AG, Germany). Anaesthesia was maintained throughout the rest of the experiment and additional ketamine i.m. boluses were given whenever necessary. Eppendorf tubes were changed hourly and systemic blood was drawn at the same time points. At the end of the experiment with abiraterone capsules, cranial part of the small intestine was exposed in all animals to verify complete capsule dissolution. The animals were killed by anaesthetic overdose.

2.5 | Lymphatic transport studies with cycloheximide

Two separate two-period, one sequence, crossover studies were conducted to compare the bioavailability of either abiraterone capsule or cinacalcet oil solution after oral dosing with and without pre-treatment with chylomicron flow blocking agent cycloheximide. The crossover study design in rats was chosen and conducted as described previously (Boleslavská, Rychecký, et al., 2020). Both studies were conducted similarly. In both periods, rats were fasted for at least 4 h before and 4 h after the dosing. In the first period, the test drug (abiraterone 4 mg or cinacalcet 3 mg) was administered via oral gavage with no additional treatment. In the second period, the animals were pre-treated with 3 mg kg^{-1} of cycloheximide administered intraperitoneally 1 h before dosing. The cycloheximide DMSO solution was diluted in normal saline in a concentration of 3 mg ml^{-1} for this purpose. The wash-out period lasted 48 and 72 h in abiraterone and cinacalcet study, respectively. Systemic blood draws were taken at 1, 2, 3, 4, 5, 7 and 10 h after abiraterone administration and at 1, 2, 3, 4, 5, 6, 8, 12 and 24 h after cinacalcet administration. In the second period, a pre-dose blood sample was taken additionally (0 h) to verify lack of carry over effect.

2.6 | Lymphatic transport study with both cycloheximide and lymph duct cannulation

In order to directly assess the cycloheximide effect on lymphatically and non-lymphatically absorbed amount of drug, a study with cycloheximide pre-treated and lymph duct cannulated rats was conducted. Cycloheximide 3.0 mg kg^{-1} was administered i.p. immediately before the surgery. The lymph duct, duodenum and jugular vein were cannulated within 60 min as described for lymphatic transport studies in cannulated animals. After the surgery and exactly 60 min after the cycloheximide pre-treatment, cinacalcet oil solution was administered over 30 min via duodenal catheter. The lymph and blood were sampled hourly as described above.

2.7 | Bioavailability studies

Absolute oral bioavailability of cinacalcet oil solution was evaluated in a two-period, one sequence (i.v. - p.o.), cross-over bioavailability study and parallel comparison of two groups (i.v. - p.o.) was conducted for abiraterone capsule. Right jugular vein was cannulated in both studies. After overnight recovery, the rats were i.v. dosed with cinacalcet or abiraterone (both 1 mg kg⁻¹). Systemic blood was drawn at 10 and 30 min and at 1, 2, 3, 5, 8, 12 and 24 h after cinacalcet administration or at 5 and 15 min and at 0.5, 1, 1.5, 2, 2.5, 3, 4, 5 and 7 h after abiraterone administration. The p.o. dosing and sampling were performed as described for the cycloheximide lymphatic transport studies (see above).

2.8 | Cinacalcet biodistribution study

Cinacalcet biodistribution was compared between cycloheximide pre-treated and control rats. The rats were fasted for 12 h before and 4 h after dosing. Six rats were dosed with cinacalcet via oral gavage (3 mg) with no further treatment. Nine other rats were pre-treated with cycloheximide before the cinacalcet administration. The animals were killed at 8 and 24 h (both groups) and at 48 h (cycloheximide group) by cervical dislocation under deep isoflurane anaesthesia. Systemic blood sample was taken and the abdominal cavity was exposed. Small intestine, liver, right kidney and spleen were harvested. The kidney and the spleen were homogenized (IKA® T10 basic Ultra-Turrax®) in 100% DMSO solution. A 1 to 2 mg sample was taken from the liver and homogenized. The small intestine was longitudinally cut and washed thoroughly to remove all intraluminal contents. The organ was then homogenized as a whole.

Moreover, a single group extended cinacalcet pharmacokinetic study with cycloheximide pre-treatment was conducted. The blood draws were taken at 4, 8, 18, 21, 24, 28, 32, 42 and 48 h to cover the late pharmacokinetic profile.

2.9 | Sample processing

Blood samples were centrifuged (1811x g for 10 min) and serum was extracted. Lymph volume was measured gravimetrically and the samples were further processed without additional adjustment. Organ homogenates were centrifuged (1431x g for 10 min) and the DMSO supernatant was extracted. All samples were stored in -80°C until analysis. Laboratory was unaware of animal assignment to particular experimental group (laboratory blinding).

2.10 | Analytical methods

Determination of cinacalcet in studied samples was performed using the Shimadzu UHPLC Nexera X3 coupled with a Triple Quad 8045 tandem mass spectrometer (Shimadzu, Kyoto, Japan). Poroshell 12 SB

AQ column (100 mm × 2.1 mm, 2.6 µm particle size) from Agilent Technologies (Waldbronn, Germany) was used for the analysis. The mobile phase consisted of 0.1% formic acid in deionized water (Solvent A) and acetonitrile (Solvent B). The flow rate of the mobile phase was maintained at 0.45 ml min⁻¹ and the injection volume was 1 µl. The temperature of the column was kept at 40°C and samples were thermostated at 5°C. The optimized gradient program (min/% B) was 0/30, 1.0/30, 3.0/80, 4.0/80, 4.5/30 and 6.5/30. The MS/MS measurements (operated in positive mode) were performed in the selected reaction mode (SRM). Two SRM transitions were monitored for cinacalcet: Quantifier transition was 358.2 > 155.2 (Q1 pre-bias -18 V, Q3 pre-bias -29 V and collision energy -20 V), and qualifier transition was 358.2 > 208.2 (Q1 pre-bias -16 V, Q3 pre-bias -25 V and collision energy -15 V). The transition 362.2 > 155.2 (Q1 pre-bias -18 V, Q3 pre-bias -28 V and collision energy -18 V) was monitored for cinacalcet-d₄ (internal standard, IS). The ion source was set as follows: interface temperature: 300°C, desolvation line temperature: 250°C, heat block temperature: 400°C, nebulizing gas flow: 3 L min⁻¹, heating gas flow: 10 L min⁻¹ and drying gas flow: 10 L min⁻¹.

The concentration of cinacalcet was determined in serum, lymph and different tissues (dimethyl sulfoxide extracts). Before the LC-MS/MS analysis, 20 µl of sample (serum, lymph or tissue extracts) was deproteinized with 60 µl of 100% acetonitrile containing IS (cinacalcet-d₄, c = 30 ng ml⁻¹) in an Eppendorf tube by vortexing for 15 s. Then, samples were centrifuged at 16,500×g for 8 min and 50 µl of supernatant was transferred into LC vials. The method was validated in terms of linearity, lower limit of quantification (LLOQ), upper limit of quantification (ULOQ), accuracy, precision, selectivity, recovery and matrix effects. Selectivity was monitored by injecting six samples of each matrix (serum, lymph and all studied tissue extract samples) with mass spectrometer set in scan mode. The obtained chromatograms showed no interfering compound within the retention time window of cinacalcet. Moreover, the developed method uses a tandem mass spectrometer in specific SRM mode, which ensures high selectivity. The calibration curves were constructed in each blank matrix (serum, lymph and pooled tissue extracts) with seven concentrations by plotting the ratio of the peak area of cinacalcet to that of IS against cinacalcet concentration. The weighted least-squares linear regression method was used with weighting factor of 1 x⁻², which improved the accuracy in low concentrations. Due to the use of cinacalcet-d₄ as the IS, no significant difference in calibration curves in different matrices was observed. The method was linear (coefficients of determination [R²] higher than 0.9997) in the concentration range of 0.5–1,600 ng ml⁻¹. LLOQ, which was the lowest calibration standard, was 0.5 ng ml⁻¹ with precision and accuracy up to 10% (back calculated). ULOQ, which was the highest calibration standard, was 1,600 ng ml⁻¹ with precision and accuracy up to 4% (back calculated). The accuracy and precision of back-calculated concentrations of other calibration points were within 5% of the nominal concentration. Method accuracy and precision were evaluated by measuring five replicates at three different concentrations of 1, 50 and 1,000 ng ml⁻¹ in each

matrix on two different days. The accuracy was expressed as the relative error, RE (%) = (measured concentration – expected concentration)/expected concentration × 100 and the precision expressed by repeatability as the relative standard deviation (RSD). The inter-day and intra-day precisions (RSD %) ranged from 0.9% to 6.5%, and the relative accuracy (RE%) was within ±6.1%. The same samples were also used as quality control samples. Quality control samples were injected after each sixth sample to assess the validity of the analytical method. Recovery was evaluated by comparing the area of the cinacalcet standard peak of the pre-protein-precipitation spiked sample with that of the corresponding post-protein-precipitation spiked sample at three concentrations (1, 50 and 1,000 ng ml⁻¹). The recovery ranged in each matrix from 98.9% to 101.1%. Matrix effect was determined by comparing the area of the cinacalcet standard peak of the post-protein-precipitation spiked sample with that of the 80% acetonitrile (without matrix effect). It was evaluated at three concentration levels (1, 50 and 1,000 ng ml⁻¹) using six different samples of each matrix. The matrix effect ranged from 74% to 102%. In our method, the matrix effect is eliminated by the use of an isotopically labelled standard because the analyte/IS response ratio remains unaffected, even when the absolute responses of the analyte and IS are affected significantly. The LC-MS/MS validation proved the suitability of our analytical method for the determination of cinacalcet in different matrices.

Abiraterone concentrations in serum and lymph were analysed using LC-MS as described previously (Boleslavská, Světlík, et al., 2020). The method was validated for the same validation parameters and using the same procedure as for cinacalcet for both studied matrices, that is, serum and lymph. The LC-MS/MS was selective since no interfering endogenous components were observed at the retention time of abiraterone. A 7-point calibration curve was constructed using the analyte-to-internal standard peak area ratio in each matrix. Weighted least-squares linear regression (1 x⁻² weighting factor) was used. The developed method was linear in the range of 0.5–600 ng ml⁻¹ (R² > 0.9996). The accuracy and precision of back-calculated concentrations of all calibration points deviated within 8% of the nominal concentration, except for LLOQ (0.5 ng ml⁻¹), which deviated by ±15%. The accuracy and precision (five replicates at concentrations of 1, 50 and 500 ng ml⁻¹ in each matrix on two different days) were between 1.2% to 7.8% and 0.8% to 4.9%, respectively. The recovery of abiraterone and matrix effect (1, 50 and 500 ng ml⁻¹) ranged from 97% to 102% and 85% to 105%, respectively. The mentioned validation performance parameters confirmed that LC-MS/MS method is suitable for quantification of abiraterone in serum and lymph samples.

2.11 | Data analysis and statistics

Serum concentrations in all pharmacokinetic studies were dose normalized to 1 mg kg⁻¹ prior to further calculations. AUC values were determined using linear trapezoidal rule. Exact actual sampling times were used for this purpose. Scheduled sampling times were used for

mean concentration plotting in the graphs. In the cinacalcet biodistribution study, dose normalized (1 mg kg⁻¹) absolute amount of drug in DMSO supernatant was determined and further normalized to weight of the homogenized organ sample (1 g⁻¹). Lymph drug concentrations were dose normalized to 1 mg kg⁻¹ as well. Lymph pharmacokinetic profiles were plotted in the graphs using drug concentrations measured in the sampled lymph as actual concentrations in the middle of each collection period, that is, assuming linear absorption. GraphPad Prism version 9.1.0 (GraphPad Software, San Diego, CA, USA) was used for all statistical analyses. Unpaired Student's *t*-test was used to compare pharmacokinetic and lymphatic transport parameters. Level of significance was set to *p* < 0.05.

2.12 | Bioavailability and lymphatic transport calculations

Absolute bioavailability via lymph (F_{AL}) was defined as percentage of administered drug dose absorbed into the lymph. It was determined directly from lymph volume and drug concentration in lymph duct cannulated rats. Absolute bioavailability via portal vein (F_{AP}) was analogically defined as percentage of administered drug dose reaching the systemic circulation after direct absorption into blood. It was calculated using the following equation:

$$F_{AP} = AUC_{ent} \times AUC_{iv}^{-1}, \quad (1)$$

where AUC_{ent} is the area under the dose normalized blood concentration-time curve after enteral dosing in lymph duct cannulated (i.e. lymph deprived) rats and AUC_{iv} is the respective parameter in a separate intravenously dosed group. Total absolute bioavailability (F) in lymph duct cannulated rats was calculated as a sum of F_{AL} and F_{AP} . In intact, non-cannulated animals, F was calculated using standard formula for oral bioavailability:

$$F = AUC_{po} \times AUC_{iv}^{-1} \quad (2)$$

Relative bioavailability via lymph (F_{RL}) was defined as percentage of systemically available drug that was absorbed via lymph. It was calculated using the following equation:

$$F_{RL} = F_{AL} \times F^{-1}. \quad (3)$$

F_{RL} in the cycloheximide studies was calculated directly by comparing dose normalized AUC with and without cycloheximide pretreatment:

$$F_{RL} = (AUC_{po} - AUC_{cycloheximide}) \times AUC_{po}^{-1}. \quad (4)$$

2.13 | Materials

Abiraterone acetate commercial tablets (Zytiga[®]) and abiraterone acetate powder were kindly donated by Zentiva, k.s. (Prague, Czech Republic), Cinacalcet hydrochloride powder and its internal standard, cycloheximide solution 100 mg ml⁻¹ in 100% DMSO, Kolliphor HS 15 and Cremophor EL were purchased from Sigma-Aldrich, Prague, Czech Republic. All solvents used were at least of HPLC grade. Xylazine 20 mg ml⁻¹ solution (Romestar[®], Bioveta a.s., Czech Republic), Ketamine 100 mg ml⁻¹ solution (Narkamon[®], Bioveta a.s., Czech Republic) and isoflurane (IsoFlo[®], Zoetis/Pfizer, Czech Republic) were used for animal anaesthesia. Ketoprofen 100 mg ml⁻¹ (Ketodolor[®], Le Vet Beheer B.V., Netherlands) was used as analgesic. Heparin solution 5,000 IU ml⁻¹ (Zentiva k.s., Czech Republic) was used for catheter patency maintenance. T61[®] (Intervet International B.V., Netherlands) was used for killing the animals at the end of experiments.

2.14 | Nomenclature of targets and ligands

Key protein targets and ligands in this article are hyperlinked to corresponding entries in the IUPHAR/BPS Guide to PHARMACOLOGY <http://www.guidetopharmacology.org> and are permanently archived in the Concise Guide to PHARMACOLOGY 2019/20 (Alexander et al., 2019).

3 | RESULTS

Basic pharmacokinetic parameters for abiraterone and cinacalcet after oral and intravenous dosing to rats as well as pharmacokinetic parameters after cycloheximide pre-treatment are summarized in Tables 1 and 2. The corresponding pharmacokinetic profiles are shown in Figures 1 and 2.

Absolute oral bioavailability of abiraterone after administration of capsules was 7.0%. Cycloheximide pre-treatment significantly decreased both the rate and extent of absorption of abiraterone as indicated by threefold C_{max} decrease and a twofold AUC decrease. Although the mean half-life was approximately 2 h after both oral and intravenous administrations, it was apparently prolonged to 18 h in the cycloheximide pre-treated group.

Absolute oral bioavailability of cinacalcet was 28.7% (pharmacokinetic profile from the p.o. period of the bioavailability study not shown). Cinacalcet pharmacokinetic profile up to 12 h was substantially flattened by cycloheximide pre-treatment. From 12 h onwards, the mean serum concentration rose surprisingly to its maximum at the last sampling point at 24 h. This pattern was seen consistently in all animals after pre-treatment with cycloheximide. The mean C_{max} values were similar between the periods; however, T_{max} was significantly delayed after cycloheximide pre-treatment.

Tissue cinacalcet concentrations after oral dosing with and without cycloheximide pre-treatment are shown in Supporting Information S1. Particularly high concentrations were observed in the

TABLE 1 Mean \pm SD pharmacokinetic parameters of abiraterone after oral administration of capsule (4 mg) to rats with or without cycloheximide (CHX) pre-treatment and mean \pm SD pharmacokinetic parameters of abiraterone after intravenous administration (1 mg kg⁻¹)

	p.o. (n = 8)	p.o. + CHX (n = 6)	i.v. (n = 5)
C_{max} (ng ml ⁻¹)	4.2 \pm 2.4	1.4 \pm 1.0*	N/A
T_{max} (h)	2.9 \pm 0.8	3.5 \pm 1.1	N/A
$T_{1/2}$ (h)	1.9 \pm 0.7	17.9 \pm 12.6*	2.1 \pm 1.0
AUC_{0-7} (ng h ml ⁻¹)	12.3 \pm 5.5	5.5 \pm 4.3*	197.8 \pm 24.4
V_{ss} (L kg ⁻¹)	N/A	N/A	3.7 \pm 0.5

Note: All concentration and AUC values are dose normalized (1 mg kg⁻¹).

* $P < 0.05$ versus p.o. dosing.

	Cycloheximide study (n = 8)		Bioavailability study (n = 6)	
	p.o.	p.o. + CHX	p.o.	i.v.
C_{max} (ng ml ⁻¹)	5.2 \pm 1.2	4.6 \pm 1.8	21.7 \pm 5.6	N/A
T_{max} (h)	10.0 \pm 2.6	24.2 \pm 0.1*	6.8 \pm 2.7	N/A
$T_{1/2}$ (h)	4.8 \pm 0.3	N/A	2.7 \pm 0.3	6.8 \pm 3.3
AUC_{0-12} (ng h ml ⁻¹)	36.3 \pm 6.7	10.9 \pm 4.5*	137.3 \pm 38.1	514 \pm 117
AUC_{0-24} (ng h ml ⁻¹)	66.6 \pm 12.3	46.2 \pm 14.4*	196.9 \pm 62.8	633 \pm 200
V_{ss} (L kg ⁻¹)	N/A	N/A	N/A	11.6 \pm 5.1

Note: All concentration and AUC values are dose normalized (1 mg kg⁻¹). $T_{1/2}$ was not estimated in the cycloheximide profile due to increasing concentrations towards the last sampling in all subjects.

* $P < 0.05$ versus p.o. dosing.

TABLE 2 Mean \pm SD pharmacokinetic parameters of cinacalcet after oral administration of oil solution (3 mg) to rats with or without cycloheximide (CHX) pre-treatment and mean \pm SD pharmacokinetic parameters of cinacalcet after intravenous administration (1 mg kg⁻¹)

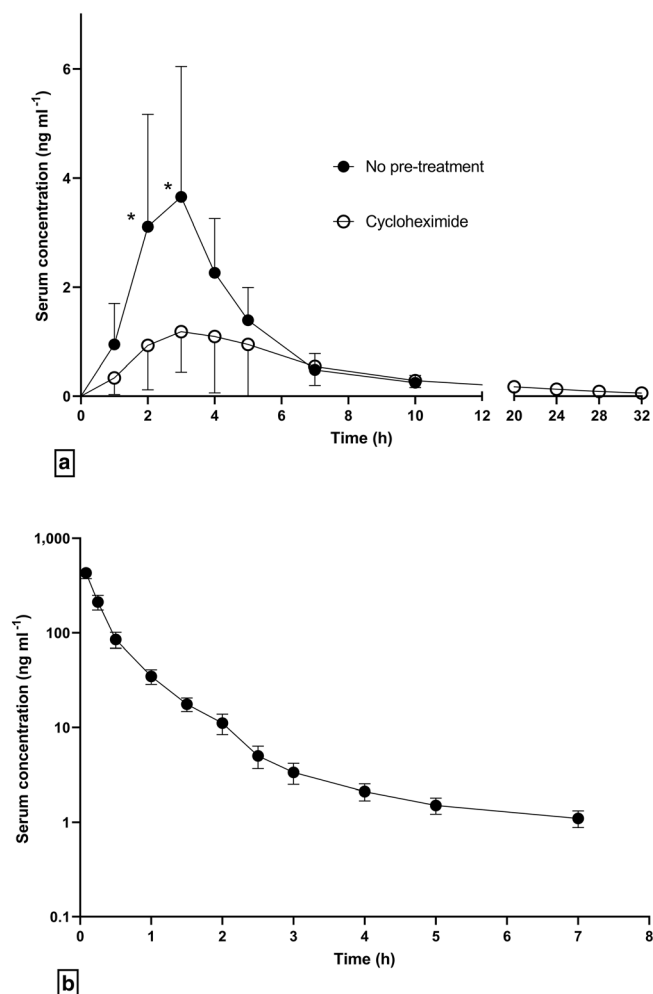


FIGURE 1 Dose normalized abiraterone serum pharmacokinetic profiles. (a) Mean \pm SD pharmacokinetic profiles of abiraterone administered orally to rats as capsule (4 mg) with or without cycloheximide pre-treatment. Profiles are derived from one group of animals (two-period, crossover study design, cycloheximide given in the second period), $n = 8$. * $P < 0.05$ versus cycloheximide. (b) Mean \pm SD abiraterone pharmacokinetic profile after intravenous dosing (1 mg kg^{-1}), $n = 5$

intestinal wall and in the spleen. In animals without cycloheximide pre-treatment, the mean tissue drug concentrations in all organs dropped, following a maximum noted at 8 h sampling time. In the cycloheximide pre-treated rats, cinacalcet tissue level remained low in the first 24 h. It rose then and the peak concentration was achieved at 48 h in all investigated organs. There was no cinacalcet depot found responsible for the late serum concentration increase.

The rising concentrations pattern was confirmed in the extended pharmacokinetic study in a separate group of cycloheximide pre-treated rats (Supporting Information S1), where the late increase of serum cinacalcet concentrations started 20 h post-dose and the concentrations oscillated around maximum between approximately 24 and 48 h. Mean C_{max} and T_{max} were 9.1 ng ml^{-1} and 37.7 h, respectively. Thus, the plateau phase was comparably high to

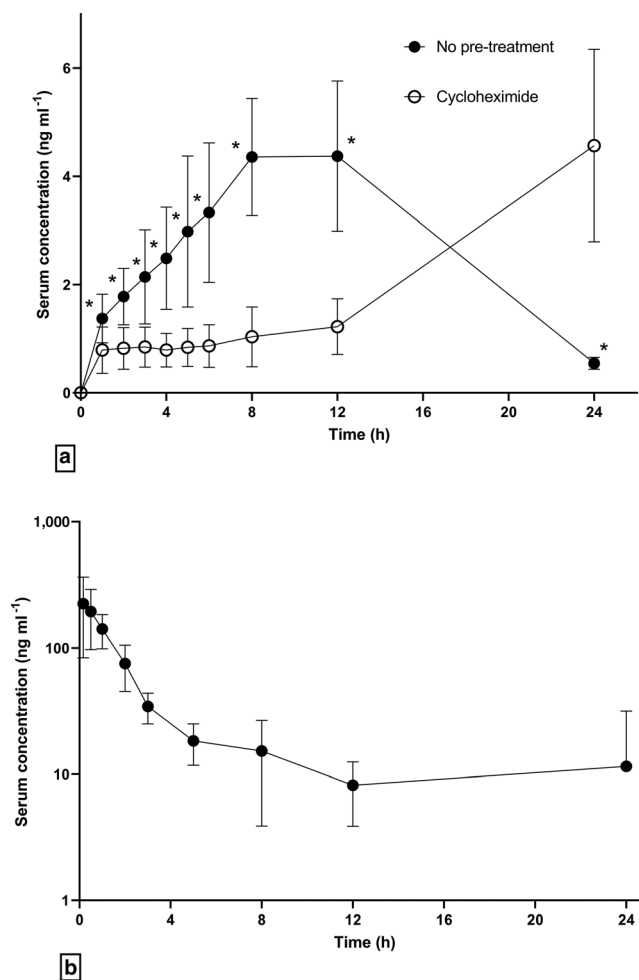


FIGURE 2 Dose normalized cinacalcet pharmacokinetic profiles. (a) Mean \pm SD pharmacokinetic profiles of cinacalcet administered orally to rats as oil solution (3 mg) with or without cycloheximide pre-treatment. Profiles are derived from one group of animals (two-period, crossover study design, cycloheximide given in the second period), $n = 8$. * $P < 0.05$ versus cycloheximide. (b) Mean \pm SD cinacalcet pharmacokinetic profile after intravenous dosing (1 mg kg^{-1}), $n = 6$

cinacalcet C_{max} value observed in animals with no pre-treatment. Mean AUC at 12, 24 and 48 h was 16.5, 43.8 and $179.5 \text{ ng h ml}^{-1}$, respectively.

Lymphatic concentration profiles and cumulative lymphatic transport of abiraterone and cinacalcet in lymph duct cannulated rats are displayed in Figures 3 and 4. Drug concentrations achieved in the lymph were considerably higher (two orders) compared to serum concentrations after oral dosing for both drugs. Mean dose normalized lymphatic C_{max} was 434 ng ml^{-1} for abiraterone and $1,180 \text{ ng ml}^{-1}$ for cinacalcet. The cumulative lymphatic transport curve had a sigmoidal shape in both drugs with slower absorption onset and faster intermediate transport which later decelerated. Cycloheximide pre-treatment in the lymph duct cannulated rats severely inhibited both lymphatic transport and portal absorption of cinacalcet (Figure 4).

Table 3 presents parameters of lymphatic transport for abiraterone and cinacalcet obtained via cannulation and cycloheximide chylomicron flow blocking methods. Absolute and relative bioavailability via lymph assessed using cannulation method was lower for abiraterone than for cinacalcet. Absorption of abiraterone did not increase after administration of abiraterone acetate in the form of oil solution in a separate experiment (Supporting Information S2). The absorption from abiraterone oil solution resulted in mean total absolute bioavailability of 1.7%, absolute bioavailability via lymph of 0.1% and relative bioavailability via lymph of 4.0% (at 7 h).

Cycloheximide chylomicron flow blocking method significantly overestimated the parameters of lymphatic transport for both drugs except for cinacalcet absolute bioavailability via lymph, for which the twofold higher mean value versus cannulation method did not reach statistical significance. The difference between the methods was particularly high in the estimation of relative bioavailability via lymph

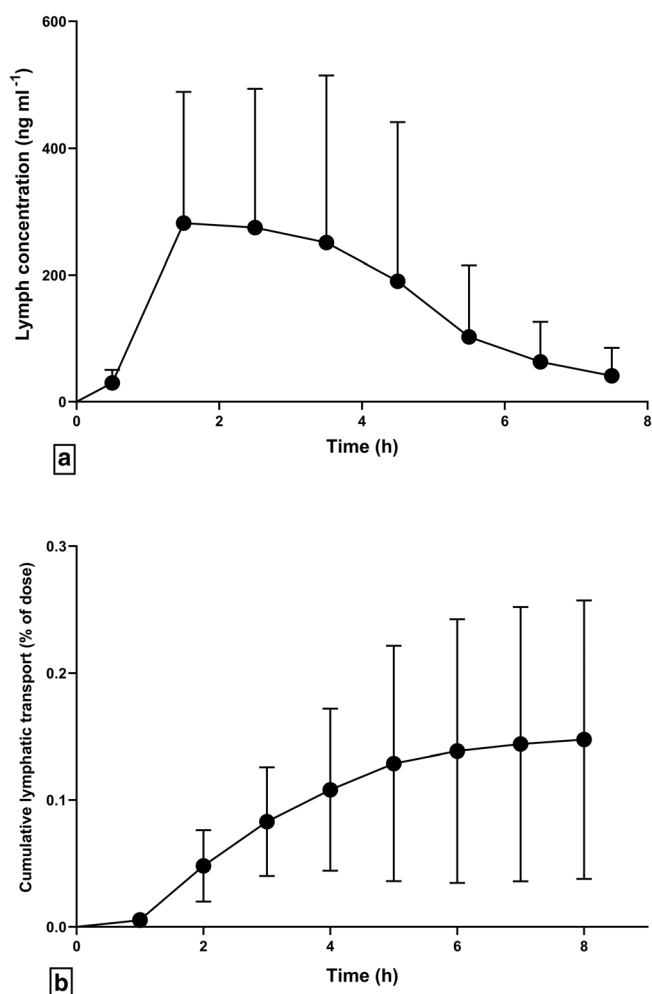


FIGURE 3 Lymphatic transport of abiraterone after enteral administration of abiraterone capsule (4 mg) to lymph duct cannulated anaesthetised rats, $n = 6$. (a) Mean \pm SD dose normalized lymph concentration profile; (b) mean \pm SD cumulative lymphatic transport

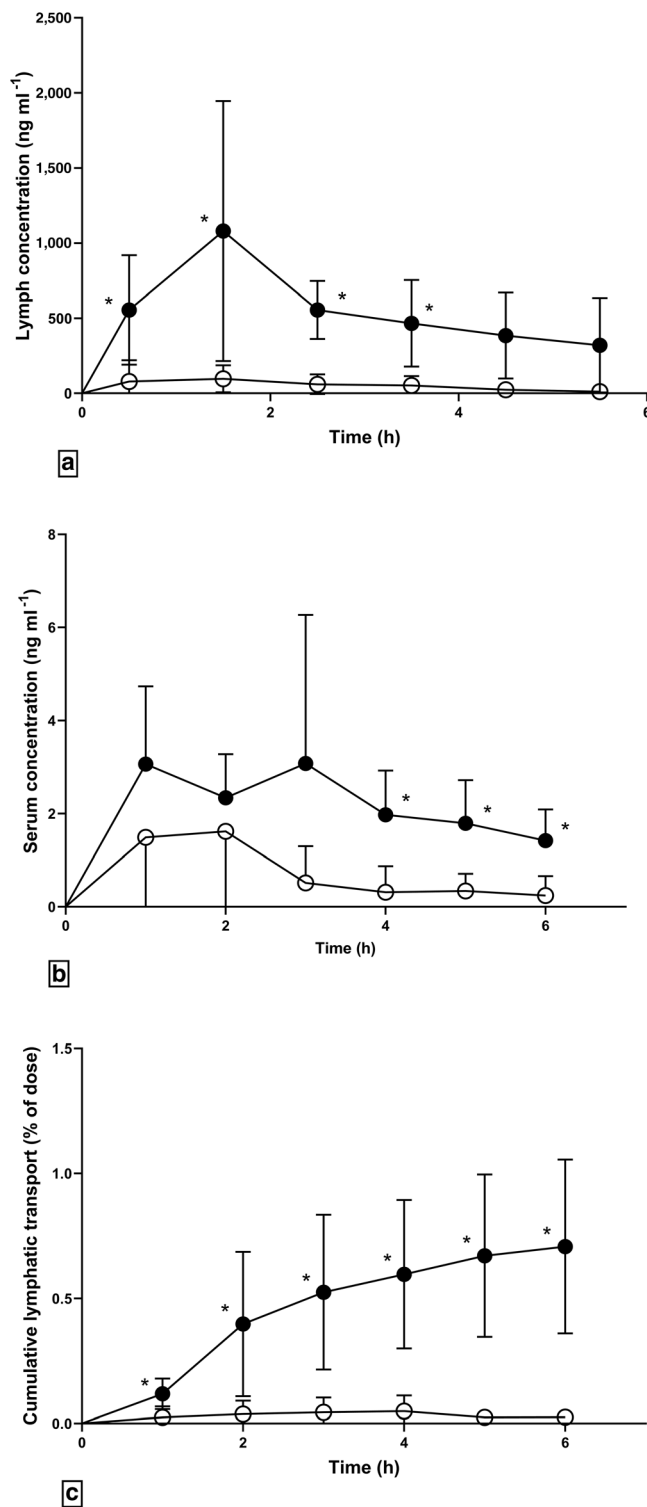


FIGURE 4 Lymphatic transport and portal absorption of cinacalcet after enteral administration of cinacalcet (3 mg) oil solution to lymph duct cannulated anaesthetised rats (closed circles, $n = 6$) and to lymph duct cannulated anaesthetised and cycloheximide pre-treated rats (open circles, $n = 5$). (a) Mean \pm SD dose normalized lymph concentration profiles; (b) mean \pm SD dose normalized serum concentration profiles; (c) mean \pm SD cumulative lymphatic transport. * $P < 0.05$ versus cycloheximide group

TABLE 3 Mean \pm SD lymphatic transport parameters of abiraterone and cinacalcet after oral and duodenal administration of abiraterone capsule and cinacalcet oil solution assessed by lymph duct cannulation in anaesthetised rats and by cycloheximide chylomicron flow blocking method

	Method	n	Time (h)	F (%)	F _{AL} (%)	F _{RL} (%)
Abiraterone capsules	Cannulation	5	7.0	21.1 \pm 22.0	0.15 \pm 0.11	2.0 \pm 2.1
	Cycloheximide	6	7.0	6.8 \pm 3.0	4.1 \pm 3.0*	56.4 \pm 28.6*
Cinacalcet oil solution	Cannulation	6	6.0	3.7 \pm 1.6	0.71 \pm 0.35	21.0 \pm 8.4
	Cycloheximide	8	6.0	2.3 \pm 0.8*	1.4 \pm 0.9	57.5 \pm 21.8*

Abbreviations: F, total absolute bioavailability; F_{AL}, absolute bioavailability via lymph; F_{RL}, relative bioavailability via lymph.

*P < 0.05 versus cannulation method.

where cycloheximide method showed 28-fold higher value for abiraterone and 2.7-fold higher value for cinacalcet compared with cannulation method.

4 | DISCUSSION

Abiraterone serum pharmacokinetic parameters after oral and intravenous administration obtained in the current study correspond with previously published data (Gurav et al., 2012). Its low oral bioavailability (<10%) has been confirmed in intact animals and the value is very similar to the previously reported absolute bioavailability of 4.1% (Gurav et al., 2012). In lymph duct cannulated animals, the total absolute bioavailability was higher which could correspond with olive oil premedication as opposed to fasted state in the bioavailability study.

Absolute bioavailability of cinacalcet after oral administration in rats has not been previously reported. Although the oral bioavailability of 29% observed in our study is less compared to the 80% bioavailability reported in man, it corresponds to the range of 35–69% seen in animal mass balance studies in other species (G. N. Kumar et al., 2004). Oil solution administered in our study resulted in approximately two times longer T_{max} compared with previous study in rats receiving cinacalcet in aqueous drug dosing forms (Kuijpers, 2004).

Lymphatic transport of abiraterone administered as capsules was low in lymph duct cannulated rats despite achieving approximately 100 times higher lymphatic concentrations compared with serum. Long chain triglycerides present in the drug formulation or in the food ingested concurrently with the drug administration are inevitable for a significant extent of lymphatic transport (Han, Hu, Quach, Simpson, Trevaskis, & Porter, 2016b; Khoo et al., 2003). Therefore, abiraterone oil solution was tested in a separate study, but its oral bioavailability decreased compared to capsules, although the relative bioavailability via lymph was approximately twice as high. We assume that the main factor limiting lymphatic transport of abiraterone is its insufficient lipophilicity. There is strong evidence that lymphatic transport contributes significantly ($F_{RL} > 10\%$) to the drug absorption only in compounds with $\log P > 5$ (Charman & Stella, 1986). $\log P$ value of abiraterone predicted by multiple calculation algorithms (ChemAxon, ALOGPS, PubChem) is approximately 4.5. Hence, it is relatively close

under the cut point, which also corresponds to the 'borderline' lymphatic transport (F_{RL} of several %). Other molecules with similar $\log P$ and known extent of lymphatic transport are [seocalcitol](#) ($\log P$ 4.8, F_{RL} 7.4%) and [ontazolast](#) ($\log P$ 4.0, F_{RL} 6.8%) with comparable results (Grove et al., 2006; Hauss et al., 1998).

Both absolute and relative bioavailability via lymph increase with increasing bodyweight of animal species tested (dog > rat > mouse; Trevaskis et al., 2013). Using recently published allometric scaling formulas (Trevaskis et al., 2020), abiraterone F_{AL} in humans could be expected approximately fourfold higher than in rats, meaning 0.60% for the capsule formulation. Given the low absolute bioavailability, this could result in F_{RL} of 10–15% in men. Therefore, other factors than lymphatic transport seem to be more important for the extremely pronounced positive food effect on intestinal absorption of abiraterone, such as intraluminal solubilization in the presence of lipids and bile after food intake (Schultz et al., 2020) or enhanced supersaturation in the gastrointestinal fluids, which seems to be the driving factor for the drug absorption as reported *in vitro* (Stappaerts et al., 2015).

Cinacalcet lymphatic transport was shown to play a significant role in the intestinal drug absorption in our cannulation study. The results fit into the range of reported lymphatic transport parameters for compounds with similar lipophilicity while being close to those of [venetoclax](#) ($\log P$ 6.9, F_{RL} 18.8%; Choo et al., 2014). Predicted human F_{AL} of 2.8% and F_{RL} of ~50% calculated according to the allometric scaling formulas mentioned above suggest that lymphatic transport is highly relevant for cinacalcet absorption and it also likely contributes to the known food effect in humans.

Cycloheximide chylomicron flow blocking method has been used extensively in the last few years in the development of new drug formulations and investigation of their lymphatic transport. During the last 5 years, 46% of studies focusing on lymphatic drug transport applied the cycloheximide method (Rysanek et al., 2020). The main reason for its popularity is that the method does not require advanced surgical skills compared with the delicate lymph duct cannulation. Furthermore, it is inexpensive and overall easy to conduct. However, as the results of our current comparability studies demonstrate, cycloheximide method substantially overestimates lymphatic transport. It provided significantly higher F_{RL} values for both tested drugs when

compared to cannulation method. The overestimation was more pronounced in the less lipophilic abiraterone than in cinacalcet.

The lipophilicity dependent extent of overestimation seems to well correspond with the results published so far, where cycloheximide method yielded comparable lymphatic transport parameters to cannulation in highly lipophilic cholecalciferol (log P 7.5; Dahan & Hoffman, 2005) and halofantrine (log P 8.9; Lind et al., 2008). On the other hand, there are suspicious data for drugs with low lipophilicity that are not likely to be significantly transported through intestinal lymph vessels. Exorbitantly high lymphatic transport parameters have been reported for **topotecan** (log P 0.8, F_{RL} 53% for aqueous dosing solution; Wang et al., 2017), **docetaxel** (log P 2.4, F_{RL} 91%; Valicherla et al., 2016) and **paclitaxel** (log P 3, F_{RL} 60%; Zhang et al., 2016). Some of these unusually high lymphatic transport results have been attributed by the authors to the properties of the advanced drug formulations that should target and enhance lymphatic transport. However, the reliability of these data is questioned by the comparability evidence provided in our study and the performance of the advanced drug formulations supported solely by the cycloheximide chylomicron flow blocking method is uncertain.

Analysis of the limited amount of comparability data between cycloheximide and cannulation methods provided relationship between lipophilicity and the extent of F_{RL} overestimation in the cycloheximide method (Supporting Information S3). The reason why the lymphatic transport of less lipophilic drugs seems to be more overestimated by the cycloheximide method may lie in the proportion of inhibition of different ways involved in the drug absorption. In the combined cycloheximide/cannulation study, cycloheximide was shown to have deleterious effect both on lymphatic and non-lymphatic ways of cinacalcet absorption.

Another fact is that mean AUC decrease of abiraterone and cinacalcet after cycloheximide administration was 56% and 57%, respectively, that is, absorption and total bioavailability of both drugs were impaired similarly. Hence, the degree of F_{RL} overestimation was derived from the real extent of lymphatic transport assessed by lymph exposure measurement which was minimal in abiraterone but considerable in cinacalcet. These results correspond to data from cycloheximide studies published so far where there is no significant difference between cycloheximide induced AUC decrease ($\approx F_{RL}$) in compounds with log $P < 5$ and log $P > 5$ (median AUC decrease of 47.3% vs. 70.7%, $P > 0.05$; Rysanek et al., 2020). In this regard, the overestimation effect of cycloheximide method is inversely related to the real extent of lymphatic transport assessed in lymph duct cannulated animals, which is generally low in compounds with log $P < 5$ but can play a significant role in more lipophilic drugs.

It is evident that the effects of cycloheximide are complex. We observed rather unusual pattern of cinacalcet serum/tissue concentration increase in cycloheximide pre-treated animals that started approximately 20 h after the drug dosing. This pattern was consistent across all three experiments and was also apparent in all animals studied. Scanning the literature, such an increase was also seen in halofantrine, where the authors assumed there would be a depot from which the drug would later be released (Lind et al., 2008). Respecting

the proposed cycloheximide mechanism of action (inhibition of intestinal chylomicron assembly), we hypothesized that this depot could be formed in the intestinal wall. However, this hypothesis was not supported by our biodistribution study results. Cinacalcet levels in the intestinal wall followed similar pattern to other organs or serum with no signs of early drug accumulation and subsequent release. We assume therefore that the late increase in cinacalcet concentrations was primarily due to delayed absorption from gastrointestinal lumen that was caused by severely reduced gastrointestinal motility, although possible contribution of impaired elimination by cycloheximide cannot be ruled out based on our data.

Previous *in vivo* cycloheximide studies have indeed shown multiple negative effects on gastrointestinal tract including delayed gastric emptying, reduced gastric secretion, reduced intestinal motility and various histopathologic changes (Plattner et al., 2001; Verbin et al., 1971; Yeh & Shils, 1969a, 1969b). These reports are not in concordance with the report by Dahan and Hoffman (2005) on good cycloheximide tolerability. In our study, the health status of the animals in the cycloheximide arms was frequently deteriorating. Within 4 to 5 h after cycloheximide treatment, about half of the rats were apathic and had bristled fur or diarrhoea-like exudate. This is linked to the fact that the administered cycloheximide dose in the standard protocol for chylomicron flow blocking method is close to its known LD_{50} (3.7 mg kg⁻¹; Cycloheximide Safety Datasheet, 2019).

Moreover, for the molecules like cinacalcet (and halofantrine), in which cycloheximide causes delayed and long-lasting increase of serum concentrations, the estimates of AUC and thus bioavailability strongly depend on the timeframe over which the study is conducted. The absorption was not only delayed but also significantly enhanced by cycloheximide if the pharmacokinetic profiles were measured well beyond the usual timeframe. Even 48 h after a single cinacalcet dose, the absorption phase was not completed, which indicates that the model lacks physiological relevance for absorption studies.

5 | CONCLUSION

Non-invasive cycloheximide chylomicron flow blocking method does not provide correct and reliable estimate on lymphatic transport of drugs and therefore should not be used to address this process of drug absorption anymore. The cycloheximide method largely overestimates the true lymphatic absorption measured directly as drug exposure in lymph collection.

Comparison of lymphatic transport data generated by direct drug concentration measurements in lymph collection and cycloheximide chylomicron flow method in rats has been conducted for two modern highly lipophilic compounds, that is, abiraterone acetate and cinacalcet hydrochloride. Whereas the lymphatic transport in direct measurement was shown to play a significant role in the intestinal absorption of cinacalcet, lymphatic transport of abiraterone was low. Absolute bioavailability following oral dosing of both drugs has also been described.

ACKNOWLEDGEMENTS

This work was supported by the Charles University (Univerzita Karlova v Praze) Project Progres Q25, grant No. SVV 260 523 and Charles University Research Centre program no. UNCE/SCI/014. PR, JR, JK and TB wish to acknowledge the support provided by Pharmaceutical Applied Research Centre (The Parc) for their scientific work.

AUTHOR CONTRIBUTIONS

PR, MŠ and OS were responsible for study design, study conduct, data analysis and manuscript writing. TB, JB and FŠ prepared the drug dosing forms. TG, PL and JP performed the animal surgery. JR, JK and NKC conducted the study. PK and TK were responsible for bioanalysis.

CONFLICT OF INTEREST

The authors declare no conflict of interest.

DECLARATION OF TRANSPARENCY AND SCIENTIFIC RIGOUR

This declaration acknowledges that this paper adheres to the principles for transparent reporting and scientific rigour of preclinical research as stated in the BJP guidelines for [Design and Analysis](#) and [Animal Experimentation](#), and as recommended by funding agencies, publishers and other organizations engaged with supporting research.

DATA AVAILABILITY STATEMENT

All data generated during the study are available from the corresponding author upon reasonable request.

ORCID

Pavel Ryšánek  <https://orcid.org/0000-0001-6727-1663>

Martin Šíma  <https://orcid.org/0000-0002-6541-738X>

REFERENCES

- Alexander, S. P. H., Kelly, E., Mathie, A., Peters, J. A., Veale, E. L., Armstrong, J. F., Faccenda, E., Harding, S. D., Pawson, A. J., Sharman, J. L., Southan, C., Buneman, O. P., Cidlowski, J. A., Christopoulos, A., Davenport, A. P., Fabbro, D., Spedding, M., Striessnig, J., Davies, J. A., ... Wong, S. S. (2019). The concise guide to pharmacology 2019/20: Introduction and other protein targets. *British Journal of Pharmacology*, 176, S1–S20. <https://doi.org/10.1111/bph.14747>
- Boleslavská, T., Rycheký, O., Krov, M., Žvátora, P., Dammer, O., Beránek, J., Kozlík, P., Křížek, T., Hořínková, J., Ryšánek, P., Roušarová, J., Canová, N. K., Šíma, M., Slanař, O., & Štěpánek, F. (2020). Bioavailability enhancement and food effect elimination of abiraterone acetate by encapsulation in surfactant-enriched oil marbles. *The AAPS Journal*, 22(6), 122. <https://doi.org/10.1208/s12248-020-00505-5>
- Boleslavská, T., Světlík, S., Žvátora, P., Bosák, J., Dammer, O., Beránek, J., Kozlík, P., Křížek, T., Kutinová Canová, N., Šíma, M., Slanař, O., & Štěpánek, F. (2020). Preclinical evaluation of new formulation concepts for abiraterone acetate bioavailability enhancement based on the inhibition of pH-induced precipitation. *European Journal of Pharmaceutics and Biopharmaceutics*, 151, 81–90. <https://doi.org/10.1016/j.ejpb.2020.04.005>
- Caliph, S. M., Charman, W. N., & Porter, C. J. (2000). Effect of short-, medium-, and long-chain fatty acid-based vehicles on the absolute oral bioavailability and intestinal lymphatic transport of halofantrine and assessment of mass balance in lymph-cannulated and non-cannulated rats. *Journal of Pharmaceutical Sciences*, 89(8), 1073–1084. [https://doi.org/10.1002/1520-6017\(200008\)89:8<1073::aid-jps12>3.0.co;2-v](https://doi.org/10.1002/1520-6017(200008)89:8<1073::aid-jps12>3.0.co;2-v)
- Charman, W. N. A., & Stella, V. J. (1986). Estimating the maximal potential for intestinal lymphatic transport of lipophilic drug molecules. *International Journal of Pharmaceutics*, 34(1–2), 175–178. [https://doi.org/10.1016/0378-5173\(86\)90027-X](https://doi.org/10.1016/0378-5173(86)90027-X)
- Chi, K. N., Spratlin, J., Kollmannsberger, C., North, S., Pankras, C., Gonzalez, M., Bernard, A., Stieltjes, H., Peng, L., Jiao, J., Acharya, M., Kheoh, T., Griffin, T. W., Yu, M. K., Chien, C., & Tran, N. P. (2015). Food effects on abiraterone pharmacokinetics in healthy subjects and patients with metastatic castration-resistant prostate cancer. *Journal of Clinical Pharmacology*, 55(12), 1406–1414. <https://doi.org/10.1002/jcph.564>
- Choo, E. F., Boggs, J., Zhu, C., Lubach, J. W., Catron, N. D., Jenkins, G., Souers, A. J., & Voorman, R. (2014). The role of lymphatic transport on the systemic bioavailability of the Bcl-2 protein family inhibitors navitoclax (ABT-263) and ABT-199. *Drug Metabolism and Disposition*, 42(2), 207–212. <https://doi.org/10.1124/dmd.113.055053>
- Cycloheximide Safety Datasheet. (2019). Retrieved from <https://www.caymanchem.com/msdss/14126m.pdf>
- Dahan, A., & Hoffman, A. (2005). Evaluation of a chylomicron flow blocking approach to investigate the intestinal lymphatic transport of lipophilic drugs. *European Journal of Pharmaceutical Sciences*, 24(4), 381–388. <https://doi.org/10.1016/j.ejps.2004.12.006>
- Grove, M., Nielsen, J. L., Pedersen, G. P., & Mullertz, A. (2006). Bioavailability of seocalcitol IV: Evaluation of lymphatic transport in conscious rats. *Pharmaceutical Research*, 23(11), 2681–2688. <https://doi.org/10.1007/s11095-006-9109-z>
- Gurav, S., Punde, R., Farooqui, J., Zainuddin, M., Rajagopal, S., & Mullangi, R. (2012). Development and validation of a highly sensitive method for the determination of abiraterone in rat and human plasma by LC-MS/MS-ESI: Application to a pharmacokinetic study. *Biomedical Chromatography*, 26(6), 761–768. <https://doi.org/10.1002/bmc.1726>
- Han, S., Hu, L., Quach, T., Simpson, J. S., Edwards, G. A., Trevaskis, N. L., & Porter, C. J. (2016a). Lymphatic transport and lymphocyte targeting of a triglyceride mimetic prodrug is enhanced in a large animal model: Studies in greyhound dogs. *Molecular Pharmaceutics*, 13(10), 3351–3361. <https://doi.org/10.1021/acs.molpharmaceut.6b00195>
- Han, S., Hu, L., Quach, T., Simpson, J. S., Trevaskis, N. L., & Porter, C. J. H. (2016b). Constitutive triglyceride turnover into the mesenteric lymph is unable to support efficient lymphatic transport of a biomimetic triglyceride prodrug. *Journal of Pharmaceutical Sciences*, 105(2), 786–796. <https://doi.org/10.1002/jps.24670>
- Hauss, D. J., Fogal, S. E., Ficorilli, J. V., Price, C. A., Roy, T., Jayaraj, A. A., & Keirns, J. J. (1998). Lipid-based delivery systems for improving the bioavailability and lymphatic transport of a poorly water-soluble LTB4 inhibitor. *Journal of Pharmaceutical Sciences*, 87(2), 164–169. <https://doi.org/10.1021/js970300n>
- Holm, R., Porter, C. J., Mullertz, A., Kristensen, H. G., & Charman, W. N. (2002). Structured triglyceride vehicles for oral delivery of halofantrine: Examination of intestinal lymphatic transport and bioavailability in conscious rats. *Pharmaceutical Research*, 19(9), 1354–1361. <https://doi.org/10.1023/a:1020311127328>
- Khoo, S. M., Edwards, G. A., Porter, C. J. H., & Charman, W. N. (2001). A conscious dog model for assessing the absorption, enterocyte-based metabolism, and intestinal lymphatic transport of halofantrine. *Journal of Pharmaceutical Sciences*, 90, 1599–1607. <https://doi.org/10.1002/jps.1110>
- Khoo, S. M., Shackelford, D. M., Porter, C. J., Edwards, G. A., & Charman, W. N. (2003). Intestinal lymphatic transport of halofantrine

- occurs after oral administration of a unit-dose lipid-based formulation to fasted dogs. *Pharmaceutical Research*, 20(9), 1460–1465. <https://doi.org/10.1023/a:1025718513246>
- Kuijpers, G. (2004). Pharmacology and toxicology review of NDA (Application number 21–688).
- Kumar, G. N., Sproul, C., Poppe, L., Turner, S., Gohdes, M., Ghorah, H., Padhi, D., & Roskos, L. (2004). Metabolism and disposition of calcimimetic agent cinacalcet HCl in humans and animal models. *Drug Metabolism and Disposition*, 32(12), 1491–1500. <https://doi.org/10.1124/dmd.104.000604>
- Kumar, S. V., Rudresha, G., Gurav, S., Zainuddin, M., Dewang, P., Kethiri, R. R., Rajagopal, S., & Mullangi, R. (2013). Validated RP-HPLC/UV method for the quantitation of abiraterone in rat plasma and its application to a pharmacokinetic study in rats. *Biomedical Chromatography*, 27(2), 203–207. <https://doi.org/10.1002/bmc.2776>
- Lilley, E., Stanford, S. C., Kendall, D. E., Alexander, S. P., Cirino, G., Docherty, J. R., George, C. H., Insel, P. A., Izzo, A. A., Ji, Y., Panettieri, R. A., Sobey, C. G., Stefanska, B., Stephens, G., Teixeira, M., & Ahluwalia, A. (2020). ARRIVE 2.0 and the *British Journal of Pharmacology*: Updated guidance for 2020. *British Journal of Pharmacology*, 177, 3611–3616. <https://doi.org/10.1111/bph.15178>
- Lind, M. L., Jacobsen, J., Holm, R., & Mullertz, A. (2008). Intestinal lymphatic transport of halofantrine in rats assessed using a chylomicron flow blocking approach: The influence of polysorbate 60 and 80. *European Journal of Pharmaceutical Sciences*, 35(3), 211–218. <https://doi.org/10.1016/j.ejps.2008.07.003>
- Padhi, D., Salfi, M., & Harris, R. Z. (2007). The pharmacokinetics of cinacalcet are unaffected following consumption of high- and low-fat meals. *American Journal of Therapeutics*, 14(3), 235–240. <https://doi.org/10.1097/01.mjt.0000212703.71625.26>
- Percie du Sert, N., Hurst, V., Ahluwalia, A., Alam, S., Avey, M. T., Baker, M., Browne, W. J., Clark, A., Cuthill, I. C., Dirnagl, U., Emerson, M., Garner, P., Holgate, S. T., Howells, D. W., Karp, N. A., Lalic, S. E., Lidster, K., MacCallum, C. J., Macleod, M., ... Würbel, H. (2020). The ARRIVE guidelines 2.0: Updated guidelines for reporting animal research. *British Journal of Pharmacology*, 177(16), 3617–3624. <https://doi.org/10.1111/bph.15193>
- Plattner, V., Leray, V., Leclair, M. D., Aube, A. C., Cherbut, C., & Galmiche, J. P. (2001). Interleukin-8 increases acetylcholine response of rat intestinal segments. *Alimentary Pharmacology & Therapeutics*, 15(8), 1227–1232. <https://doi.org/10.1046/j.1365-2036.2001.01009.x>
- Porter, C. J., Trevaskis, N. L., & Charman, W. N. (2007). Lipids and lipid-based formulations: Optimizing the oral delivery of lipophilic drugs. *Nature Reviews. Drug Discovery*, 6(3), 231–248. <https://doi.org/10.1038/nrd2197>
- Rysanek, P., Grus, T., Sima, M., & Slanar, O. (2020). Lymphatic transport of drugs after intestinal absorption: Impact of drug formulation and physicochemical properties. *Pharmaceutical Research*, 37(9), 166. <https://doi.org/10.1007/s11095-020-02858-0>
- Schultz, H. B., Meola, T. R., Thomas, N., & Prestidge, C. A. (2020). Oral formulation strategies to improve the bioavailability and mitigate the food effect of abiraterone acetate. *International Journal of Pharmaceutics*, 577, 119069. <https://doi.org/10.1016/j.ijpharm.2020.119069>
- Shackleford, D. M., Faassen, W. A., Houwing, N., Lass, H., Edwards, G. A., Porter, C. J., & Charman, W. N. (2003). Contribution of lymphatically transported testosterone undecanoate to the systemic exposure of testosterone after oral administration of two andriol formulations in conscious lymph duct-cannulated dogs. *The Journal of Pharmacology and Experimental Therapeutics*, 306(3), 925–933. <https://doi.org/10.1124/jpet.103.052522>
- Stappaerts, J., Geboers, S., Snoeys, J., Brouwers, J., Tack, J., Annaert, P., & Augustijns, P. (2015). Rapid conversion of the ester prodrug abiraterone acetate results in intestinal supersaturation and enhanced absorption of abiraterone: In vitro, rat in situ and human in vivo studies. *European Journal of Pharmaceutics and Biopharmaceutics*, 90, 1–7. <https://doi.org/10.1016/j.ejpb.2015.01.001>
- Trevaskis, N. L., Caliph, S. M., Nguyen, G., Tso, P., Charman, W. N., & Porter, C. J. (2013). A mouse model to evaluate the impact of species, sex, and lipid load on lymphatic drug transport. *Pharmaceutical Research*, 30(12), 3254–3270. <https://doi.org/10.1007/s11095-013-1000-0>
- Trevaskis, N. L., Hu, L., Caliph, S. M., Han, S., & Porter, C. J. (2015). The mesenteric lymph duct cannulated rat model: Application to the assessment of intestinal lymphatic drug transport. *Journal of Visualized Experiments*, 97, e52389. <https://doi.org/10.3791/52389>
- Trevaskis, N. L., Lee, G., Escott, A., Phang, K. L., Hong, J., Cao, E., Katneni, K., Charman, S. A., Han, S., Charman, W. N., Phillips, A. R. J., Windsor, J. A., & Porter, C. J. H. (2020). Intestinal lymph flow, and lipid and drug transport scale allometrically from pre-clinical species to humans. *Frontiers in Physiology*, 11, 458. <https://doi.org/10.3389/fphys.2020.00458>
- Trevaskis, N. L., McEvoy, C. L., McIntosh, M. P., Edwards, G. A., Shanker, R. M., Charman, W. N., & Porter, C. J. (2010). The role of the intestinal lymphatics in the absorption of two highly lipophilic cholesterol ester transfer protein inhibitors (CP524,515 and CP532,623). *Pharmaceutical Research*, 27(5), 878–893. <https://doi.org/10.1007/s11095-010-0083-0>
- Valicherla, G. R., Dave, K. M., Syed, A. A., Riyazuddin, M., Gupta, A. P., Singh, A., Wahajuddin, Mitra, K., Datta, D., & Gayen, J. R. (2016). Formulation optimization of Docetaxel loaded self-emulsifying drug delivery system to enhance bioavailability and anti-tumor activity. *Scientific Reports*, 6, 26895. <https://doi.org/10.1038/srep26895>
- Verbin, R. S., Longnecker, D. S., Liang, H., & Farber, E. (1971). Some observations on the acute histopathologic effects of cycloheximide in vivo. *The American Journal of Pathology*, 62(1), 111–125.
- Wang, T., Shen, L., Zhang, Z., Li, H., Huang, R., Zhang, Y., & Quan, D. (2017). A novel core-shell lipid nanoparticle for improving oral administration of water soluble chemotherapeutic agents: Inhibited intestinal hydrolysis and enhanced lymphatic absorption. *Drug Delivery*, 24(1), 1565–1573. <https://doi.org/10.1080/10717544.2017.1386730>
- Yeh, S. D. J., & Shils, M. E. (1969a). Cycloheximide effect on vitamin B12 absorption and intrinsic factor production in the rat. *Proceedings of the Society for Experimental Biology and Medicine*, 130(4), 1260–1264. <https://doi.org/10.3181/00379727-130-33768>
- Yeh, S. D. J., & Shils, M. E. (1969b). Cycloheximide inhibition of gastric secretion in the rat. *Proceedings of the Society for Experimental Biology and Medicine*, 130(3), 807–810. <https://doi.org/10.3181/00379727-130-33660>
- Zhang, B., Xue, A., Zhang, C., Yu, J., Chen, W., & Sun, D. (2016). Bile salt liposomes for enhanced lymphatic transport and oral bioavailability of paclitaxel. *Pharmazie*, 71(6), 320–326. Retrieved from <https://www.ncbi.nlm.nih.gov/pubmed/27455550>

SUPPORTING INFORMATION

Additional supporting information may be found in the online version of the article at the publisher's website.

How to cite this article: Ryšánek, P., Grus, T., Lukáč, P., Kozlík, P., Křížek, T., Pozniak, J., Roušarová, J., Královičová, J., Kutinová Canová, N., Boleslavská, T., Bosák, J., Štěpánek, F., Šíma, M., & Slanar, O. (2021). Validity of cycloheximide chylomicron flow blocking method for the evaluation of lymphatic transport of drugs. *British Journal of Pharmacology*, 1–12. <https://doi.org/10.1111/bph.15644>



Application of Oil-in-Water Cannabidiol Emulsion for the Treatment of Rheumatoid Arthritis

Petr Jelínek,^{1,†} Jaroslava Roušarová,^{2,†} Pavel Ryšánek,² Martina Ježková,¹ Tereza Havlůjová,¹ Jiří Pozniak,³ Petr Kozlík,⁴ Tomáš Křížek,⁴ Tomáš Kučera,⁵ Martin Šíma,² Ondřej Slanař,² and Miroslav Šoós^{1,*}

Abstract

Introduction: Rheumatoid arthritis (RA) is a chronic autoimmune disease with unknown cause. It mainly affects joints and, without proper treatment, negatively impacts their movement, causes painful deformities, and reduces the patients' quality of life. Current treatment options consist of various types of disease-modifying anti-rheumatic drugs (DMARDs), however 20–30% of patients are partially resistant to them. Therefore, development of new drugs is necessary. Possible options are compounds exhibiting their action via endocannabinoid system, which plays an important role in pain and inflammation modulation. One such compound – cannabidiol (CBD) has already been shown to attenuate synovitis in animal model of RA in *in vivo* studies. However, it has low bioavailability due to its low water solubility and lipophilicity. This issue can be addressed by preparation of a lipid containing formulation targeting lymphatic system, another route of absorption in the body.

Materials and Methods: CBD-containing emulsion was prepared by high-shear homogenization and its droplet size distribution was analysed by optical microscopy. The relative oral bioavailability compared to oil solution as well as total availability of CBD were assessed in a cross-over study in rats and absorption of CBD via lymphatic system was observed. The effect of CBD on the animal model of RA was determined.

Results: Compared to oil solution, the emulsion exhibited higher absolute oral bioavailability. Significant lymphatic transport of CBD was observed in all formulations and the concentrations in lymph were calculated. The therapeutic effect of CBD on RA was confirmed as an improvement in clinical symptoms as well as morphological signs of disease activity were observed during the study.

Conclusion: In this work, we prepared a simple stable emulsion formulation, determined the pharmacokinetic parameters of CBD and calculated its absolute bioavailability in rats. Moreover, we successfully tested the pharmaceutical application of such a formulation and demonstrated the positive effect of CBD in an animal model of RA.

Keywords: rheumatoid arthritis; cannabidiol; emulsion; *in vivo* study; bioavailability; lymphatic absorption

Introduction

Rheumatoid arthritis (RA) is a chronic autoimmune inflammatory disease affecting mainly small joints, but it can also spread to other tissues and organs; for example, skin, lungs, or heart. RA can progress into periarticular bone and cartilage damage resulting in debilitating deformities, significantly reducing quality of life. As RA

is a chronic disease with an unknown cause, the main therapeutic objective is to stop the progression of the disease and achieve sustained remission; that is, to reduce the pain and inflammation of affected joints, maximize their function, and prevent irreversible periarticular damage.¹

Current treatment options consist of synthetic, targeted synthetic, and biologic disease-modifying

¹Department of Chemical Engineering, Faculty of Chemical Engineering, University of Chemistry and Technology, Prague, Czech Republic.

²Institute of Pharmacology, First Faculty of Medicine, Charles University and General University Hospital in Prague, Prague, Czech Republic.

³Third Department of Surgery, First Faculty of Medicine, Charles University in Prague and Motol University Hospital, Prague, Czech Republic.

⁴Department of Analytical Chemistry, Faculty of Science, Charles University, Prague, Czech Republic.

⁵Institute of Histology and Embryology, First Faculty of Medicine, Charles University, Prague, Czech Republic.

[†]Equally contributing authors.

*Address correspondence to: Prof. MUDr. Ondřej Slanař, PhD, Institute of Pharmacology, First Faculty of Medicine, Charles University and General University Hospital in Prague, Kateřinská 32, Prague 121 08, Czech Republic, E-mail: ondrej.slanař@lf1.cuni.cz; Prof. Ing. Miroslav Šoós, PhD, Department of Chemical Engineering, Faculty of Chemical Engineering, University of Chemistry and Technology, Technická 1905/5, Prague 16628, Czech Republic, E-mail: miroslav.soos@vscht.cz

antirheumatic drugs (DMARDs), supplemented by glucocorticoids, nonsteroidal antirheumatic drugs, and analgesics for symptomatic treatment of pain and inflammation. However, the disease is rather heterogeneous, and a combination of DMARDs is often necessary for inducing remission and maintaining low disease activity. Although the introduction of biologics dramatically improved the prognosis of patients as well as therapeutic outcomes, there are still ~20–30% of patients partially resistant to current treatment options. Other downsides are high cost of biologic DMARDs and the need for parenteral administration. For this reason, new therapies are urgently needed.²

One group of candidate drugs with therapeutic potential for RA treatment are natural compounds exhibiting their action through the endocannabinoid system, which plays an important role in pain and inflammation modulation. There are two types of cannabinoid (CB) receptors. CB1 receptors, expressed mainly in the central nervous system, are responsible for neurobehavioral effects and nociceptive transmission in the brain.

The other type, CB2 receptors, found in immune cells, lymph nodes, and nodular corona of Peyer patches, plays an important role in immunomodulation and inflammatory pain response. The activation of CB2 receptors mediates immune cell suppression. It inhibits the production of proinflammatory cytokines, autoantibodies, and matrix metalloproteinases (MMPs). Furthermore, it suppresses the proliferation of fibroblast-like synoviocytes, NF κ B-dependent apoptotic responses, and T-helper-mediated functions.³

Cannabidiol (CBD), obtained from *Cannabis sativa*, is a promising nonpsychoactive compound affecting endocannabinoid system. CB are widely commercially available as food supplements, not only for humans but also for animals. CBD itself has been shown to attenuate synovitis and joint destruction in collagen-induced arthritis (CIA), an animal model of RA in *in vivo* studies.^{4,5}

Despite this, Epidiolex/Epidyolex, a solution of CBD and flavorings in sesame oil used to treat seizures in rare forms of epilepsy, and Sativex, oromucosal spray for spastic symptoms of multiple sclerosis, remain the only Food and Drug Administration- and European Medicines Agency (EMA)-approved oral drugs that contain CBD.⁶ This is because although CBD has high solubility in lipids and organic solvents, it is almost insoluble in water. Low water solubility leads to low bioavailability and subsequently noneffective plasma concentrations after oral administration. Nevertheless, there is a promising way to increase the absorption from the gastroin-

testinal tract by targeting another specific means of drug transport in the body; the lymphatic system.

Lymphatic transport is an important pharmacokinetic characteristic of numerous highly lipophilic compounds.⁷ Robust evidence suggests that only compounds with $\log p > 5$ have an inherent affinity toward intestinal lymph.^{8,9} The presence of drug in the lymph can have major pharmacokinetic and pharmacodynamic implications, as oral bioavailability increases due to higher absorption and circumvention of liver first-pass effect.

Furthermore, the lymphatic system plays an important role in immunomodulation due to presence of leukocytes in lymph and associated lymph nodes. Therefore, it is an important potential target for immunomodulatory drugs, and better treatment efficacy is expected. CBD with its high lipophilicity ($\log p$ 6.3), significant first-pass metabolism, and immunomodulatory effect is a suitable candidate to exploit all these advantages.¹⁰

Therefore, assessment of CBD lymphatic transport is of great importance for the pharmaceutical science. Zgair et al. have already reported a significant CBD concentration in mesenteric lymph (250 times higher compared with plasma) after the administration of the sesame oil formulation.¹¹ However, a precise and comprehensive quantification of CBD lymphatic transport assessing its absolute and relative contribution to overall systemic bioavailability is still lacking.

To enable lymphatic absorption, the presence of a lipidic excipient is necessary, as it helps solubilize the drug and mediates its association with chylomicrons.^{11,12} Therefore, most CBD-containing formulations used in *in vivo* studies are oil based.^{4,13,14} Emulsions, formulations consisting of both oil and aqueous phase, are tolerable, and another advantage is their enhanced surface area for absorption due to increase in droplet area, which can enhance bioavailability, as demonstrated by Francke et al¹⁵ for CBD-containing nanoemulsion. Despite this success, careful selection of excipients is crucial because different oil vehicles and surfactants can affect the bioavailability of CBs, and thus, the efficiency of RA treatment.¹⁶ Consequently, an appropriate combination of *in vitro* and *in vivo* investigations is essential for formulation optimization.

Based on the information discussed above, we prepared CBD microemulsion composed of surfactant-stabilized oil droplets dispersed in water. We determined its droplet size and tested coalescence stability. The main focus of this study was characterization of CBD pharmacokinetic parameters and therapeutic effect in the treatment of RA.

Materials and Methods

Chemicals

The following chemicals were used for the preparation of CBD formulations. CBD (98.9 wt %) was purchased from PharmaHemp® (Slovenia). Sunflower oil (standardized product of pharmaceutical quality) was purchased from Fagron a.s. (Czech Republic). L- α -Lecithin (soybean, >94% phosphatidylcholine) manufactured by Calbiochem® was purchased from Sigma-Aldrich (Germany). Capryol® PGMC and Transcutol® P were kindly donated by Gattefossé (France). Kolliphor® EL was purchased from BASF (Germany). Aqual® Ultrapur demineralized water was used for the preparation of the formulations.

Preparation of formulations containing CBD

The emulsion formulation for oral delivery composed of sunflower oil and water (1:4 wt ratio) was prepared by high-shear homogenization. First, CBD (112.5 mg) was dissolved in sunflower oil (3 g) in a glass vial using mild magnetic stirring. Then, lecithin (1.5 g) was added to the oil phase. Ultra-Turrax® T 25 (IKA; Germany) disperser with S25N-10G-ST dispersing tool was immersed in the vial with the CBD oil phase and lecithin. Approximately half of the aqueous phase fraction (12 g) was added to the mixture to reach the necessary immersion level of the dispersing tool.

The stirring speed was set to 15,000 rpm for 5 min, during which the rest of the aqueous phase was manually dripped into the vial using a syringe with long needle. After the high-shear homogenization, the emulsion was shaken for 1 min using a vortex mixer (Vortex mixer VV3, VWR) to eliminate the surface foam. The final concentration of CBD in the emulsion was 7.5 mg/mL. The oil solution, which was used as a reference with the same CBD concentration, was prepared by dissolution of CBD (24.4 mg) in sunflower oil (3 g) applying mild magnetic stirring.

The formulation for intravenous delivery was composed of CBD (60 mg), Capryol PGMC (0.4 g), Cremophor EL (1 g), Transcutol P (0.6 g), and distilled water up to the total volume of 6 mL. First, CBD was dissolved in the mixture of nonaqueous components. Then, water was added, and the concoction was stirred magnetically (900 rpm). The final concentration of CBD in the emulsion was 1 mg/100 μ L.

Optical microscopy and image analysis of the emulsion containing CBD

Optical microscopy was performed using a system composed of Resolv4K lenses (Navitar, the United States)

and Olympus (the United States) objective lenses connected to the high-speed camera PL-D725MU-T (Pixelink; Navitar). Emulsion droplet was placed between the support and cover glass slide. Image analysis was performed using software ImageJ (NIH, the United States). Maximum Feret diameters were calculated considering 500–600 oil droplets.

Animals

Wistar rats (300–450 g) were purchased from Velaz (Prague, Czech Republic). The rats were housed under standard conditions (temperature of $22 \pm 2^\circ\text{C}$, relative humidity of $50 \pm 10\%$, 12-h light–dark cycle). The animals had access to water and standard granulated diet *ad libitum*. All parts of experiment were carried out with respect to Guiding Principles for the Use of Animals at Charles University, First Faculty of Medicine. The permission for the experimental animal project was conferred by the Ministry of Education, Youth and Sports, Czech Republic (MSMT-26838/2021–4).

General anesthesia was induced using isoflurane (IsoFlo, 250 mL; Zoetis/Pfizer, Czech Republic), ketamine (Narkamon, 100 mg/mL, inj. Sol.; Bioveta, Ivanovice na Hané, Czech Republic), and xylazine (Rometa, 20 mg/mL, inj. Sol.; Bioveta). Heparin (Heparin Léčiva, inj. Sol., 1×10 mL/50 KU; Zentiva, Czech Republic), ketoprofen (Ketodolor, inj. Sol., 100 mL; LeVet Pharma b.v., Netherlands), and Carbethopendecinium bromide (Ophthalmo-Septonex, eye ointment, 1×5 g; Zentiva) were used in pursuance of the perioperative anticoagulant, analgesic, and antiseptic treatment, respectively.

Bovine type II collagen and incomplete Freund's adjuvant for arthritis induction were purchased from Chondrex. The combination of mebezonium iodide, embutramide, and tetracaine hydrochloride (T 61, inj. Sol.; Intervet International, B.V., Netherlands) was used for the euthanasia at the end of the experiment.

CBD bioavailability

To allow repeated blood sampling, a polyurethane catheter (3Fr; Intech Laboratories, Plymouth Meeting, the United States) was inserted into the external jugular vein 3 days before first dosing. The procedure was performed under general anesthesia using 2.5–5% isoflurane followed by 100 mg/kg of intramuscular ketamine and 5 mg/kg of intramuscular xylazine. At the end of the surgical procedure, 5 mg/kg ketoprofen was administered subcutaneously as an analgesic. The catheter was flushed with 200 μ L saline and 50 μ L heparin, and sealed with a combination of 20 μ L glycerol and heparin.

The relative oral bioavailability of CBD emulsion compared with simple oil solution was assessed in a randomized, single-dose, two-sequence, and two-period, laboratory-blinded, crossover bioequivalence study. Adult male rats were fasted with unrestricted access to water for 4 h before and after dosing. The administration of 1 mL (equivalent to 7.5 mg of CBD) of both the oil and emulsion formulation was conducted using oral gavage. Systemic blood samples (120 μ L) were collected predose (second period) and at 1, 2, 3, 4, 5, 6, 8, 10, and 24 h postdose (both periods) from the jugular vein catheter. Each blood sample was substituted with an equal volume of saline. The washout period between the first and the second dosing took 72 h.

In addition, another group of animals was dosed intravenously for the purpose of absolute bioavailability calculation of both formulations used in the bioequivalence study. For this experiment, both jugular veins were cannulated. CBD formulation (1 mg, 100 μ L) was administered into the left jugular vein. Blood samples were then drawn from the right jugular vein catheter at 5, 15, and 30 min and at 1, 2, 4, 6, and 10 h.

Blood samples were centrifuged for 10 min (2000 g, 4°C), and serum was extracted. Serum samples were stored at -80°C until analysis.

CBD lymphatic absorption

Anesthetized mesenteric lymph duct cannulated rat model was used as previously described with slight modifications.¹⁷ Adult male rats were left on a normal diet and given 1 mL olive oil 1 h before surgery to visualize the mesenteric lymph duct. They were anesthetized using isoflurane, ketamine, and xylazine as described above. Transverse laparotomy was performed. The mesenteric duct was identified cranially to the superior mesenteric artery and cannulated using heparin prefilled 0.97 mm O.D., 0.58 mm I.D. polyethylene catheter (Instech Laboratories, Plymouth Meeting, the United States).

The catheter was fixed in place with two to three drops of tissue adhesive (Surgibond[®]; SMI AG, Belgium). A duodenal catheter (same parameters as for the lymphatic catheter) was also placed through a small duodenotomy and fixed with tissue adhesive. The abdominal wall was sutured with both catheters leaving the abdominal cavity through the right flank of the animal. At the end of the procedure, the right jugular vein was cannulated for blood sampling. The rats were placed on heated pads and covered with blankets to prevent heat loss.

After the surgery, 1 mL of oil solution or emulsion (both containing 7.5 mg of CBD) was dosed through

duodenal catheter for >30 min. The whole lymph was collected in regularly changed Eppendorf tubes from the time drug administration started. Rats were continuously hydrated with normal saline at a rate of 3 mL/h intraduodenally using an infusion pump (Perfusor[®] compact plus; B. Braun, Melsungen AG, Germany). Anesthesia was maintained throughout the rest of the experiment, and additional ketamine i.m. boluses were administered whenever necessary. Eppendorf tubes were changed every 1 h, and systemic blood was drawn at the same time points.

Lymph samples were processed without further adjustments and stored at -80°C until analysis.

CBD emulsion in the treatment of CIA

Collagen emulsion for CIA induction was prepared according to the Chondrex protocol by emulsification of incomplete Freund's adjuvant with collagen dissolved in 0.05 M acetic acid. The initial 0.2 mL emulsion dose was applied subcutaneously into the bases of adult female rats' tails. The 0.1 mL booster injection was administered 7 days later. Rats in the negative control group were injected with the same volumes of saline.

The required number of rats suffering from CIA was obtained 17 days after the first immunization. On this day (Day 0), the CIA rats were symmetrically randomized into two groups. The first group (CBD group) was treated orally with 2 mL microemulsion containing 15 mg CBD once daily ($n=6$), and the second group (Placebo group) was treated with the same volume of saline ($n=6$). Rats in the negative control group were administered saline ($n=3$). Treatment lasted 24 days in all three groups.

The treatment progression was monitored throughout the experiment by visually assessing and recording the state of both hind paws of each rat every 3 days. The four-point scoring scale per leg was used with the following grading: 0 = normal joint; 1 = swelling or redness in 1 joint; 2 = swelling or redness in >1 joint; 3 = whole-paw swelling; 4 = joint deformity or ankylosis, immobility. Ankle edema was evaluated by measuring the width of both hindlimb ankles using digital calipers on the day of randomization (Day 0) and at the end of the experiment (Day 24).

Blood samples were taken on Day 0 and Day 24 to evaluate MMP-3 levels in serum. Blood was sampled from the tail on Day 0 and from the myocardium immediately before the euthanasia on Day 24. Blood was centrifuged and the obtained serum was stored at

–20°C until analysis. MMP-3 levels were determined using an enzyme-linked immunosorbent assay (Rat MMP3 ELISA kit ab270216; Abcam, Cambridge, United Kingdom).

On Day 24, immediately after the euthanasia, each rat's right hindlimb was amputated above the ankle. The samples were fixed in 4% formaldehyde in PBS, and subsequently decalcified in the 10% formic acid solution. This process lasted 2–3 months with solution replacement twice a week. After decalcification, the phalangeal part was separated, rinsed in water, and embedded in paraffin using a common procedure. Seven-micrometer-thick sections were stained with hematoxylin eosin and mounted in Canada balsam.

The imaging was performed using Leica DMLB microscope and LAS software (Leica Microsystems GmbH, Wetzlar, Germany). Sections through the phalangeal joints were scored according to the level of structural damage and disease activity. The structural damage score was based on the following characteristics: cartilage erosion, bone erosion and resorption, and synovial inflammation plus pannus invasion. The levels were 0=healthy joint; 1=mild changes; 2=advanced changes; and 3=severe damage. The disease activity score was established as follows: 0=no osteoclasts, 1=occasional osteoclasts present; 2=focal presence of osteoclasts; 3=widespread infiltration of osteoclasts.

Analytical methods

The concentration of CBD in serum and lymph was determined. For serum and lymph samples, protein precipitation was used. The samples were processed as follows: 80 μ L of 100% acetonitrile (containing 30.0 ng/mL CBD-d3 as an internal standard) were added to 20 μ L of the sample. The mixture was vortexed and centrifuged at 10,000 g for 8 min. Sixty microliters of supernatant were transferred to an chromatography vial. For the UHPLC-MS/MS analysis, the Shimadzu UHPLC Nexera X3 coupled with a Triple Quad 8045 tandem mass spectrometer (Shimadzu, Kyoto, Japan) was used. Chromatographic analysis was performed on a Poroshell 120 EC-C18 column (50 \times 2.1 mm; 1.9 μ m; Agilent Technologies, Inc., Santa Clara, CA, the United States).

The mobile phase consisted of 0.1% formic acid in deionized water (Solvent A) and methanol with 0.1% formic acid (Solvent B). The flow rate of the mobile phase was maintained at 0.4 mL/min, and the injection volume was 2 μ L. The column temperature was kept at

40°C, and the samples were thermostated at 10°C. The optimized gradient elution was carried out as follows (min/% B): 0/50, 0.5/50, 2.5/90, 3.5/90, 4.0/50, and 5.5/50. The MS/MS spectrometer was operated in a positive mode.

The applied conditions of the electrospray ion source were as follows: nebulizing gas flow: 3 L/min, heating gas flow: 10 L/min, interface temperature: 300°C, desolvation line temperature: 250°C, heat block temperature: 400°C, and drying gas flow: 10 L/min. The MS/MS measurement was performed in multiple reaction-monitoring mode (MRM). MRM transitions of 315.2 > 193.1 (Q1 prebias –16 V, Q3 prebias –20 V, and collision energy –22 V) and 318.2 > 196.1 (Q1 prebias –16 V, Q3 prebias –22 V, and collision energy –35 V) were monitored for CBD and CBD-d3, respectively.

The calibration curves were constructed in each blank matrix (serum and lymph) with seven concentrations by plotting the ratio of the peak area of CBD to that of internal standard against CBD concentration. The weighted least-squares linear regression method was used with a weighting factor of $1/x^2$, which improved the accuracy in low concentrations. The method was linear (coefficients of determination [R^2] > 0.9997) in the concentration range of 1–1000 ng/mL. The method was validated according to the requirements of the EMA Guideline on bioanalytical method validation and the guideline acceptance criteria.¹⁸

Data analysis and statistics

Serum and lymph concentrations in all pharmacokinetic studies were dose-normalized to 1 mg/kg before further calculations. Exact actual sampling times were used for all pharmacokinetic calculations, while scheduled sampling times were used only for plotting of mean pharmacokinetic profiles in the graphs. Pharmacokinetic analysis was performed using Phoenix WinNonlin[®] (Certara, Princeton, the United States) and PK solver add-on for MS Excel. Area under the curve (AUC) was calculated using the trapezoidal rule, while C_{max} and T_{max} were directly observed.

Lymphatic transport parameters were calculated as previously described.¹⁹ In brief, absolute bioavailability through the lymphatic system (F_{AL}) was defined as the percentage of administered drug that appeared in the intestinal lymph. It was determined directly using lymph volume and CBD concentrations in lymph duct cannulated rats. Analogically, absolute bioavailability through portal vein (F_{AP}) was defined as the

percentage of administered drug dose reaching the systemic circulation after direct absorption into the blood.

It was calculated as $F_{AP} = AUC_{ent}/AUC_{iv}$, where AUC_{ent} is the area under the dose-normalized blood concentration–time curve after enteral dosing in lymph duct cannulated (i.e., lymph-deprived) rats, and AUC_{iv} is the respective parameter in a separate intravenously dosed group. Total absolute bioavailability (F) in lymph duct cannulated rats was calculated as the sum of F_{AL} and F_{AP} . Finally, relative bioavailability through lymph (F_{RL}) was defined as the percentage of systemically available drug that was absorbed through lymph. It was calculated as $F_{RL} = F_{AL}/F$.

GraphPad Prism version 9.1.0 (GraphPad Software, San Diego, CA, the United States) was used for statistical analyses and graph plotting. Paired t -test was used to compare mean serum concentrations, whereas the Wilcoxon nonparametric test was used to compare median T_{max} values. The AUC and C_{max} values were compared by applying the standard ANOVA model for bioequivalence assessment using 90% confidence interval for the ratio of geometric least-squares means. Comparison of the results of arthritis score, MMP-3 levels, ankle widths, rat weights, and histological scores between the treatment groups was evaluated using the Mann–Whitney U -test. The level of statistical significance was set to $p < 0.05$.

Results and Discussion

Emulsion formulation

Sunflower oil droplets containing CBD were stabilized using soybean lecithin in the aqueous phase (the final CBD concentration was 7.5 mg/mL). The emulsion consisted of droplets with diameters ranging from 2 to 293 μm with the average Feret diameter equal to $42 \pm 47 \mu\text{m}$ immediately after the preparation (see Day 1 in Fig. 1). As can be seen in Figure 2, on Day 1, the droplet distribution was bimodal with two characteristic peaks ~ 8 and 80 μm . After a weeklong storage at 4°C, the droplet size distribution shifted slightly in favor of larger droplets, as shown in images referring to Day 8 in Figure 1. On Day 8, the minimal and maximal Feret diameters were 3 and 374 μm , respectively, and the average Feret diameter increased by $\sim 25\%$ to $52 \pm 59 \mu\text{m}$ (see Fig. 2). However, the bimodal character of the size distribution remained preserved.

Although mild droplet coalescence was observed, a few seconds of vortex mixing eliminated the presence of large droplets on Day 8 with the average Feret diameter dropping from 52 ± 59 to $38 \pm 33 \mu\text{m}$ (see Fig. 2). That represents an $\sim 10\%$ decrease of the average size compared with Day 1 and a 30% narrower size distribution. The emulsion was easily mixable by vortexing even a month after the preparation. Based on this

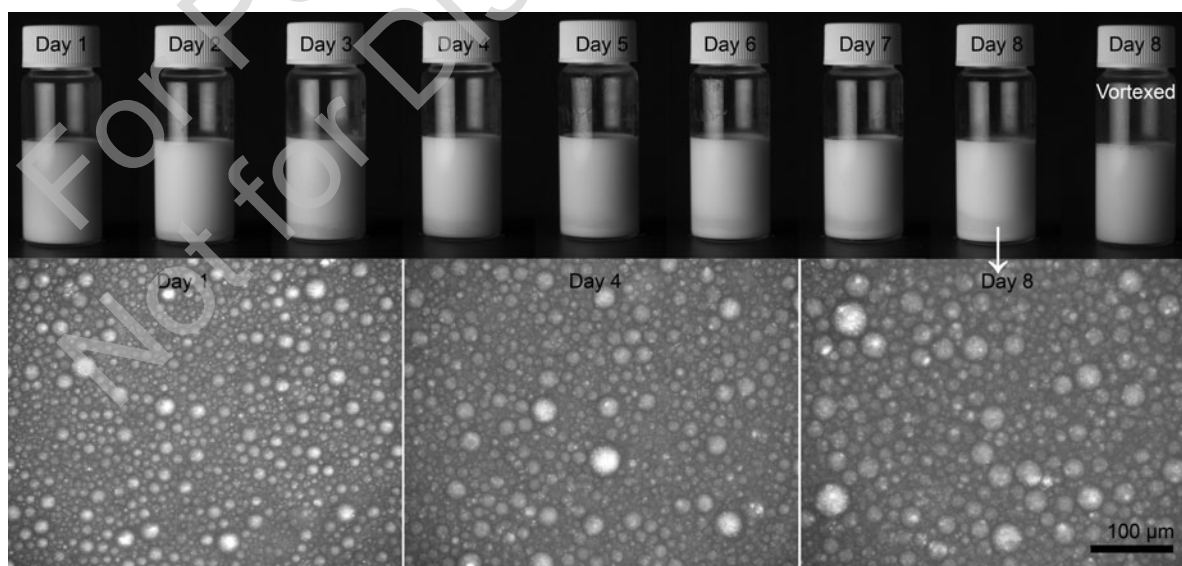


FIG. 1. An emulsion formulation captured for eight consecutive days (upper row) and analyzed by optical microscopy on Days 1, 4, and 8. After 8 days, slight phase separation was easily eliminated by brief vortex mixing (see the last vial entitled vortexed).

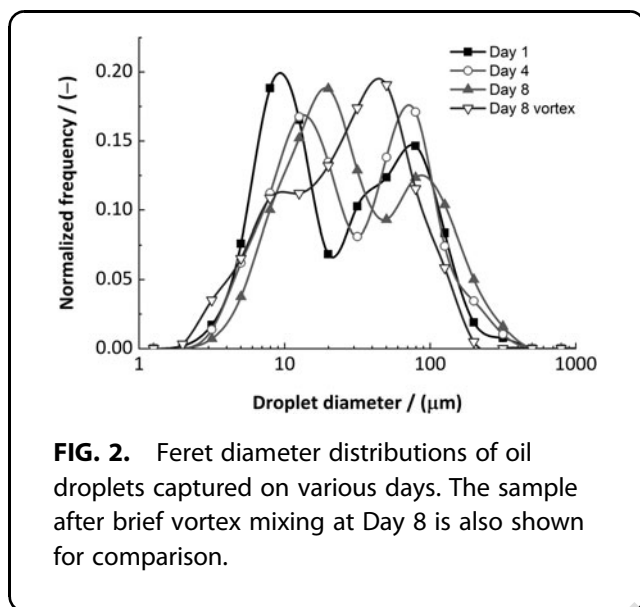


FIG. 2. Feret diameter distributions of oil droplets captured on various days. The sample after brief vortex mixing at Day 8 is also shown for comparison.

stability test, before every application, the emulsion was briefly vortexed (few seconds) to ensure the same droplet size distribution.

CBD bioavailability

Fourteen rats completed the crossover study assessing the relative performance of CBD emulsion compared with oil solution. There was a higher degree of absorption after the administration of the CBD emulsion (Table 1 and Fig. 3). There was also a trend toward higher absorption rate. Nevertheless, the difference in T_{max} did not reach statistical significance ($p=0.06$). CBD pharmacokinetic parameters after intravenous dosing are summarized in Table 2. Using mean i.v. AUC value from this experiment, the mean \pm SD absolute oral bioavailability of CBD was calculated as $24.7 \pm 3.6\%$ for emulsion and $14.4 \pm 12.2\%$ for oil solution.

Table 1. Pharmacokinetic Parameters of Cannabidiol After Administration in the Form of Oil Solution and Emulsion to Rats ($n=14$) Using a Crossover Study Design

Formulation	CBD oil solution	CBD emulsion
C_{max} (ng/mL)	8.95 (5.6–14.2)	34.4 (29.8–39.8)
Emulsion/oil solution	–	324 (181–581)
C_{max} (%)		
T_{max} (h)	4.05 (2.05–7.98)	2.54 (2.02–5.00)
AUC_{inf} (ng·h/mL)	66.8 \pm 20.8 (46.0–96.8)	153 \pm 11 (142–163)
Emulsion/oil solution	–	210 (124–355)
AUC_{inf} (%)		

C_{max} , AUC_{inf} and emulsion/solution ratios are given as geometric mean (90% confidence interval). T_{max} is given as median (range). All concentrations and AUCs are dose-normalized to 1 mg/kg. AUCs, area under the curves; CBD, cannabidiol.

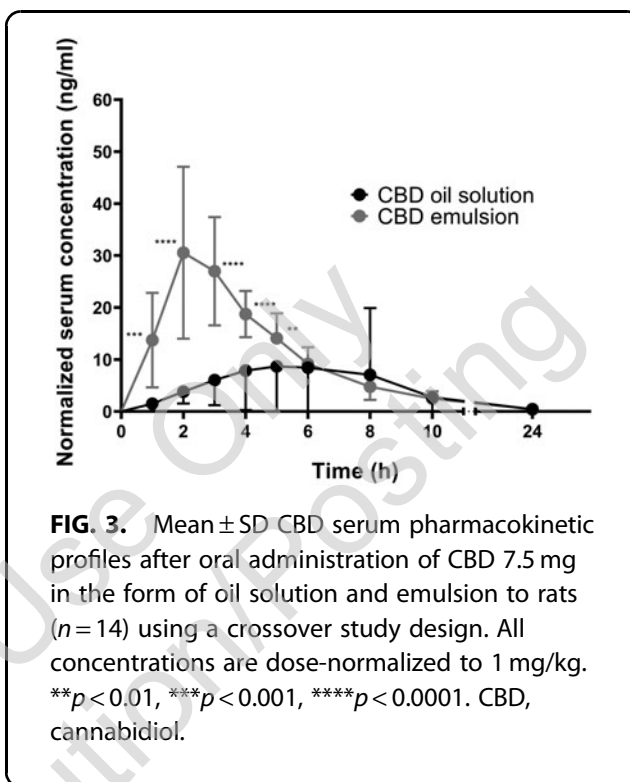


FIG. 3. Mean \pm SD CBD serum pharmacokinetic profiles after oral administration of CBD 7.5 mg in the form of oil solution and emulsion to rats ($n=14$) using a crossover study design. All concentrations are dose-normalized to 1 mg/kg. ** $p < 0.01$, *** $p < 0.001$, **** $p < 0.0001$. CBD, cannabidiol.

The observed normalized serum C_{max} concentrations of 10–35 ng/mL after oral administration of the two CBD formulations are in line with previously reported data in rats.^{16,20–23} There are only sparse reports on absolute bioavailability of CBD. The value of 25% observed after oral administration of CBD emulsion appears to slightly exceed the range of 5–20% reported in other species, including man.¹⁹

Studies using different formulations have already been published as CBs are an attractive group of compounds exhibiting a wide range of pharmacological effects throughout the body.²⁴ However, the intestinal absorption of CBD can be significantly affected by their composition. In case of emulsion formulations, which consist of two immiscible stabilized phases (oil and water), the most important excipients are as follows: solvents, cosolvents, surfactants, and cosurfactants.

Table 2. Mean \pm SD Cannabidiol Pharmacokinetic Parameters After Intravenous Cannabidiol (1 mg) Administration to Rats ($n=7$)

C_0 (ng/mL)	1178 \pm 421
$T_{1/2}$ (h)	2.5 \pm 0.5
V_{ss} (L/kg)	2.9 \pm 1.1
Cl (L/h·kg)	1.7 \pm 0.6
AUC_{inf} (ng·h/mL)	623 \pm 141

Concentration and AUC values are dose-normalized to 1 mg/kg. C_0 , maximum concentration; $T_{1/2}$ - biological half-life; V_{ss} , volume of distribution; Cl, clearance.

Feng et al.²¹ had already demonstrated that oil selection significantly affects the absorption of CBs. Izgelov et al.¹⁶ prepared formulation based on self-nano emulsifying drug delivery systems to investigate the effect of medium- and long-chain glycerides in oil phase. The subsequent pharmacokinetic studies suggested high absorption. However, all the tested formulations contained a range of surfactants combined with significant amounts of ethyl lactate together with *n*-butanol. Our results present a rather simple formulation based on fully biologically degradable compounds, where impact of various oils²¹ and droplet size on oral absorption can be easily evaluated.

Lymphatic absorption of CBD

Significant lymphatic transport after administration of both CBD emulsion and oil solution was observed (Table 3 and Fig. 4). CBD lymph concentrations were two to three orders of magnitude higher than serum concentrations. After administration of the CBD emulsion, there was a trend toward faster absorption into the lymph with lymphatic C_{max} reaching at ~4 h. On the contrary, absorption from the oil solution was more sustained, and the lymph concentrations observed at the end of the sampling period exceeded those of the CBD emulsion. Overall, the extent of lymphatic transport did not differ significantly between the two CBD formulations.

High levels of CBD in the lymph are similar to those reported by Zgair et al.¹¹ Relative bioavailability through lymph of ~50% is comparable with compounds with very high lymphatic transport, such as halofantrine and vitamin D.^{25,26} It is evident that lymphatic transport after oral administration plays a substantial role in the CBD pharmacokinetics and contributes significantly to total bioavailability. This fact is of a great importance for further pharmaceutical applications. As mentioned above, CBD undergoes first-pass metabolism, which results in low plasma concentration. It has been estimated that as much as 70–75% of

Table 3. Mean ± SD Cannabidiol Lymphatic Transport Parameters After Intraduodenal Administration of 7.5 mg of Cannabidiol in the Form of the Emulsion or Oil Solution ($n=3$ for Each Formulation) as Assessed at 8 h in Mesenteric Lymph Duct Cannulated Rats

	F (%)	F_{AL} (%)	F_{RL} (%)
CBD oil solution	4.8 ± 1.0	2.7 ± 0.7	55.3 ± 8.5
CBD emulsion	12.3 ± 12.3	3.0 ± 1.3	39.2 ± 27.1

F , total absolute bioavailability; F_{AL} , absolute bioavailability through lymph; F_{RL} , relative bioavailability through lymph.

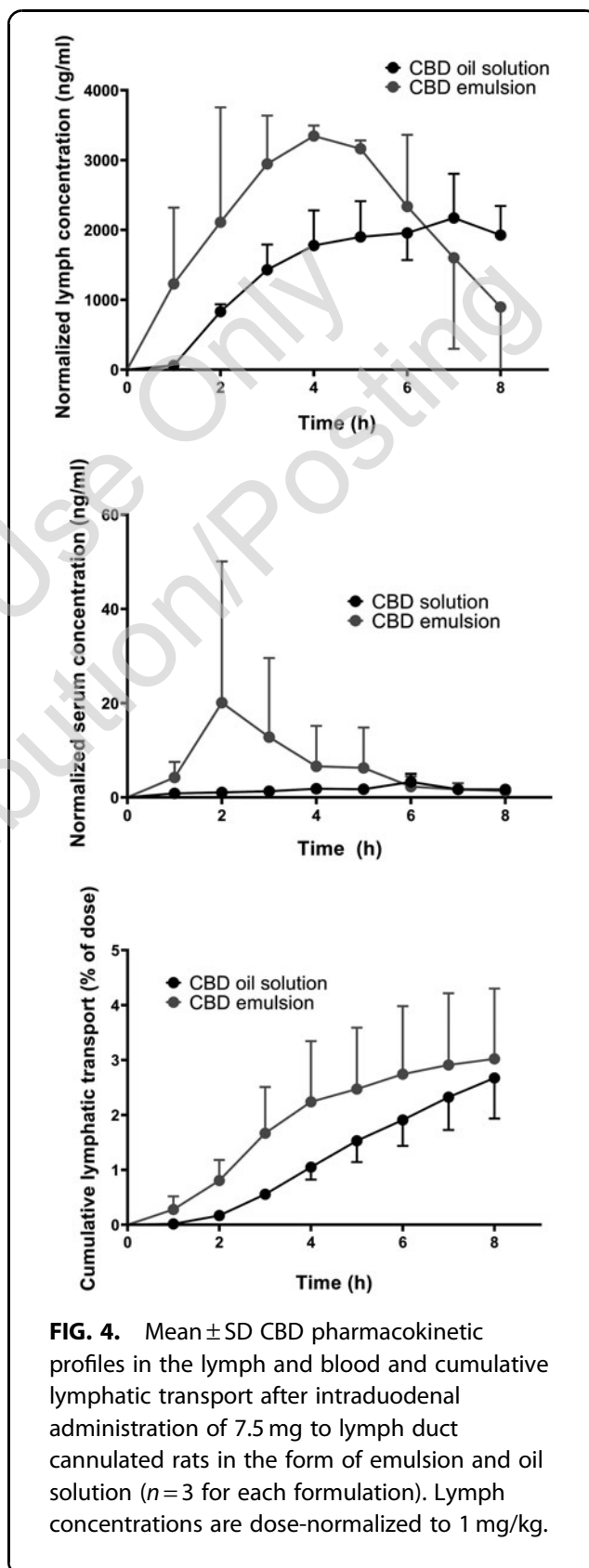


FIG. 4. Mean ± SD CBD pharmacokinetic profiles in the lymph and blood and cumulative lymphatic transport after intraduodenal administration of 7.5 mg to lymph duct cannulated rats in the form of emulsion and oil solution ($n=3$ for each formulation). Lymph concentrations are dose-normalized to 1 mg/kg.

Table 4. Mean±SD Values of Ankle Width, Weight, Matrix Metalloproteinase 3 Levels in Female Wistar Rats Suffering from Collagen-Induced Arthritis (n=6 in Cannabidiol and Placebo Group, n=3 in Negative Control Group)

	Ankle width (mm)				Weight (g)		Matrix metalloproteinase 3 (% of AU)	
	Day 0		Day 24		Day 0	Day 24	Day 0	Day 24
	Left hindlimb	Right hindlimb	Left hindlimb	Right hindlimb				
Negative control	5.44±0.05	5.31±0.43	5.70±0.20	5.77±0.22	268.33±15.33	282.33±9.88	1.00±0.27	1.00±1.30
CBD group	7.77±1.40	8.60±0.60	7.88±0.93	8.27±0.22	278.67±15.83	282.17±25.53	368.22±435.36	20.23±18.69
Placebo group	7.14±1.51	7.80±1.28	8.57±0.20	8.55±0.37	264.33±23.39	271.50±19.77	154.76±220.46	27.88±12.27

absorbed dose is metabolized before reaching systemic circulation. Therefore, improving lymphatic transport, and bypassing liver, is essential for increasing bioavailability of this compound.

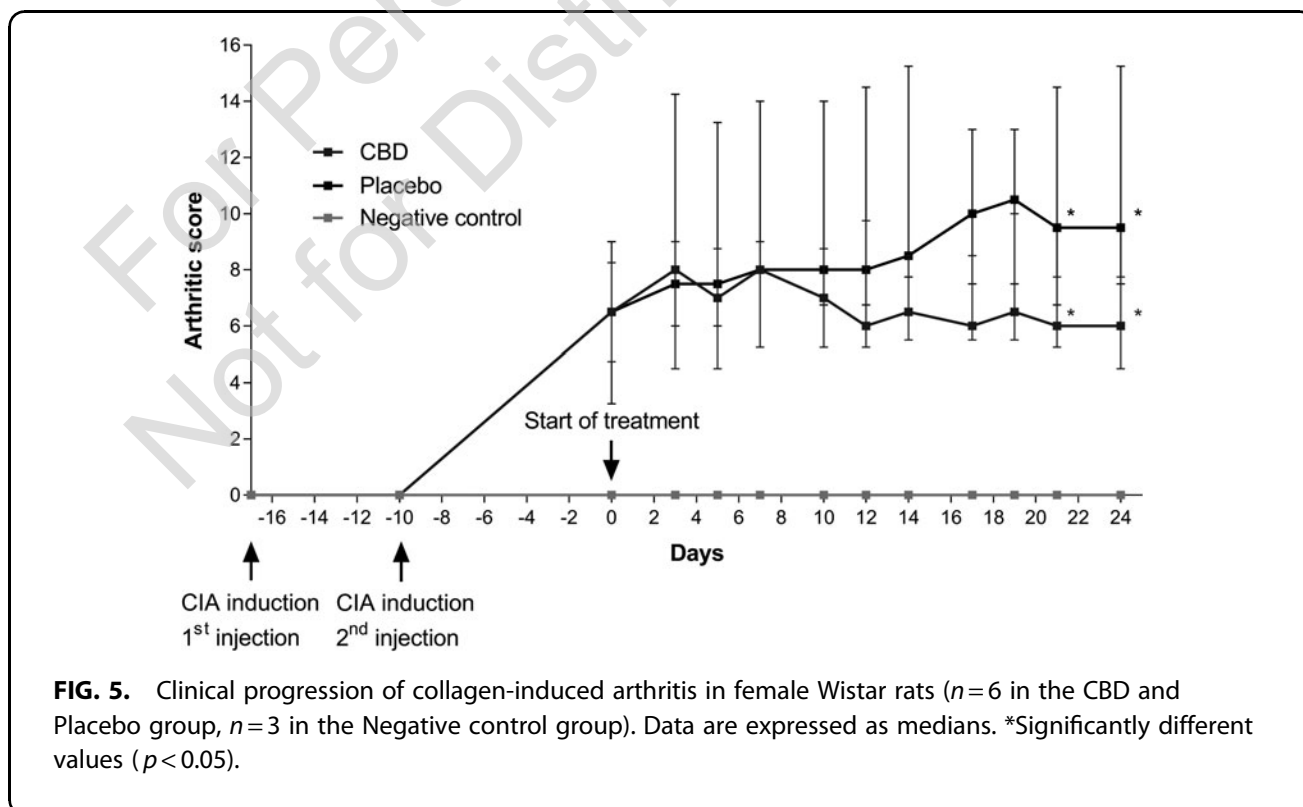
In sparse translational studies, it has been shown that lymphatic transport increases with increasing bodyweight of investigated species concerning both absolute and relative contributions to systemic bioavailability.²⁷ Based on these works, absolute bioavailability through lymph in humans is expected to be four times higher than that in rats. We observed a CBD absolute bioavailability through lymph of ~3% for both formulations in anesthetized rats. It can be expected to be two- to threefold higher in awake animals where the total bioavailability was threefold

higher for oil solution and twofold higher for micro-emulsion. This would potentially translate to absolute bioavailability through lymph of 24–36% in humans.

Another issue is a significant food effect. Various studies have demonstrated that CBD ingestion with high-fat meal increases the C_{max} and AUC values 4 to 14 times and four to five times, respectively.²⁸ Using a formulation that already contains lipids not only increases the total bioavailability but it can also eliminate large differences in absorption in fasted and fed state, and sustain balanced levels of CBD throughout the treatment.

CBD emulsion in the treatment of CIA

The comparison of the results evaluating the efficacy of CBD emulsion on CIA is summarized in Table 4.



Although there is a trend toward decreased MMP-3 levels and ankle widths in the CBD group than in the Placebo group on Day 24, none of the values were significant. A significant RA clinical progression in the Placebo group in comparison with CBD group was observed since Day 21 according to the symptom scoring (Fig. 5). Representative examples of histological findings are shown in Figure 6.

Significantly lower activity of phalangeal disease in the CBD group (median score 0.5, interquartile range [IQR] 0.0–1.0) in comparison with the Placebo group (median score 2.0, IQR 1.0–3.0) was observed in histological assessment ($p=0.04$). The difference in histologically scored structural phalangeal damage between the CBD and the Placebo group (median score 1.5 and 3.0, IQR 1.0–2.75 and 2.25–3.0, respectively) was not statistically significant ($p=0.37$). No treatment effect in this domain was likely caused by the onset of irreversible joint damage before treatment initiation in either group of rats, as the study was designed primarily to evaluate the drug effects to diminish or stop the progression of the disease, not to describe its potential for preventing structural damage.

Clinically relevant parameters, that is, clinical symptoms scores as well as morphological signs of disease/osteoclast activity, have shown significant improvements in the treatment groups. This was accompanied by only nonsignificant, but favorable trends in the course of the serum biomarker of the disease progres-

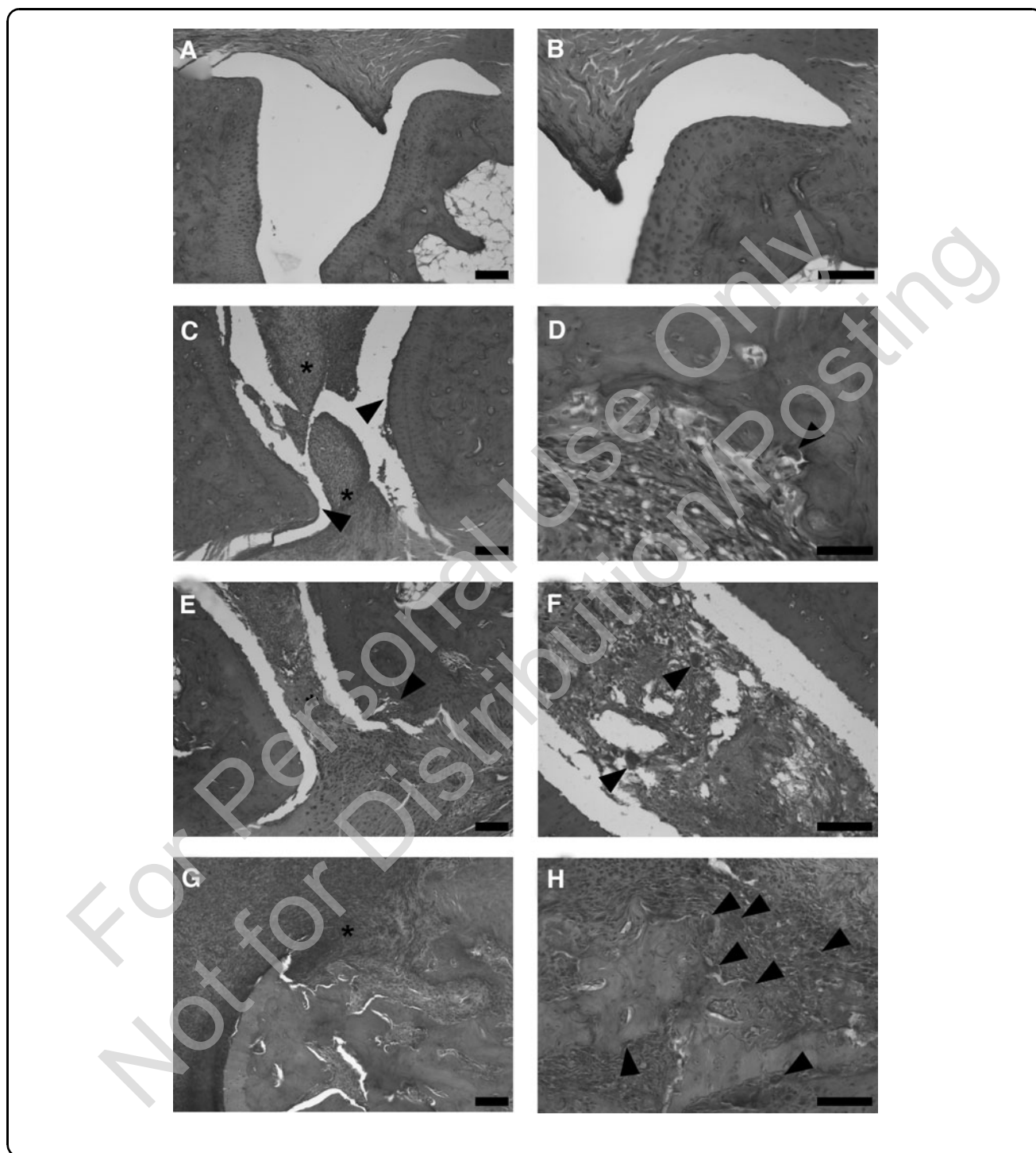
sion MMP-3 or in the ankle diameter measurements. The lack of significance for the MMP-3 biomarker was likely caused by an imbalance at the beginning of the treatment between both the CBD and Placebo groups, corresponding to the fact that the study was not balanced for this parameter.

In summary, our results from the rat CIA model demonstrate the therapeutic effect of CBD emulsion in the treatment of RA, represented by improvement in clinical symptoms as well as lower osteoclast activity and favorable trend in MMP-3 levels and lower paw swelling. Even though CBD did not show sufficient pharmacological effect in monotherapy, positive effect on the disease is still present. The lack of sufficient response could be dose dependent as the actual therapeutic dose in this indication is still unknown. There is a possibility to use CBD as an adjuvant in combination with conventional therapy—DMARDs, as its presence might have a positive impact on the efficacy of such treatment or ameliorate its adverse effects. Similar beneficial effect has already been demonstrated by El-Sheikh et al,²⁹ for a combination of methotrexate or leflunomide and another natural compound affecting endocannabinoid system; that is, beta-caryophyllene.

Conclusions

Presented work was focused on evaluation of CBD absorption after oral administration with special focus

FIG. 6. Representative images of interphalangeal joints' histological scoring for tissue damage and level of disease/osteoclast activity. **(A)** Histopathological damage – Score 0. The image shows a physiological interphalangeal joint; articulating bones covered with intact cartilage and normal morphological synovial membranes with a maximum double layer of synovialocytes. **(B)** Disease/osteoclast activity – Score 0. A higher magnification of **(A)** shows an intact joint with no osteoclasts and no signs of cartilage or bone erosion. **(C)** Histopathological damage – Score 1. The inflammatory synovial pannus protrudes into the joint cavity (*). Articular cartilages are morphologically intact (*arrowheads*). **(D)** Disease/osteoclast activity – Score 1. An isolated osteoclast in Howship's lacuna next to the subchondral bone. **(E)** Histopathological damage – Score 2. Interphalangeal joint with an inflammatory synovial pannus (*), which penetrates beyond a partially eroded articular cartilage into the subchondral bone (*arrowhead*). **(F)** Disease/osteoclast activity – Score 2. Two osteoclasts (*arrowheads*) are found within the inflammatory synovial pannus. **(G)** Histopathological damage – Score 3. Joint with the highly cellular inflammatory synovial pannus completely filling the joint cavity. The pannus penetrates through heavily eroded articular cartilage across the subchondral bone deep into the bone cavity (*). **(H)** Disease/osteoclast activity – Score 3. Multiple osteoclasts (*arrowheads*) adjacent to eroding bone or within the inflammatory pannus filing the joint cavity. **(A–H)** Hematoxylin-eosin staining. Scale bars in **A, C, E, F, G,** and **H** = 100 μm , in **B** and **D** = 50 μm .



on lymphatic transport and possible therapeutic application in RA treatment. For this reason, two types of simple lipid-containing formulations, sunflower oil solution and sunflower oil microemulsion stabilized by soybean lecithin, were used. Prepared emulsion exhibited good size stability and only marginal coalescence,

which was easily redispersed by shaking even after long-term storage.

In comparison with simple oil solution, our formulation exhibited improved bioavailability with 3.2 times higher C_{max} and 2.1 times higher AUC. Further pharmacokinetic experiments showed that both

formulations (oil as well as emulsion) were lymphatically absorbed to a great extent, and CBD concentrations in the lymph were two to three orders of magnitude higher than serum concentrations, thus, confirming the importance of this route of transport.

Although treatment with our formulation resulted in significant improvement in clinical symptoms and disease activity, the effect on ankle swelling, joint damage as well as the MMP-3 levels was only minor. Overall, our emulsion did not exhibit sufficient efficacy in monotherapy in the model of RA, although this may change with the dose.

We have demonstrated the beneficial effect of emulsion formulation on lymphatic absorption and subsequent increase in absolute oral bioavailability. This is important, because with further optimization even higher values could be achieved. In fact, our formulation is rather simple, and thus provides robust platform for additional testing of various components and formulation parameters; that is, oil type, droplet diameter, droplet size distribution. Furthermore, as CBD exhibits a wide range of effects on human body, its therapeutic value is not limited to RA. Understanding how to maximize its absorption is crucial, and lymphatic transport is proving to be an important pathway for highly lipophilic molecule suffering from extensive first-pass metabolism such as CBD.

Authors' Contributions

P.J., J.R., and M.J. conducted investigation; P.R. and T.K. contributed to methodology and investigation; T.H. performed writing—review and editing; J.P. provided resources; P.K. performed formal analysis and methodology; M. Šíma contributed to methodology and supervision; O.S. performed supervision and project administration; M. Šoóš contributed to supervision, writing—original draft, and project administration.

Author Disclosure Statement

All authors declare that they have no conflicts of interest.

Funding Information

This work was supported by AZV grant No. AZV NU22-08-00346, specific university research grant No. A1_FCHI_2022_006, Charles University grant GAUK No. 102322, and Charles University Program Cooperation (research area PHAR).

References

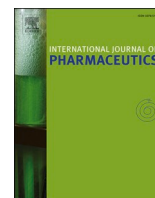
- Ajeganova S, Huizinga T. Sustained remission in rheumatoid arthritis: latest evidence and clinical considerations. *Ther Adv Musculoskelet Dis*. 2017;9:249–262.
- Kerschbaumer A, Sepriano A, Smolen JS, et al. Efficacy of pharmacological treatment in rheumatoid arthritis: a systematic literature research informing the 2019 update of the EULAR recommendations for management of rheumatoid arthritis. *Ann Rheum Dis*. 2020;79:744–759.
- Kaur I, Behl T, Bungau S, et al. The endocannabinoid signaling pathway as an emerging target in pharmacotherapy, earmarking mitigation of destructive events in rheumatoid arthritis. *Life Sci*. 2020;257:118109.
- Malfait AM, Gallily R, Sumariwalla PF, et al. The nonpsychoactive cannabis constituent cannabidiol is an oral anti-arthritis therapeutic in murine collagen-induced arthritis. *Proc Natl Acad Sci U S A*. 2000;97:9561–9566.
- Trentham DE, Townes AS, Kang AH. Autoimmunity to type II collagen an experimental model of arthritis. *J Exp Med*. 1977;146:857–868.
- EMA. Epidyolex; [cited 2022 May 1]. Available from: <https://www.ema.europa.eu/en/medicines/human/EPAR/epidyolex>
- Porter CJ, Trevaskis NL, Charman WN. Lipids and lipid-based formulations: optimizing the oral delivery of lipophilic drugs. *Nat Rev Drug Discov*. 2007;6:231–248.
- Charman WNA, Stella VJ. Estimating the maximal potential for intestinal lymphatic transport of lipophilic drug molecules. *Int J Pharm*. 1986;34:175–178.
- Ryšánek P, Grus T, Šíma M, et al. Lymphatic transport of drugs after intestinal absorption: impact of drug formulation and physicochemical properties. *Pharm Res*. 2020;37:166.
- Huestis MA. Human cannabinoid pharmacokinetics. *Chem Biodivers*. 2007;4:1770–1804.
- Zgair A, Lee JB, Wong JCM, et al. Oral administration of cannabis with lipids leads to high levels of cannabinoids in the intestinal lymphatic system and prominent immunomodulation. *Sci Rep*. 2017;7:14542.
- Franco V, Gershkovich P, Perucca E, et al. The interplay between liver first-pass effect and lymphatic absorption of cannabidiol and its implications for cannabidiol oral formulations. *Clin Pharmacokinet*. 2020;59:1493–1500.
- Lowin T, Tingting R, Zurmahr J, et al. Cannabidiol (CBD): a killer for inflammatory rheumatoid arthritis synovial fibroblasts. *Cell Death Dis*. 2020;11:714.
- Millar SA, Stone NL, Yates AS, et al. A systematic review on the pharmacokinetics of cannabidiol in humans. *Front Pharmacol*. 2018;9:1365.
- Francke NM, Schneider F, Baumann K, et al. Formulation of cannabidiol in colloidal lipid carriers. *Molecules*. 2021;26:1469.
- Izgelov D, Shmoeli E, Domb AJ, et al. The effect of medium chain and long chain triglycerides incorporated in self-nano emulsifying drug delivery systems on oral absorption of cannabinoids in rats. *Int J Pharm*. 2020;580:119201.
- Trevaskis NL, Hu L, Caliph SM, et al. The mesenteric lymph duct cannulated rat model: application to the assessment of intestinal lymphatic drug transport. *J Vis Exp*. 2015:52389.
- EMA. ICH guideline M10 on bioanalytical method validation and study sample analysis; [cited 2022 May 1]. Available from: https://www.ema.europa.eu/en/documents/scientific-guideline/ich-guideline-m10-bioanalytical-method-validation-step-5_en.pdf
- Ryšánek P, Grus T, Lukáč P, et al. Validity of cycloheximide chylomicron flow blocking method for the evaluation of lymphatic transport of drugs. *Br J Pharmacol*. 2021;178:4663–4674.
- Deiana S, Watanabe A, Yamasaki Y, et al. Plasma and brain pharmacokinetic profile of cannabidiol (CBD), cannabidivarin (CBDV), Δ^9 -tetrahydrocannabinol (THCV) and cannabigerol (CBG) in rats and mice following oral and intraperitoneal administration and CBD action on obsessive-compulsive behaviour. *Psychopharmacology (Berl)*. 2012;219:859–873.
- Feng W, Qin C, Chu Y, et al. Natural sesame oil is superior to pre-digested lipid formulations and purified triglycerides in promoting the intestinal lymphatic transport and systemic bioavailability of cannabidiol. *Eur J Pharm Biopharm*. 2021;162:43–49.
- Hložek T, Uttl L, Kadeřábek L, et al. Pharmacokinetic and behavioural profile of THC, CBD, and THC + CBD combination after pulmonary, oral, and subcutaneous administration in rats and confirmation of conversion

- in vivo of CBD to THC. *Eur Neuropsychopharmacol.* 2017;27:1223–1237.
23. Kok LY, Bannigan P, Sanaee F, et al. Development and pharmacokinetic evaluation of a self-nanoemulsifying drug delivery system for the oral delivery of cannabidiol. *Eur J Pharm Sci.* 2022;168:106058.
 24. Stella B, Baratta F, Della Pepa C, et al. Cannabinoid formulations and delivery systems: current and future options to treat pain. *Drugs.* 2021;81:1513–1557.
 25. Dahan A, Hoffman A. Evaluation of a chylomicron flow blocking approach to investigate the intestinal lymphatic transport of lipophilic drugs. *Eur J Pharm Sci.* 2005;24:381–388.
 26. Karpf DM, Holm R, Kristensen HG, et al. Influence of the type of surfactant and the degree of dispersion on the lymphatic transport of halofantrine in conscious rats. *Pharm Res.* 2004;21:1413–1418.
 27. Trevaskis NL, Lee G, Escott A, et al. Intestinal lymph flow, and lipid and drug transport scale allometrically from pre-clinical species to humans. *Front Physiol.* 2020;11:458.
 28. Perucca E, Bialer M. Critical aspects affecting cannabidiol oral bioavailability and metabolic elimination, and related clinical implications. *CNS Drugs.* 2020;34:795–800.
 29. El-Sheikh SMA, Abd El-Alim AEF, Galal AAA, et al. Anti-arthritis effect of β -caryophyllene and its ameliorative role on methotrexate and/or leflunomide-induced side effects in arthritic rats. *Life Sci.* 2019;233:116750.

Cite this article as: Jelínek P, Roušarová J, Ryšánek P, Ježková M, Havlůjová T, Pozniak J, Kozlík P, Křížek T, Kučera T, Šíma M, Slanař O, and Sooš M (2022) Application of oil-in-water cannabidiol emulsion for the treatment of rheumatoid arthritis, *Cannabis and Cannabinoid Research X:X*, 1–13, DOI: 10.1089/can.2022.0176.

Abbreviations Used

AUC = area under the curve
 CB = cannabinoid
 CBD = cannabidiol
 CIA = collagen-induced arthritis
 DMARDs = disease-modifying antirheumatic drugs
 EMA = European Medicines Agency
 IQR = interquartile range
 MMPs = matrix metalloproteinases
 MRM = multiple reaction-monitoring mode
 RA = rheumatoid arthritis



Serum and lymph pharmacokinetics of nilotinib delivered by yeast glucan particles *per os*

Petra Šalamúnová^{a,1}, Tereza Krejčí^{a,b,1}, Pavel Ryšánek^{c,1}, Ivan Saloň^a, Jiřina Kroupová^a, Anna Hubatová-Vacková^a, Jakub Petřík^{b,d}, Tomáš Grus^e, Peter Lukáč^e, Petr Kozlák^f, Tomáš Krížek^f, Ondřej Dammer^b, Josef Beránek^b, Martin Šíma^c, Ondřej Slanář^c, František Štěpánek^{a,*}

^a Department of Chemical Engineering, University of Chemistry and Technology Prague, Technická 5, 166 28 Prague, Czech Republic

^b Zentiva, k.s., U Kabelovny 130, 102 37 Prague, Czech Republic

^c Institute of Pharmacology, First Faculty of Medicine, Charles University and General University Hospital in Prague, Albertov 4, 128 00 Prague, Czech Republic

^d Department of Analytical Chemistry, University of Chemistry and Technology Prague, Technická 5, 166 28 Prague, Czech Republic

^e Department of Cardiovascular Surgery, First Faculty of Medicine, Charles University and General University Hospital in Prague, U Nemocnice 499/2, 128 08 Prague, Czech Republic

^f Department of Analytical Chemistry, Faculty of Science, Charles University, Hlavova 2030/8, 128 43 Prague, Czech Republic

ARTICLE INFO

Keywords:

Glucan particles
Nilotinib hydrochloride
Encapsulation
Macrophages
Bioavailability
Lymphatic transport

ABSTRACT

Nilotinib is a selective tyrosine-kinase inhibitor approved for the treatment of chronic myeloid leukemia. It is poorly soluble in aqueous media and has a low oral bioavailability. Nilotinib encapsulation into yeast glucan particles (GPs) was investigated in this work as a means of increasing bioavailability. The amorphization of nilotinib in GPs resulted in an increased dissolution rate, which was confirmed by *in vitro* experiments using biorelevant dissolution media. Simultaneously, GPs containing nilotinib were effectively taken up by macrophages, which was quantified *in vitro* on cell cultures. The overall oral bioavailability in a rat model was approximately 39 % for nilotinib delivered in a reference formulation (Tasigna) and was almost doubled when delivered in GPs. The contribution of glucan particles to the lymphatic transport of nilotinib was quantified. When delivered by GPs, cumulative nilotinib absorption via the lymphatic system increased by a factor of 10.8 compared to the reference, but still represented a relative bioavailability of only 1.12 %. The cumulative uptake of GPs in the lymph was found to be 0.54 mg after a single dose of 50 mg. Yeast glucan particles can therefore serve as a drug delivery vehicle with a dual function: dissolution rate enhancement by amorphization, and, to a smaller extent, lymphatic delivery due to macrophage uptake.

1. Introduction

Nilotinib is a selective tyrosine-kinase inhibitor indicated for the treatment of chronic myelogenous leukemia and Philadelphia-positive acute lymphoblastic leukemia (Ph+ CML) (Zhang et al., 2014). Globally, CML has an incidence of 1–2 per 100,000 people per year and nilotinib is one of the most widely prescribed anti-cancer drugs, with sales over \$2 bn in 2021 alone. According to the Biopharmaceutics Classification System (BCS), nilotinib is a Class IV compound, which means that it possesses low aqueous solubility and medium/low absorption. The currently marketed formulation of nilotinib (Tasigna)

exhibits approximately 30% bioavailability following oral administration (Tasigna, 2021). Low bioavailability represents not only an economic loss but also an environmental burden (cytostatic residues in waste waters). In addition to poor solubility and absorption, nilotinib exhibits a positive food effect, which results in increased systemic levels following administration with a high-fat diet (Wolf et al., 2011; Tian et al., 2018). In order to improve the bioavailability of a BCS Class IV drug, two aspects need to be addressed: solubility and absorption.

To improve nilotinib solubility, several approaches have been proposed in the literature. These include the formation of an amorphous solid dispersion by spray drying with polymeric excipients, the

* Corresponding author.

E-mail address: Frantisek.Stepanek@vscht.cz (F. Štěpánek).

¹ These authors contributed equally to this work.

formulation of supersaturating formulations (Zhu et al., 2022), the formation of hybrid nilotinib nanoparticles with polymers and surfactants using supercritical CO₂, or the incorporation of nilotinib into a lipid-based suspension system or polymers and non-ionic surfactants (Herbrink et al., 2017; Jesson et al., 2014; Koehl et al., 2019; Koehl et al., 2020; Koehl et al., 2020). However, solubility enhancement alone might not be sufficient in cases where the rate-limiting step is absorption. To overcome the problem of incomplete absorption, a combined swellable and floating gastro-retentive drug delivery system has been investigated, in which the controlled release of nilotinib in the stomach was regulated by polymeric excipients (Lin et al., 2020). In the specific case of nilotinib, an additional complication is its pH-dependent solubility. Nilotinib is a weak base with pK_{a1} 3.0 and pK_{a2} 6.2. The solubility of nilotinib decreases with increasing pH. It is slightly soluble at pH 1 (less than 1 mg/mL) and almost insoluble (less than 0.1 mg/mL) in a phosphate buffer with pH above 4.5 (Tian et al., 2018).

An alternative strategy to improve nilotinib bioavailability could be the enhancement of absorption in the gastro-intestinal tract by some other mechanism than simple diffusion of a freely dissolved drug. One such strategy includes drug delivery by means of carrier particles that promote lymphatic transport (Han et al., 2022; Miao et al., 2021) such as yeast glucan particles (GPs). Glucan particles are porous polysaccharide shells obtained from baker's yeast (*Saccharomyces cerevisiae*) by a series of extraction and purification steps. GPs have a characteristic size of 3–5 µm and retain the morphology and surface features of original yeast cells. A full physico-chemical characterisation of GPs including spectroscopic, thermal and colloidal properties is reported in our previous work (Saloň et al., 2016).

It has also been reported in the literature that GPs derived from *Saccharomyces cerevisiae* possess immunomodulatory activity when administered orally and therefore, they are taken up by macrophages that reside in Peyer's patches (De Smet et al., 2013; Baert et al., 2015; Soares et al., 2018; Soto et al., 2019). These findings have been supported by histological and optical analyses proving the presence of GPs in the lymphatic organs (Xie et al., 2016; Xie et al., 2016; Zhang et al., 2017; Wu et al., 2020; Gao et al., 2021). Owing to their porous nature, GPs have been successfully used for the encapsulation of a wide variety of bioactive compounds. These include peptides, proteins, vitamins and caffeine, siRNA, natural compounds, anti-inflammatory compounds and antibiotics (Xie et al., 2016; Yu et al., 2015; Saloň et al., 2016; Bajgar et al., 2019; Aouadi et al., 2009; Soto and Ostroff, 2008; Tesz et al., 2011; Plavcová et al., 2019; Young and Nitin, 2019; Rotrekl et al., 2020; Ruphuy et al., 2020; Soto et al., 2010). In the case of poorly water-soluble drugs, it has been shown that encapsulation into GPs can result in amorphization and consequently dissolution rate enhancement (Šalamúnová et al., 2021).

Therefore, we hypothesize that nilotinib encapsulation into glucan particles might result in bioavailability enhancement by two complementary mechanisms: dissolution rate enhancement due to amorphization, and lymphatic absorption via macrophage uptake. Despite the promise of GPs as a potential drug delivery vehicle, full pharmacokinetic studies of orally administered GPs either alone or in comparison with an existing drug have not been reported in the literature so far. Crucially, no direct comparison of serum and lymph pharmacokinetics profiles of a clinically approved drug administered via GPs and the same drug administered as an existing marketed formulation has been conducted to date.

The present work is concerned with the encapsulation of nilotinib into GPs, the physico-chemical characterization of the GP-nilotinib (GP-nil) composites and their *in vitro* dissolution behavior, as well the quantitative determination of nilotinib pharmacokinetics *in vivo* with a specific focus on the contribution of lymphatic absorption. Using fluorescently labelled glucan particles in combination with precise lymph sampling methodology (Ryšánek et al., 2021), we present a quantitative evaluation of GPs lymphatic uptake after oral administration and use this information to interpret the pharmacokinetics of nilotinib

administered via glucan particles.

2. Materials and methods

2.1. Glucan particles preparation and nilotinib loading

Glucan particles were prepared from dried baker's yeast *Saccharomyces cerevisiae* (Lesaffre Česko, a.s.) using a published protocol (Plavcová et al., 2019). Concisely, 150 g of dried yeast was redispersed in 600 mL of 1 M NaOH solution and heated to 90 °C for 60 min. Then, the suspension was centrifuged for 3 min (6,000 × g) and the supernatant was removed. The alkali extraction of the yeast was repeated 3 times in total. Next, the alkali mixture was adjusted with HCl to pH about 4.5 and heated to 75 °C for 2 h. Again, the supernatant was discarded after every centrifugation of the suspension (3 min, 6,000 × g) and the solid part was washed by deionized water (3 times), isopropanol (4 times) and acetone (2 times). After each washing step, the centrifugation with the same parameters was applied. The final product was lyophilized for 48 h and subsequently stored in a refrigerator, protected against air moisture.

GP-nil composites with nilotinib loading ranging from 0.1 % to 15 % (w/w) were prepared by the slurry evaporation method (Plavcová et al., 2019; Šalamúnová et al., 2021). Nilotinib hydrochloride was kindly provided by Zentiva Group a.s. A suspension of glucan particles in ethanol was prepared by combining dry glucan particles, a stock solution of nilotinib in ethanol, and pure ethanol in the desired ratios specified in Table 1. The suspension was mixed in a round-bottom flask for approximately 5 min (IKA® T10 basic Ultra-Turrax®) until it was visually homogeneous. Ethanol was then slowly evaporated (175 RPM, 480 mbar and 60 °C, followed by 15 min. at 80 mbar) to obtain a dry powder (Plavcová et al., 2019). The GP-nil composites were then lyophilized for 2 days to remove any residual solvent and stored in a refrigerator protected from light and air moisture.

2.2. Characterization of glucan particle composites

2.2.1. Structural characterization

The prepared GP-nil composites were visualized using optical and fluorescence microscopy (Olympus IX81, WU fluorescence cube with excitation in 330 – 385 nm range and detection at wavelengths higher than 420 nm). Olympus UPLSAPO Objective 40× was employed. The Scanning Electron Microscope (SEM) Jeol JCM-5700 was used for the morphological characterization of the prepared GPs with nilotinib. Before SEM analysis, the samples were sputter-coated with a 5-nm gold layer (Emitech K550X). The crystallinity of the samples was analyzed by X-ray powder diffraction analysis (PANalytical X'Pert Pro with High Score Plus diffractometer; 5° to 50° 2θ angle). The XRPD patterns are reported in the Supplementary Information.

2.2.2. Nilotinib assay

To determine the amount of nilotinib loaded into the GP-nil composites, 10 mL of methanol was added to 10 mg of composites and ultrasonic bath was used to extract the compounds for 10 min. The supernatant was separated by centrifugation (10 min, 6,000 × g) and filtered through 0.2 µm filters. The nilotinib content was then determined on the Water UPLC Acquity system equipped with Acquity UPLC BEH C18 column (1.7 µm; 2.1 × 100 mm) and PDA detector. The following gradient of 10 mM NH₄H₂PO₄ pH 8.5/acetonitrile at flow rate 0.3 mL/min was used: linear change from 70/30 to 20/80 (0–1.2 min) followed by steady state (1.2–2.8 min) and a linear change to starting conditions (2.8–3.8 min) followed by steady state for 1.5 min to re-equilibrate. The data were processed using the Empower software.

2.2.3. Dissolution tests

Dissolution testing was conducted using a USP 2 dissolution apparatus equipped with mini-paddles (Sotax, Switzerland) and coupled to

Table 1

Summary of feedstocks and final composition of individual GP-nil samples prepared by slurry evaporation. The code name “GP-nil-X.Y” denotes a sample with nominal nilotinib mass fraction X.Y % (w/w).

Sample code name	Concentration of nilotinib in stock solution (mg/mL)	Volume of stock solution (mL)	Volume of added ethanol (mL)	Mass of GPs (mg)	Planned content of nilotinib (%(w/w))	Determined content of nilotinib (%(w/w))
GP-nil-0.1	0.5	0.4	19.6	200	0.1	0.08 ± 0.001
GP-nil-0.5	0.5	2.0	18.0	200	0.5	0.38 ± 0.01
GP-nil-1.0	0.5	4.0	16.0	200	1.0	1.22 ± 0.04
GP-nil-1.5	0.5	6.0	14.0	200	1.5	1.17 ± 0.05
GP-nil-2.0	0.5	8.0	12.0	200	2.0	1.54 ± 0.0004
GP-nil-2.5	0.5	10.0	10.0	200	2.5	1.98 ± 0.03
GP-nil-15.0	1.73	150.0	–	1500	15.0	13.88 ± 0.91

UV–vis spectrophotometer Specord 200 Plus (Analytik Jena, Germany). The dissolution media were kept at 37 °C and stirred at 125 RPM. The samples were added to a dissolution vessel either directly using a weighing boat or pre-dispersed in Eppendorf tubes containing 2 mL of water. The weight of GP-nil composites added to the dissolution media corresponded to 5 mg for powder dissolution experiments or 7 mg for experiments simulating dosing for rats (samples dosed as suspension). Liquid samples were taken at predefined time points, filtered through a 0.7 µm in-line filter and analyzed immediately on a UV–vis spectrophotometer at 264 nm in 5 mm cuvettes. To simulate conditions prevailing in different parts of the gastrointestinal (GI) tract, dissolution media with pH ranging from 2 to 6.8 were used. In addition, dissolution in a biorelevant medium (FaSSiF) was conducted. This medium contains taurocholate and lecithin, i.e. physiological surfactants present in the human bile.

2.3. Preparation of fluorescently labelled glucan particles

Fluorescein isothiocyanate (FITC) labelled glucan particles (GP-FITC) were prepared as follows: 1200 mg of GPs, 200 mL of 0.1 M carbonate-bicarbonate buffer with pH 9.2 (prepared by dissolving 0.477 g of sodium carbonate and 3.822 g of sodium bicarbonate in deionized water to a final volume of 200 mL), and 30 mg of FITC were mixed in a round-bottom flask and sonicated on a sonication bath for 15 min. The suspension in the covered round-bottom flask was then mixed by a magnetic stirrer at 500 RPM at 25 °C for 6 h. The content of the reaction mixture was centrifuged for 3 min at 6000 × g. The supernatant containing unreacted materials was discarded. The pellet was washed by deionized water three times, and then by 99.9 % ethanol (PENTA) ten times until no free FITC was detected by fluorescence spectroscopy. After these steps, the particle suspension was lyophilized to obtain a dry powder and stored in a refrigerator for further use. The successful attachment of FITC was verified by fluorescence spectroscopy and the remaining features of surface morphology of glucan particles were verified by scanning electron microscopy, both shown in [Figure S1](#) in the [Supplementary information](#). It has also been verified that the modification of GPs was not detrimental to their colloidal stability.

2.4. Macrophage uptake and cytotoxicity study

2.4.1. Cell culture

Two cell lines were used for the cytotoxicity study: Abelson murine leukemia macrophage cell line RAW 264.7 (ATCC® TIB-71™) and a murine reticulum sarcoma macrophage cell line J774A.1 (ATCC® TIB-67™), purchased from the American Type Culture Collection (ATCC). Both cell lines were cultured in Dulbecco's modified Eagle's medium - high glucose (DMEM, Sigma-Aldrich) supplemented with 10 % v/v fetal bovine serum (FBS, Sigma-Aldrich) and 1 % v/v antibiotic antimycotic solution (AAS, Sigma-Aldrich), hereinafter referred as the culture medium. Cells were cultivated in an incubator under the controlled environment (37 °C, 5 % CO₂, 95 % relative humidity) until they reached 70 – 80 % confluency and were subsequently passaged. For experiments,

cells between the 5th – 18th passages were used.

2.4.2. Cytotoxicity assays

To prove that nilotinib can be effectively delivered to cells in the form of GP-nil composites under pH conditions at which it is practically insoluble, cytotoxicity assays were carried out. As a positive control, nilotinib solutions in dimethylsulfoxide (DMSO) were used. The concentration of DMSO in the final cell suspension was very low (less than 0.1 %) to minimize its effect on cell viability and cell wall permeability. However, the DMSO concentration was still sufficiently high for nilotinib to be completely dissolved in the desired concentration range from 0.09 to 22.5 µM. The GP-nil composites (samples with varying nilotinib loading, listed in [Table 1](#)) were added to the culture medium in the form of a suspension homogenized by IKA® T10 basic Ultra-Turrax® at 20,000 RPM for 1 min. The quantity of GP-nil particles added to the cell culture was kept constant (500 µg/mL in the final medium); depending on the GP-nil sample used, the final nilotinib concentrations ranged from 0.09 to 22.5 µM.

The RAW 264.7 and J774A.1 cells were seeded into 96-well plates at the density of 5,000 cells per well in 100 µL of culture medium. After 24 h of pre-incubation, 10 µL of prepared nilotinib solution or GP-nil composites suspended and homogenized in the culture medium were added to the wells. The cells were incubated with the tested substances for 24 h at 37 °C under the 5 % CO₂ atmosphere. The relative viability of cells was measured by the Cell Counting Kit-8 (Sigma-Aldrich). The number of living cells is proportional to the amount of created formazan dye detected by measuring absorbance at 450 nm. The viability of control cells was assigned as 100 %. The control cells were treated with DMSO solution without nilotinib in the case of nilotinib solutions, or with the pure cell culture medium in the case of GP-nil series. As a reference, the viability of cells treated with GPs without any encapsulated nilotinib was determined as well. All samples were measured in triplicates and the tests were performed twice.

2.5. In vivo studies

2.5.1. Chemicals

Xylazine (Rometa 20 mg/mL inj sol, Bioveta a.s., Czech Republic), ketamine (Narkamon 100 mg/mL inj sol, Bioveta a.s., Czech Republic) and isoflurane (IsoFlo 250 mL, Zoetis/Pfizer, Czech Republic) were used for the animal anaesthesia. Ketoprofen (Ketodolor inj 100 mL, LeVet Pharma b.v., Netherlands) was used for perioperative analgesia. Heparin (Heparin Léčiva inj 1x10 mL/50kU, Zentiva k.s., Czech Republic) was used for catheter patency maintenance. Omeprazole was used as Helicid 40 Inf. (Zentiva, Czech Republic).

2.5.2. Animals

All animal experiments were performed in accordance with the Guiding Principles for the Use of Animals in Charles University, First Faculty of Medicine, and every effort was made to minimize the animal suffering. The number of animals enrolled in each study was chosen so as to minimise the number of animals used while maximising the statistical

robustness of the studies. The project was approved by the Ministry of Education, Youth and Sports, Czech Republic under No. MSMT-9445/2018–8. Male Wistar rats (weight 300–450 g, age 3–5 months) were purchased from Velaz s.r.o., Prague, Czech Republic. They were housed under standard conditions (12-hour light/dark cycle, 22 °C temperature and 50 % relative humidity) and fed on water and standard granulated diet *ad libitum*. The acclimation period took at least one week. Wistar rats were chosen based on previous experience and validation of lymph transport studies (Ryšánek et al., 2021).

2.5.3. Comparative bioavailability study

A randomized, single dose, laboratory-blinded, 2-period, 2-sequence, crossover study was conducted under fasting conditions in rats to compare the bioavailability of nilotinib after oral administration. The test formulation was GP-nil composites, and the reference formulation was Tasigna (Novartis Europharm Ltd., Ireland). Both test and reference (powder emptied from the Tasigna capsule) were weighed into a glass vial and suspended in deionized water prior to dosing. The dose of nilotinib was 7 mg per 2 mL of suspension in both cases.

All rats underwent cannulation of the right jugular vein with catheters made from medical grade polyurethane (3Fr, Instech Laboratories, Plymouth Meeting, USA). Prior to surgery, 2.5–3.5 % isoflurane was used to anesthetize the rats, continued with ketamine (100 mg/kg, i.m.) and xylazine (5 mg/kg, i.m.). Ketoprofen (5 mg/kg, s.c.) was applied after the cannulation. Catheters were flushed with saline 200 µL, diluted heparin 50 µL and sealed by glycerol with heparin 20 µL. The third day after the cannulation, rats were randomly assigned into study groups and the dosing of nilotinib formulations was performed.

The access of the animals to food was restricted between 4 h prior to dosing and 4 h thereafter. To prevent extensive dissolution of GP-nil-15.0 (see Fig. 2), the rats were pretreated with omeprazole (20 mg/kg) two hours before the dosing. The dosing itself consisted of 2 mL of suspension (reference or test formulation, both containing 7 mg of nilotinib) followed by 1 mL of water via oral gavage. Blood samples (100 µL) were then collected for 24 h (0, 1, 2, 3, 4, 5, 6, 10 and 24 h) after the dosing. Volume replacement with 100 µL of saline was provided after each sampling and 50 µL of heparinized saline flush (1250 IU/mL) of the catheter used to secure the catheter patency. Wash out period of 96 h between consecutive doses was applied.

2.5.4. Absolute oral bioavailability study

Nilotinib intravenous formulation was prepared in concentration 2 mg/mL. The mixture contained 10 % of *N,N*-dimethylacetamide, 20 % of Cremophor EL, and 70 % of a 5 % aqueous solution of dextrose (Xia et al., 2012). Absolute oral bioavailability of nilotinib was evaluated in a two-period, one sequence (i.v. - p.o.), cross-over study. Right jugular vein was cannulated. After overnight recovery, the rats were i.v. dosed with nilotinib (1 mg/kg). Systemic blood was drawn at 10 and 30 min and at 1, 2, 4, 6, 10 and 24 h after nilotinib administration. The p.o. dosing and sampling was performed as described for the comparative bioavailability study (see above). Wash out period of 96 h between consecutive doses was applied.

2.5.5. Lymphatic transport study

Mesenteric lymph duct cannulated anaesthetized rat model was used as previously described with slight modifications (Trevaskis et al., 2015). Rats were left on normal diet and given 1 mL olive oil one hour prior to surgery to facilitate the mesenteric lymph duct visualisation. They were anaesthetized with an i.m. combination of xylazine (5 mg/kg) and ketamine (100 mg/kg) after a rapid 2.5–3.5 % isoflurane induction. Transverse laparotomy was performed. Mesenteric duct was identified cranially to superior mesenteric artery and cannulated with heparin prefilled 0.97 mm O.D., 0.58 mm I.D. polyethylene catheter (Instech Laboratories, Plymouth Meeting, USA). The catheter was fixed in place with two to three drops of tissue adhesive (Surgibond®, SMI AG, Belgium). A duodenal catheter was also placed (same parameters as for

lymphatic catheter) via a small duodenotomy and fixed with a purse string suture or tissue adhesive. The abdominal wall was sutured in two layers with both catheters leaving the abdominal cavity on the right side of the animal. At the end of the procedure, the right jugular vein was cannulated for blood sampling (3 Fr polyurethane catheter, Instech Laboratories, Plymouth Meeting, USA). The rats were then placed on heated pads and covered with blanket to prevent heat loss.

Two mL of suspension (reference or test formulation, both containing 7 mg of nilotinib) or 2 mL of suspension with GP-FITC for quantitative lymph transport study were dosed via duodenal catheter over 30 min. Whole lymph was collected in regularly changed Eppendorf tubes from the time when suspension was inserted into duodenum. The rats were continuously hydrated with normal saline at a rate of 3 mL/h intraduodenally using the infusion pump (Perfusor® compact plus, B. Braun, Melsungen AG, Germany). Anaesthesia was maintained throughout the rest of the experiment and additional ketamine i.m. boluses were given whenever necessary. Eppendorf tubes were changed every 1 h and systemic blood was drawn at the same time points.

2.5.6. Biodistribution study

Nilotinib biodistribution after administration of reference (Tasigna) and test (GP-nil composites) formulations were compared. The rats were fasted for 4 h before and 4 h after dosing. The animals were sacrificed at 24 h after dosing by cervical dislocation in terminal isoflurane anaesthesia. Systemic blood sample was taken via cardiac puncture, and the abdominal cavity was exposed. The jejunum, ileum, Peyer's patches, mesenteric lymph nodes, spleen, liver and right kidney were harvested. Subsequently, the jejunum and ileum were longitudinally cut and washed thoroughly to remove all intraluminal contents. All tissues were then homogenized (IKA® T10 basic Ultra-Turrax®) in 100 % DMSO.

2.5.7. Sample processing

Blood samples were centrifuged for 10 min (2264 × g, 4 °C) and serum aliquots were extracted. Lymph volume was measured gravimetrically, and the samples were further processed without additional adjustment. Organ homogenates were centrifuged for 10 min (2264 × g, 4 °C) and the DMSO supernatant was extracted. All samples were stored in –80 °C until analyzed.

2.5.8. Nilotinib bioanalytical assay

Determination of nilotinib in different tissues, serum, and lymph samples was carried out using the Nexera X3 UHPLC coupled with a Triple Quad 8045 tandem mass spectrometer (Shimadzu, Kyoto, Japan). UPLC BEH Phenyl column (100 × 2.1 mm; 1.7 µm particle size) from Waters (Milford, MA, USA), thermostated at 40 °C, was used for the analysis. Mobile phase (A: 0.1 % formic acid in deionized water, B: 0.1 % formic acid in methanol) was pumped in a flow rate of 0.3 mL/min and the following optimized gradient program was applied (min/%B) 0/40, 0.5/40, 1.5/90, 3.0/90, 3.5/40, and 6.5/40. The injection volume was 1 µL, and samples were kept at 10 °C. Effluent from the column was directed to the MS ion source between 2.5 and 4.0 min only. For the rest of the time, the effluent was directed to the waste. The tandem mass spectrometry operated in multiple reaction-monitoring mode (MRM) using positive electrospray ionization. MRM transitions of 530.2 > 289.1 (Q1 pre-bias –26 V, Q3 pre-bias –20 V and collision energy –31 V) and 536.2 > 295.1 (Q1 pre-bias –26 V, Q3 pre-bias –14 V and collision energy –31 V) were monitored for nilotinib and nilotinib-d6 as internal standard (IS), respectively. The ion source was set as follows: nebulizing gas flow: 3 L/min, heating gas flow: 10 L/min, interface temperature: 350 °C, desolvation line temperature: 300 °C, heat block temperature: 350 °C, and drying gas flow: 10 L/min.

Studied samples were processed as follows. 20 µL of the sample (serum, lymph, or tissue extracts) was deproteinized with 60 µL of 100 % acetonitrile containing IS (nilotinib-d6, c = 50 ng/mL) in an Eppendorf tube by vortexing for 15 s. Then, samples were centrifuged at 16500 × g for 8 min, and 50 µL of supernatant was transferred into LC vials. The

method was validated with respect to linearity, the limit of detection (LOD), the lower limit of quantification (LLOQ), the upper limit of quantification (ULOQ), accuracy, precision, selectivity, recovery, and matrix effects. Method selectivity was monitored by injecting six samples of each matrix (serum, lymph, and all studied tissue extract samples) with a mass spectrometer set in scan mode. The obtained chromatograms showed no interfering compound within the retention time window of nilotinib. The eight-point calibration curves were constructed in each blank matrix (serum, lymph, and pooled tissue extracts) by plotting the ratio of the peak area of nilotinib to that of IS against nilotinib concentration.

The weighted least-squares linear regression method was used with a weighting factor of $1/x^2$, which improved the accuracy in low concentrations. Due to the use of nilotinib-d6 as the IS, no significant difference in calibration curves in different matrices was observed. The method was linear (coefficients of determination (R^2) higher than 0.9995) in the concentration range of 0.25–1000 ng/mL. LOD was determined as the detector response with the minimum signal to noise ratio of 3, LLOQ as the lowest quantified concentration level with the minimum signal to noise ratio of 10 providing results of accuracy and precision up to 15 % (back-calculated). ULOQ was determined as the highest quantified concentration level in the linear calibration range with accuracy and precision up to 5 % (back-calculated). The LOD corresponded to 0.04 ng/mL, the LLOQ was at a concentration level of 0.25 ng/mL, and the ULOQ was 1000 ng/mL. Accuracy and precision were determined via analysis of the fortified blank samples of each matrix at three concentration levels (0.5, 50, and 500 ng/mL) at six replicates ($n = 6$). The accuracy was expressed as the relative error, RE (%) = (measured concentration – expected concentration)/expected concentration \times 100, and the precision expressed by repeatability as the relative standard deviation (RSD). All determined values of accuracy were within the range of 1.2–7.3 % and precisions (RSD %) ranged from 0.6 to 5.5 %.

Recovery of the method was assessed by comparison of nilotinib concentration found in a different matrix sample spiked with the standard before precipitation of proteins and concentration found in a sample spiked after precipitation of proteins at three concentration levels (0.5, 50, and 500 ng/mL). Since there is no reference material of different tissues containing nilotinib, the recovery was simulated by fortifying different tissue homogenates with the standard. Recovery ranged in each matrix from 96.6 to 101.1 %. Matrix effect was determined by comparing the area of the nilotinib standard peak of the post-protein-precipitation spiked sample with that of the 80 % acetonitrile (without matrix effect). It was evaluated at three concentration levels (0.5, 50, and 500 ng/mL) using 6 different samples of each matrix. The matrix effect ranged from 85 to 105 %. Calibration was performed every day before measuring samples and quality control samples were injected after each 6th sample.

2.5.9. Determination of GP-FITC in rat lymph

To understand the time-resolved transport of glucan particles in the lymphatic system after oral administration, experiments using GPs labelled with fluorescein isothiocyanate (GP-FITC) were conducted. The concentration of GP-FITC in rat lymph was determined by fluorescence spectrophotometry (Cary Eclipse Fluorescence Spectrometer, Agilent Technologies, USA) at excitation and emission wavelengths of $\lambda_{ex} = 495$ nm and $\lambda_{em} = 525$ nm, respectively. For analysis, 20 μ L of the lymph sample was mixed with deionized water to a final volume of 2 mL. Prior to measurement, all samples were homogenized using IKA® T10 basic Ultra-Turrax® (20 000 rpm, 1 min). The mass of GP-FITC present in each sample was calculated based on a previously constructed calibration curve (Supplementary information, Figure S3) and multiplied to the total volume of the original sample.

2.5.10. Data analysis and statistics

Serum concentrations in all pharmacokinetic studies were dose- and body weight-normalized prior to further calculations. Exact actual

sampling times were used for all pharmacokinetic calculations, while scheduled sampling times were used only for plotting of mean pharmacokinetic profiles in the graphs.

Pharmacokinetic analysis was performed using Phoenix WinNonlin® (Certara, Princeton, USA). C_{max} , t_{max} and AUC were evaluated. The natural logarithmic transformation of C_{max} and AUC was used for all statistical inference. AUC was calculated using the trapezoidal rule, while C_{max} and t_{max} were taken directly from the observed data. The pharmacokinetic parameters were analyzed using an ANOVA model. The fixed factors included in this model were the effects of subject, treatment, period, and sequence. The 90% confidence interval for the ratio of geometric least-squares means between the test and reference products was calculated.

In the nilotinib biodistribution study, dose and body weight normalized absolute amount of drug in DMSO supernatant was determined and further normalized to weight of the homogenized organ sample. Lymph drug concentrations were dose and body weight normalized as well. GraphPad Prism version 9.1.0 (GraphPad Software, San Diego, CA, USA) was used for statistical analyses. Mann-Whitney U test was used to compare serum and tissue nilotinib concentrations after administration of reference and test formulation, respectively. Statistical significance was considered at $P \leq 0.05$.

Lymphatic drug transport calculations were performed as previously shown in the literature (Rysánek et al., 2020). Absolute bioavailability via lymph (F_{AL}) was defined as percentage of administered drug dose absorbed into the lymph. It was determined directly from lymph volume and drug concentration in lymph duct cannulated rats. Analogically, absolute bioavailability via portal vein (F_{AP}) was defined as percentage of administered drug dose reaching the systemic circulation after direct absorption into the blood and was calculated as $F_{AP} = AUC_{ent} / AUC_{iv}$, where AUC_{ent} is the area under the dose and body weight normalized blood concentration–time curve after enteral dosing in lymph duct cannulated (i.e. lymph deprived) rats and AUC_{iv} is the respective parameter in a separate intravenously dosed group. Total absolute bioavailability (F) in lymph duct cannulated rats was calculated as a sum of F_{AL} and F_{AP} . In the bioavailability study group, F was calculated using the standard formula $F = AUC_{po} / AUC_{iv}$. Relative bioavailability via lymph (F_{RL}) was defined as percentage of systemically available drug that was absorbed via lymph. It was calculated as $F_{RL} = F_{AL} / F$.

3. Results

3.1. Properties of GP-nil composites

The physical appearance, *in vitro* dissolution behavior and macrophage uptake of the GP-nil composites were investigated first. The size and morphology (Fig. 1) of GP-nil composites were identical to those of original yeast (no aggregation or deformation has occurred), which is consistent with previously reported properties of GPs containing a variety of bioactive payloads (Salón et al., 2016; Šalamúnová et al., 2021). Thanks to its fluorescence (Fig. 1) it was confirmed that nilotinib was uniformly distributed across individual particles. The content of nilotinib extracted from GP-nil composites is summarized in Table 1. Additionally, all samples were found to contain only amorphous nilotinib (Supplementary information, Figure S2 showing XRPD results). It was visually inspected that the GP-nil powders had a good wettability and were well dispersible in aqueous dissolution media. From these results it can be concluded that nilotinib is predominantly present as an amorphous dispersion within the porous wall of the glucan particles.

As the intention was to investigate the delivery of nilotinib via lymphatic system, dissolution in the GI tract was counterintuitively an undesired effect. Dissolution profiles were hence assessed in aqueous buffers of pH ranging from pH 2 to pH 6.8 to estimate the effect of pH on the release rate from the GP-nil composites in various parts of the GI tract (Mudie et al., 2010). Moreover, dissolution profile was also assessed in biorelevant media simulating the intestinal fluid in the fasted

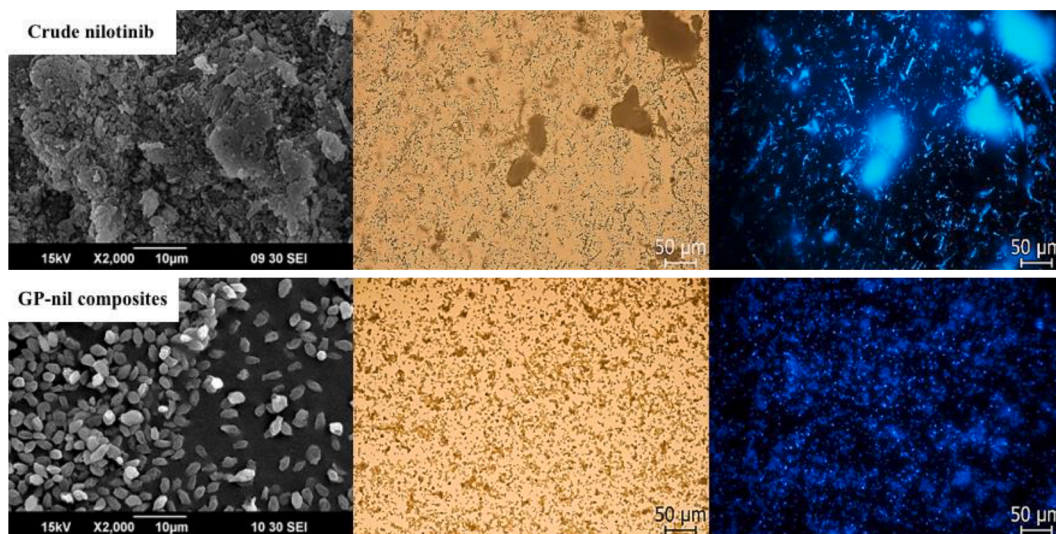


Fig. 1. SEM, optical and fluorescence micrographs of crude nilotinib (top) GP-nil-15.0 composites (bottom).

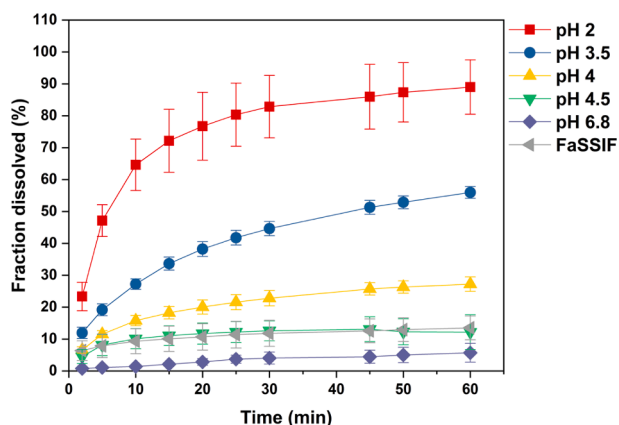


Fig. 2. Dissolution profiles of nilotinib composites (GP-nil-15.0) in various 200 mL media at 37 °C and mini-paddles set at 125 RPM.

state (FaSSIF). As shown in Fig. 2, nilotinib dissolves well when the composites are dispersed in pH 2 and pH 3.5 due to nilotinib protonation. As pH is increased, nilotinib dissolution is suppressed. At pH 4, pH 4.5 and pH 6.8, as much as 75 %, 90 % and 95 %, respectively, of nilotinib originally encapsulated in the GP-nil composites remained undissolved. Dissolution in FaSSIF was also rather slow when compared to dissolution at low pH; after 60 min, 90 % of the drug remained undissolved. It was decided to perform subsequent *in vivo* studies under such conditions that would be favorable for the intended delivery route, i.e. via lymph. Such conditions can be reproducibly achieved by the pretreatment of test animals with proton pump inhibitor omeprazole (Šíma et al., 2019).

To study the contribution of dissolution to the overall nilotinib bioavailability, dissolution test in FaSSIF was conducted with Tasigna as a reference. In this case the sample preparation simulated the dosing procedure used during *in vivo* studies where the powders were pre-dispersed in water before dosing to the animals (see Section 2.5.3). As shown in Fig. 3, both Tasigna and GP-nil-15.0 composites dissolved poorly in FaSSIF medium. Nevertheless, there were differences in the behavior of both formulations: the fraction dissolved after 60 min reached 15 % for the GP-nil-15.0 composites but only 7 % for Tasigna. XRPD analysis of residual solid material after the dissolution experiment confirmed that nilotinib remained in the amorphous state, i.e. there was no recrystallization (Supplementary information, Figure S2).

The ability of GP-nil-15.0 composites to be effectively phagocytosed was quantified by comparing the cytotoxic effect of nilotinib delivered to RAW 264.7 and J774A.1 cells in the form of GP-nil suspension and DMSO solution, respectively. The results of cytotoxicity tests are summarized in Fig. 4. For nilotinib added as a DMSO solution, the relative viability of RAW 264.7 and J774A.1 cells decreased from approximately 90 % at the lowest concentration of 0.09 μM to approximately 50 % at the highest concentration of 22.5 μM . It is interesting that a comparable, or even stronger cytotoxic effect has been achieved when nilotinib was applied in the form of GP-nil composites across the investigated concentration range for both cell lines (Fig. 4). While nilotinib is soluble in DMSO (100 mg/mL) its solubility in aqueous fluids at neutral pH is negligible. Therefore, the cytotoxicity observed for GP-nil composites cannot be attributed to freely dissolved nilotinib. This implies that nilotinib must have entered the cells in the undissolved form via phagocytosis of GP-nil composites rather than by the diffusion of freely dissolved nilotinib. Since the endosomal pH is known to be acidic, it can be assumed that nilotinib was released from the GP-nil composites once inside the cells. The direct observation of phagocytosis of GPs containing encapsulated drugs was reported recently (Šalamúnová et al., 2021).

3.2. Bioavailability studies

To evaluate the performance of GP-nil composites under *in vivo* conditions, a comparative bioavailability study was performed using Tasigna as a reference (cf. Section 2.5.3). All six rats enrolled to this cross-over study completed both periods. The weight of rats ranged from 313 to 377 g, thus body weight-normalized nilotinib dose ranged between 18.6 and 22.4 mg/kg. All nilotinib serum concentrations of pre-dose blood samples in the second period were below the limit of quantification, confirming that the wash-out period between dosing was sufficient. The mean nilotinib dose and body weight-normalized pharmacokinetic profiles after administration of both formulations are shown in Fig. 5, and the pharmacokinetic parameters of both formulations are summarized in Table 2. Both the rate and extent of nilotinib absorption were substantially higher after administration of GP-nil-15.0 composites in comparison to the reference. C_{max} and AUC_{last} values were almost 2x higher than reference values. T_{max} was shorter in the case of GP-nil-15.0 composites, although the difference did not reach statistical significance ($P = 0.0649$).

To determine the absolute quantity of nilotinib absorbed into systemic circulation after oral administration, a separate absolute bioavailability study was conducted using Tasigna reference formulation for oral dosing (cf. Section 2.5.4). All 8 rats enrolled to this cross-

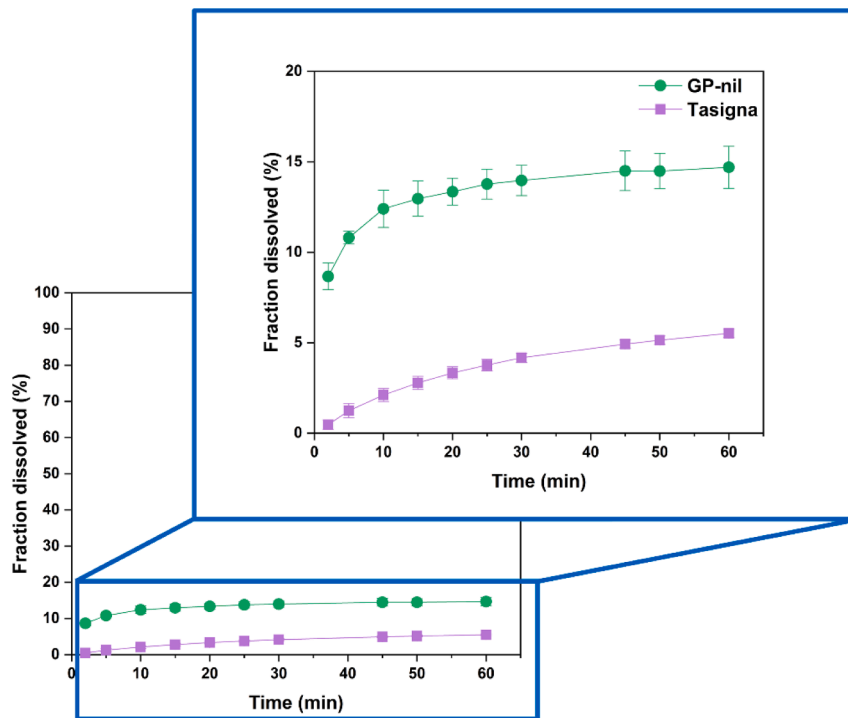
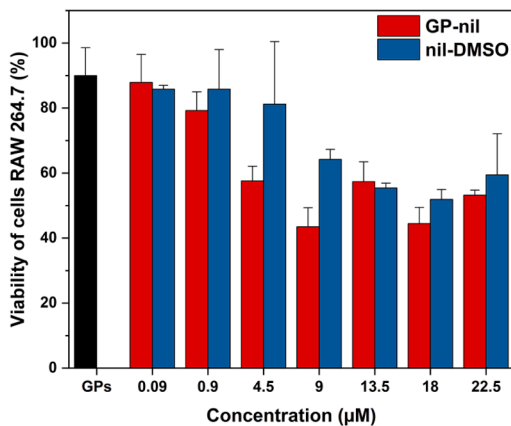
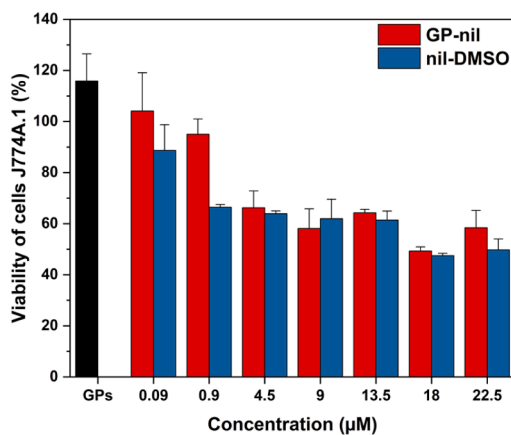


Fig. 3. Dissolution profiles of GP-nil-15.0 composites and Tasigna in FaSSiF (7 mg of nilotinib, 200 mL media, 37 °C, mini-paddles at 125 RPM).



(A)



(B)

Fig. 4. The cytotoxic effect of GP-nil-15.0 composites and nilotinib DMSO solutions in different concentrations on (A) RAW 264.7 cells and (B) J774A cells.

over study completed both periods including i.v. and p.o. administration. Body weight normalized intravenous nilotinib dose ranged from 0.987 to 1.012 mg/kg, while oral dose ranged between 16.31 and 26.31 mg/kg. Mean \pm SD body weight and dose normalized pharmacokinetic profiles of nilotinib after intravenous and oral dosing are shown in Fig. 6 and the pharmacokinetic parameters are summarized in Table 3. The absolute oral bioavailability of nilotinib was 39.0 ± 16.8 % indicated as mean \pm SD.

3.3. Lymphatic transport and biodistribution study

To determine the contribution of lymphatic absorption to the pharmacokinetics and overall bioavailability of nilotinib, a lymphatic

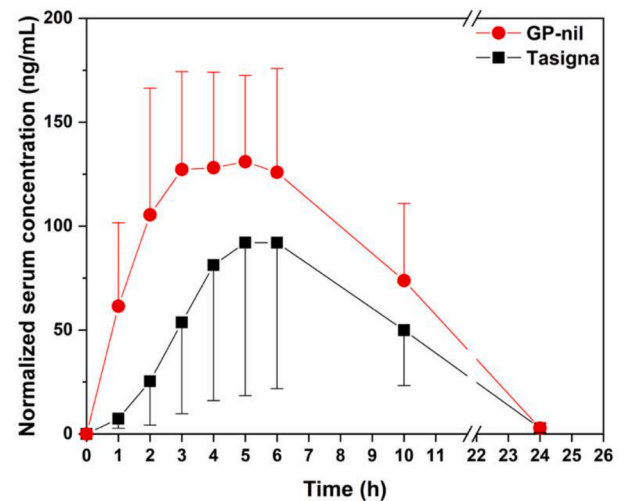


Fig. 5. Arithmetic mean (\pm SD) nilotinib pharmacokinetic profiles normalized per dose and body weight in fasted rats (n = 6) after administration of two different formulations: Tasigna as a reference and GP-nil-15.0 composites as a test.

Table 2

Nilotinib pharmacokinetic parameters normalized per dose and body weight after administration of GP-nil-15.0 composites (test) and Tasigna (reference) formulations to rats ($n = 6$) in the fasted state. C_{max} , AUC_{last} and T/R ratios are described as geometric mean (90% confidence intervals) and T_{max} values are described as range.

Formulation	C_{max} (ng/mL)	T/R C_{max} (%)	AUC_{last} (ng \times min/mL)	T/R AUC_{last} (%)	T_{max} (min)
Tasigna	78.04 (38.20–159.4)	N/A	765.0 (397.6–1472)	N/A	243–614
GP-nil-15.0	136.8 (103.0–181.6)	175.3	1455 (1067–1984)	190.2	181–361

transport study was conducted as described in Section 2.5.5. There were 10 rats enrolled. The weight of rats ranged from 457 to 608 g, thus body weight-normalized nilotinib dose ranged between 11.5 and 15.5 mg/kg. Lymphatic concentration profiles and cumulative lymphatic transport of nilotinib after intraduodenal administration of Tasigna as a reference and GP-nil-15.0 composites to the lymph duct cannulated rats are shown in Fig. 7. The pharmacokinetic parameters are summarized in Table 4.

The dose and body weight normalized lymphatic C_{max} was 4x higher, the total absolute bioavailability was approximately 2.7x higher, and the absolute bioavailability via lymph was >10x higher in the case of nilotinib delivered via glucan particles compared to the reference formulation. This trend is also apparent in the comparison of cumulative lymphatic transport, shown in Fig. 7B. However, it should be kept in mind that despite the significantly increased contribution of lymphatic

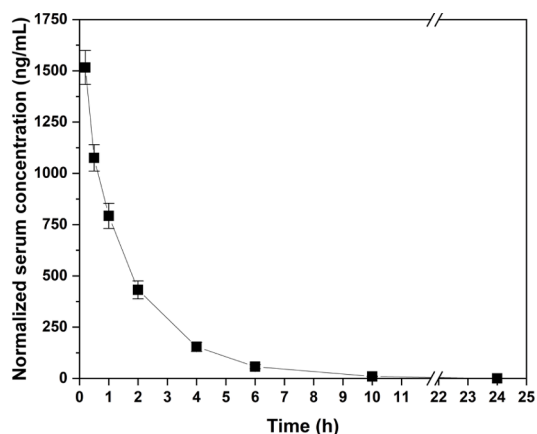
Table 3

Mean \pm SD pharmacokinetic parameters of nilotinib after oral (Tasigna® reference formulation) and intravenous (nilotinib intravenous solution) administration to rats using a cross-over study design ($n = 8$). All concentrations and AUCs are normalized to 1 mg/kg. The pharmacokinetic profiles are shown in Fig. 6.

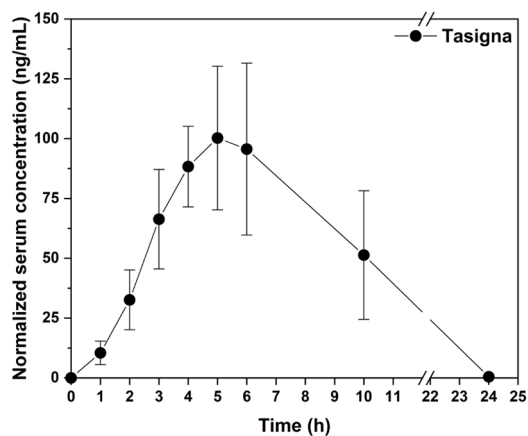
	<i>p.o.</i> administration	<i>i.v.</i> administration
C_{max} (ng/mL)	111.5 \pm 21.6	–
C_0 (ng/mL)	–	1549 \pm 214
T_{max}	5.03 \pm 0.98	–
AUC_{inf} (ng \cdot h/mL)	990 \pm 337	2756 \pm 618
V_{ss} (L/kg)	–	0.663 \pm 0.105
Cl (L/h \cdot kg)	–	0.389 \pm 0.121
Bioavailability (%)	35.9 \pm 12.2	–

absorption in the case of GP-formulated nilotinib, the relative contribution of lymphatic transport to the overall bioavailability of nilotinib still remained at a modest level ($F_{RL} = 1.12 \pm 0.93$ %). The higher nilotinib solubility from GP-nil composites under fasted condition (approximately 3x higher – cf. Fig. 3) contributed predominantly to its higher absolute bioavailability compared to the reference.

Based on the combination of *in vitro* dissolution and *in vivo* pharmacokinetic data, a potential scenario of nilotinib absorption can be outlined as follows. Part of nilotinib contained in the formulation dissolves from the GP-nil composites due to its amorphous form, which increases solubility (approximately 15 % of the dose as shown in Fig. 3).

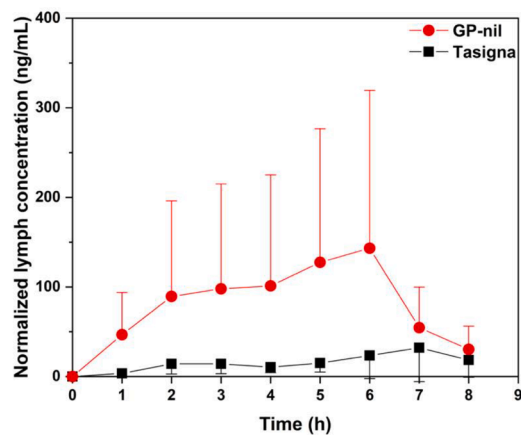


(A)

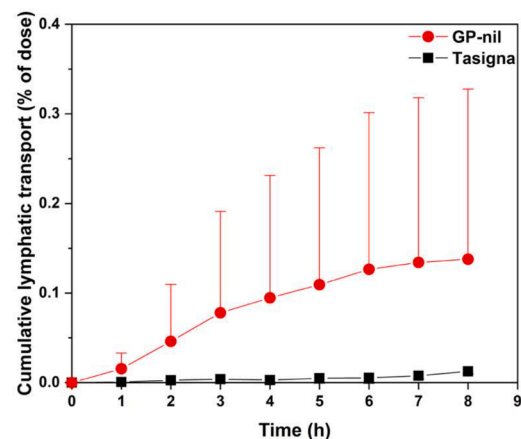


(B)

Fig. 6. Pharmacokinetic serum profiles (mean \pm SD) of nilotinib normalized per dose and body weight after (A) intravenous and (B) oral dosing to fasted rats ($n = 8$).



(A)



(B)

Fig. 7. Lymphatic transport of nilotinib after duodenal administration of Tasigna as a reference and GP-nil-15.0 composites as a test to cannulated anaesthetized rats. (A) Mean \pm SD of dose and body weight-normalized lymph concentration profile; (B) Mean \pm SD of cumulative lymphatic transport.

Table 4

Mean \pm SD lymph pharmacokinetic parameters of nilotinib after duodenal administration of Tasigna as a reference or GP-nil-15.0 composites to cannulated anaesthetized rats (normalized lymphatic C_{max} , total absolute bioavailability F, absolute bioavailability via lymph F_{AL} and relative bioavailability via lymph F_{RL}).

Formulation	C_{max} (ng/mL)	F (%)	F_{AL} (%)	F_{RL} (%)
Tasigna	35.9 \pm 23	2.95 \pm 1.00	0.013 \pm 0.003	0.44 \pm 0.06
GP-nil-15.0	147.0 \pm 140.4	8.03 \pm 7.62	0.14 \pm 0.19	1.12 \pm 0.93

A certain proportion of this dissolved nilotinib is then absorbed into systemic circulation in a similar manner as it would from the reference. The undissolved part of nilotinib that remains in the glucan particles (approximately 85 % based on *in vitro* dissolution data) is potentially available for M–cell uptake and lymphatic transport where a number of additional mechanisms can be envisaged (e.g. enhanced dissolution in the acidic pH of endosomes, partitioning of dissolved nilotinib to lipidic components of the lymph that can act as a sink, etc.). The total quantity of bioavailable nilotinib is then a superposition of these contributions.

As a complementary information, the residual nilotinib concentration in various tissues and organs 24 h after administration was determined. Specifically, lymphatic tissues and organs (Peyer's patches, mesenteric lymph nodes, spleen), absorption organs (intestine) and elimination organs (liver, kidney) were analyzed for nilotinib content as described in Section 2.5.6. A total of 6 rats (body weight of 410–501 g) were used; three rats received the reference (Tasigna) and the other three rats received GP-nil composites. The body weight normalized nilotinib dose ranged from 13.9 to 17.4 mg/kg. The median nilotinib dose-normalized concentration in the investigated tissues and organs at 24 h after administration of each formulation are summarized in Table 5. There were no significant differences in serum/tissue levels between the reference (Tasigna) and test (GP-nil-15.0) formulation, as confirmed by the corresponding *P*-values (Table 5). However, it should be pointed out, that the tissue analysis was carried out at a time point of 24 h after administration since the PK results were not yet known. With hindsight based on the PK curves shown in Fig. 5, there is not expected to be any significant difference between the test and the reference formulation at this time point.

3.4. Determination of fluorescently labelled glucan particles in rat lymph

The ability of orally administered GPs to enter the lymphatic system is known from the literature mainly thanks to qualitative or semi-quantitative histology analysis (Soto et al., 2019; Xie et al., 2016; Xie et al., 2016; Zhang et al., 2017; Wu et al., 2020; Gao et al., 2021). To better understand the time-resolved transport of glucan particles in the lymphatic system after oral administration, experiments using GPs labelled with fluorescein isothiocyanate (GP-FITC) were conducted according to the procedure described in Section 2.5.5 (*in vivo* experiments) and 2.5.9 (analysis). The study involved 4 rats with a body weight ranging from 490 to 683 g. The body weight-normalized dose of labelled glucan particles ranged between 70.1 and 97.7 mg/kg. The results of this

Table 5

Median dose-normalized concentrations and *P*-values of nilotinib after oral administration of Tasigna as a reference and GP-nil-15.0 composites as a test.

Median dose-normalized concentrations (ng/mL for serum, ng/g for other tissues)	Tasigna	GP-nil	<i>P</i> -value
Serum	0.37	0.44	0.7
Jejunum	9.92	1.77	0.2
Ileum	0.67	2.25	0.1
Peyer's patches	3.45	2.01	0.4
Mesenteric lymph nodes	0.41	0.49	0.7
Spleen	0.66	1.01	0.7
Liver	2.56	2.82	>0.9999
Kidneys	0.64	1.44	0.7

study are summarized in Fig. 8. The amount of GP-FITC present in lymph was found to reach a maximum between 2 and 4 h and then gradually declined until the end of the experiment. The absolute cumulative quantity of glucan particles found in the lymph after administration of a 50 mg dose was 0.54 ± 0.24 mg, which corresponds to an absolute lymphatic bioavailability of 1.1 ± 0.49 %. While the bioavailability figure might seem low, it should be noted that 1 mg of GPs represents approximately 4×10^9 of individual particles. This quantity of particles must have been phagocytosed and transported into the lymph through the Peyer's patches over the investigated period, which hypothetically represents approximately 70,000 individual phagocytosis events per second.

4. Discussion

The results presented above indicate that orally administered glucan particles enter the lymphatic system in measurable quantities over the period of 8 h after the administration. The quantity of GPs entering the lymphatic system in rats was found to be approximately 2.2×10^9 (0.54 mg). This can be compared with previously published results obtained after the application of 2 μ m fluorescent polystyrene latex particles (1.65×10^9 particles per dose applied) which were detected in all segments of small intestine, in Peyer's patches and lymph nodes 0.5 h after their oral application. It was found that the total number of particles detected in lymph was up to 0.14 % of the applied dose, which corresponds to 2.3×10^6 particles present in lymph (Jenkins et al., 1994). When monodisperse fluorescent polystyrene latex microparticles with a size of 2.65 μ m and 9.13 μ m were used in an absorption study in a mouse model, fluorescent activated cell sorting analysis after oral gavage of 10^8 particles in a 0.2 mL suspension revealed that approximately 0.01 % of the applied particles were absorbed after *p.o.* application. Particles from the above-mentioned experiments were also present in spleen and mesenteric lymph nodes (Ebel, 1990). Similar results were obtained in studies conducted in rats where 1 μ m polystyrene latex particles were applied the same way as described previously (Jani et al., 1992). The number of GP-FITC particles found in lymph in the present study was 3 to 5 orders of magnitude higher than in the case of fluorescent polystyrene latex particles. We hypothesize that this can be attributed to the surface chemistry and immunomodulatory properties of beta glucans, which favor phagocytosis. Curiously, yeast and barley β -glucans were detected in pig's lymph by ^1H NMR after oral ingestion, which resulted in an alteration of lipid absorption and a change of lymph viscosity (Larsen et al., 2010).

The ability of GPs to enter the lymph can be attributed to the ability

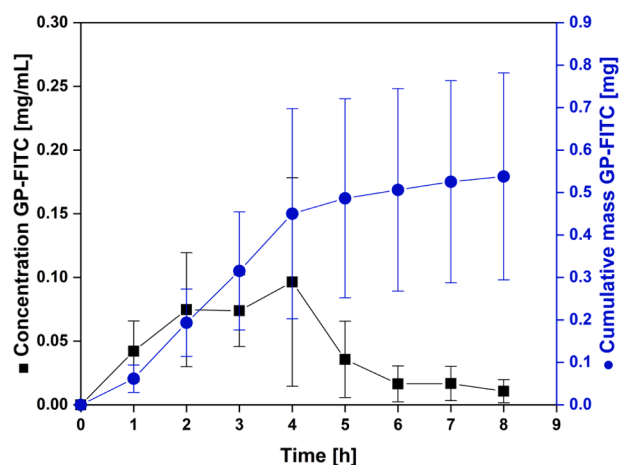


Fig. 8. Lymphatic transport of GP-FITC (mg/mL) after their duodenal administration to cannulated anaesthetized rats. Mean \pm SD of GP-FITC in lymph concentration and GP-FITC cumulative lymphatic transport.

of macrophages to take up larger quantities of glucan particles simultaneously. Referring to previously reported macrophage phagocytosing capacity experiments with fluorescently labelled yeast cells, around 6 yeast cells per 1 macrophage were found in the case of opsonized yeasts (Miliukienė et al., 2003). Fluorescent microscopy observation of GP macrophage uptake *in vitro* and *in vivo* also revealed the ability of 1 macrophage to uptake up to 10 glucan particles (Bajgar et al., 2019; Šalamúnová et al., 2021). Glucan particles thus appear to be comparable or even superior to engineered synthetic particles for drug delivery to the lymphatic system (Miao et al., 2021).

It is a well-documented fact that only highly lipophilic drugs ($\log P > 5$) have their own inherent affinity towards intestinal lymph (Charman and Stella, 1986). Examples of such molecules are halofantrine ($\log P = 8.5$) with a relative bioavailability via lymph (F_{RL}) in rats of up to 70 %, vitamin D with F_{RL} of 72 % in rats and venetoclax ($\log P = 6.9$) with F_{RL} of 19 % in dogs (Caliph et al., 2000; Dahan and Hoffman, 2005; Choo et al., 2014). Concentrations of such molecules are typically two to three orders higher in the lymph than in the blood serum. On the contrary, nilotinib ($\log P = 4.8\text{--}4.95$) lymphatic and serum concentrations observed in our study were generally comparable after administration of both formulations. Based on these observations, it can be stated that nilotinib alone is not a prime candidate for lymphatic transport. Nevertheless, it is interesting to note that nilotinib application in the form of glucan particles did result in a measurable increase of an improved absorption into the intestinal wall after better intraluminal dissolution, together with lymphatic uptake of glucan particles containing nilotinib.

Having determined the quantity of glucan particles absorbed into the lymph in a rat model, let us consider a hypothetical scenario of oral administration to humans. According to recently published allometric scaling formulas, the extent of lymphatic transport increases more than proportionally with relation to body weight regarding both absolute and relative bioavailability via lymph (Trevaskis et al., 2020). However, these formulas have been derived from experiments involving only drug formulations with standard lipophilicity-dependent partitioning between blood and lymph. Adding another mechanism of absorption, i.e., phagocytosis in Peyer's patches, results in a more complex situation with yet undefined extrapolation from preclinical species to humans. It likely enhances the lipophilic properties of the drug formulation in addition to standard lipophilicity-dependent partitioning into the lymph.

5. Conclusion

The present work has shown that orally administered nilotinib formulated in glucan particles can result in bioavailability enhancement due to two effects. The dominant contribution to the overall bioavailability of nilotinib was dissolution rate enhancement due to amorphization in the glucan particles and subsequent absorption to plasma. Simultaneously – albeit to a lesser extent – glucan particles containing undissolved nilotinib were absorbed to the lymph. A pharmacokinetic study of fluorescently labelled GPs has shown that their concentration in lymph culminated after 4 h and resulted in an absolute lymphatic absorption of 0.54 mg of glucan particles after 50 mg single oral dose. The lymph absorption of nilotinib was consequently 10.7x higher when administered via glucan particles compared to a reference (Tasigna). The present work demonstrated that even a drug substance that would not be considered suitable for lymphatic delivery based on its lipophilicity alone can be delivered to the lymphatic system when encapsulated into glucan particles. This raises several interesting questions for further research. Given the mechanism of GP uptake to the lymph, it would be interesting to determine the effect of the encapsulated drug on the life cycle of the phagocytosing cells. In particular, the ability of macrophages to transport a potentially cytotoxic payload without being killed while doing so appears to be an interesting phenomenon. Also, the

scaling from rats to other animal models and eventually to humans remains an open question for this specific drug absorption mechanism. Finally, the dose proportionality is an unknown factor at present and further studies are needed to determine how the percentage of GPs absorbed into lymph changes with the absolute dose.

CRedit authorship contribution statement

Petra Šalamúnová: Investigation, Methodology, Writing – original draft. **Tereza Krejčí:** Investigation, Methodology, Writing – original draft. **Pavel Rysánek:** Investigation, Methodology, Writing – original draft. **Ivan Saloň:** Investigation, Visualization, Methodology, Writing – original draft. **Jirina Kroupová:** Investigation, Writing – original draft. **Anna Hubatová-Vacková:** Investigation. **Peter Lukáč:** Investigation. **Tomáš Krížek:** Investigation, Visualization, Methodology. **Ondřej Dammer:** Supervision, Investigation, Methodology, Writing – review & editing. **Josef Beránek:** Supervision, Methodology, Writing – review & editing. **Martin Šíma:** Conceptualization, Investigation, Supervision, Methodology, Writing – original draft. **Ondřej Slanář:** Conceptualization, Supervision, Methodology, Writing – review & editing. **František Štěpánek:** Conceptualization, Investigation, Supervision, Funding acquisition, Methodology, Writing – original draft, Writing – review & editing.

Declaration of Competing Interest

The authors declare that they have no known competing financial interests or personal relationships that could have appeared to influence the work reported in this paper.

Data availability

Data will be made available on request.

Acknowledgement

P.R., M.Š. and O.S. were supported by the grant of the Charles University (Cooperatio - research area PHAR and SVV 260 523). P.Š., T.K. and J.K. would like to acknowledge support by Specific university research A2_FCHI_2019_034. F.Š. and I.S. acknowledge support by Czech Science Foundation (GAČR project no. 19-26127X). The authors would like to acknowledge support from The Applied Pharmaceutical Research Centre (The PARC).

Appendix A. Supplementary data

Supplementary data to this article can be found online at <https://doi.org/10.1016/j.ijpharm.2023.122627>.

References

- Aouadi, M., Tesz, G.J., Nicoloro, S.M., Wang, M., Chouinard, M., Soto, E., Ostroff, G.R., Czech, M.P., 2009. Orally delivered siRNA targeting macrophage Map4k4 suppresses systemic inflammation. *Nature* 458 (7242), 1180–1184.
- Baert, K., De Geest, B.G., De Rycke, R., Da Fonseca Antunes, A.B., De Greve, H., Cox, E., Devriendt, B., 2015. β -glucan microparticles targeted to epithelial APN as oral antigen delivery system. *J. Control. Release* 220, 149–159.
- Bajgar, A., Saloň, I., Krejčová, G., Doležal, T., Jindra, M., Štěpánek, F., 2019. Yeast glucan particles enable intracellular protein delivery in *Drosophila* without compromising the immune system. *Biomater. Sci.* 7 (11), 4708–4719.
- Caliph, S.M., Charman, W.N., Porter, C.J., 2000. Effect of short-, medium-, and long-chain fatty acid-based vehicles on the absolute oral bioavailability and intestinal lymphatic transport of halofantrine and assessment of mass balance in lymph-cannulated and non-cannulated rats. *J. Pharm. Sci.* 89 (8), 1073–1084.
- Charman, W.N.A., Stella, V.J., 1986. Estimating the Maximal Potential for Intestinal Lymphatic Transport of Lipophilic Drug Molecules. *Int. J. Pharm.* 34 (1–2), 175–178.
- Choo, E.F., Boggs, J., Zhu, C.Q., Lubach, J.W., Catron, N.D., Jenkins, G., Souers, A.J., Voorman, R., 2014. The Role of Lymphatic Transport on the Systemic Bioavailability of the Bcl-2 Protein Family Inhibitors Navitoclax (ABT-263) and ABT-199. *Drug Metab. Dispos.* 42 (2), 207–212.

- Dahan, A., Hoffman, A., 2005. Evaluation of a chylomicron flow blocking approach to investigate the intestinal lymphatic transport of lipophilic drugs. *Eur. J. Pharm. Sci.* 24 (4), 381–388.
- De Smet, R., Demoor, T., Verschuere, S., Dullaers, M., Ostroff, G.R., Leclercq, G., Allais, L., Pilette, C., Dierendonck, M., De Geest, B.G., Cuvelier, C.A., 2013. β -Glucan microparticles are good candidates for mucosal antigen delivery in oral vaccination. *J. Control. Release* 172 (3), 671–678.
- Ebel, J.P., 1990. A method for quantifying particle absorption from the small intestine of the mouse. *Pharmaceut Res* 7 (8), 848–851.
- Gao, T., Wu, Y., Wang, W., Deng, C., Chen, Y., Yi, L., Song, Y., Li, W., Xu, L., Xie, Y., 2021. Biomimetic Glucan Particles with Aggregation-Induced Emission Characteristics for Noninvasive Monitoring of Transplant Immune Response. *ACS Nano* 15 (7), 11908–11928.
- Han, X., Luo, R., Ye, N., Hu, Y., Fu, C., Gao, R., Fu, S., Gao, F., 2022. Research progress on natural β -glucan in intestinal diseases. *Int. J. Biol. Macromol.* 219, 1244–1260.
- Herbrink, M., Schellens, J.H., Beijnen, J.H., Nuijen, B., 2017. Improving the solubility of nilotinib through novel spray-dried solid dispersions. *Int. J. Pharm.* 529 (1–2), 294–302.
- Jani, P., McCarthy, D., Florence, A., 1992. Nanosphere and microsphere uptake via Peyer's patches: observation of the rate of uptake in the rat after a single oral dose. *Int. J. Pharm.* 86 (2–3), 239–246.
- Jenkins, P., Howard, K., Blackball, N., Thomas, N., Davis, S., O'hagan, D., 1994. Microparticulate absorption from the rat intestine. *J. Control Release* 29 (3), 339–350.
- Jesson, G., Brisander, M., Andersson, P., Demirbükler, M., Derand, H., Lennernäs, H., Malmsten, M., 2014. Carbon dioxide-mediated generation of hybrid nanoparticles for improved bioavailability of protein kinase inhibitors. *Pharmaceut Res* 31 (3), 694–705.
- Koehl, N.J., Holm, R., Kuentz, M., Griffin, B.T., 2019. New insights into using lipid based suspensions for 'brick dust' molecules: case study of nilotinib. *Pharmaceut Res* 36 (4), 1–13.
- Koehl, N.J., Holm, R., Kuentz, M., Jannin, V., Griffin, B.T., 2020. Exploring the impact of surfactant type and digestion: Highly digestible surfactants improve oral bioavailability of nilotinib. *Mol. Pharmaceut* 17 (9), 3202–3213.
- Koehl, N.J., Holm, R., Kuentz, M., Griffin, B.T., 2020. Chase Dosing of Lipid Formulations to Enhance Oral Bioavailability of Nilotinib in Rats. *Pharmaceut Res* 37 (7), 1–11.
- Larsen, F.H., Jørgensen, H., Engelsen, S.B., Lærke, H.N., 2010. Metabolic profiling of lymph from pigs fed with β -glucan by high-resolution 1H NMR spectroscopy. *Livest. Sci.* 133 (1–3), 38–41.
- Lin, H.-L., Chen, L.-C., Cheng, W.-T., Cheng, W.-J., Ho, H.-O., Sheu, M.-T., 2020. Preparation and characterization of a novel swellable and floating gastroretentive drug delivery system (sfGRDDS) for enhanced oral bioavailability of nilotinib. *Pharmaceutics* 12 (2), 137.
- Miao, Y.-B., Lin, Y.-J., Chen, K.-H., Luo, P.-K., Chuang, S.-H., Yu, Y.-T., Tai, H.-M., Chen, C.-T., Lin, K.-L., Sung, H.-W., 2021. Engineering nano- and microparticles as oral delivery vehicles to promote intestinal lymphatic drug transport. *Adv. Mater.* 33, 2104139.
- Miliukienė, V., Bizilevicienė, G., Pilinkienė, A., 2003. Quantitative evaluation of macrophage phagocytosing capacity by a fluorometric assay. *Acta Biol. Hung.* 54 (3–4), 347–356.
- Mudie, D.M., Amidon, G.L., Amidon, G.E., 2010. Physiological parameters for oral delivery and in vitro testing. *Mol. Pharmaceut* 7 (5), 1388–1405.
- Plavcová, Z., Šalamúnová, P., Saloň, I., Štěpánek, F., Hanuš, J., Hošek, J., 2019. Curcumin encapsulation in yeast glucan particles promotes its anti-inflammatory potential in vitro. *Int. J. Pharm.* 568, 118532.
- Rotrekl, D., Devriendt, B., Cox, E., Kavanová, L., Faldyna, M., Šalamúnová, P., Baďo, Z., Prokopec, V., Štěpánek, F., Hanuš, J., 2020. Glucan particles as suitable carriers for the natural anti-inflammatory compounds curcumin and diplacone—Evaluation in an ex vivo model. *Int. J. Pharm.* 582, 119318.
- Ruphuy, G., Saloň, I., Tomas, J., Šalamúnová, P., Hanuš, J., Štěpánek, F., 2020. Encapsulation of poorly soluble drugs in yeast glucan particles by spray drying improves dispersion and dissolution properties. *Int. J. Pharm.* 576, 118990.
- Ryšánek, P., Grus, T., Šíma, M., Slanař, O., 2020. Lymphatic transport of drugs after intestinal absorption: impact of drug formulation and physicochemical properties. *Pharmaceut Res* 37 (9), 1–17.
- Ryšánek, P., Grus, T., Lukáč, P., Kozlík, P., Krížek, T., Pozniak, J., Roušarová, J., Královicová, J., Kutinová Canová, N., Boleslavská, T., 2021. Validity of cycloheximide chylomicron flow blocking method for the evaluation of lymphatic transport of drugs. *Br. J. Pharmacol.*
- Šalamúnová, P., Saloň, I., Ruphuy, G., Kroupová, J., Balouch, M., Hanuš, J., Štěpánek, F., 2021. Evaluation of β -glucan particles as dual-function carriers for poorly soluble drugs. *Eur. J. Pharm. Biopharm.* 168, 15–25.
- Saloň, I., Hanuš, J., Ulbrich, P., Štěpánek, F., 2016. Suspension stability and diffusion properties of yeast glucan microparticles. *Food Bioprod. Process.* 99, 128–135.
- Šíma, M., Kutinová-Canová, N., Ryšánek, P., Hořínková, J., Moškořová, D., Slanař, O., 2019. Gastric pH in rats: Key determinant for preclinical evaluation of pH-dependent oral drug absorption. *Prague Med. Rep.* 120 (1), 5–9.
- Soares, E., Jesus, S., Borges, O., 2018. Oral hepatitis B vaccine: Chitosan or glucan based delivery systems for efficient HBsAg immunization following subcutaneous priming. *Int. J. Pharm.* 535 (1–2), 261–271.
- Soto, E., Kim, Y.S., Lee, J., Kornfeld, H., Ostroff, G., 2010. Glucan particle encapsulated rifampicin for targeted delivery to macrophages. *Polymers-Basel* 2 (4), 681–689.
- Soto, E.R., Ostroff, G.R., 2008. Characterization of multilayered nanoparticles encapsulated in yeast cell wall particles for DNA delivery. *Bioconjug. Chem.* 19 (4), 840–848.
- Soto, E.R., Kim, H.C., Yagita, H., De Jesus, M., Ostroff, G.R., 2019. Polydopamine Coating of Glucan Particles Increases Uptake into Peyer's Patches. *ACS Appl. Bio Mater.* 2 (9), 3748–3754.
- Tasigna: EPAR - Product Information. European Medicines Agency: https://www.ema.europa.eu/en/documents/product-information/tasigna-epar-product-information_en.pdf, 2021, p. 124.
- Tesz, G.J., Aouadi, M., Prot, M., Nicoloso, S.M., Boutet, E., Amano, S.U., Goller, A., Wang, M., Guo, C.A., Salomon, W.E., Virbasius, J.V., Baum, R.A., O'Connor Jr., M.J., Soto, E., Ostroff, G.R., Czech, M.P., 2011. Glucan particles for selective delivery of siRNA to phagocytic cells in mice. *Biochem. J.* 436 (2), 351–362.
- Tian, X., Zhang, H., Heimbach, T., He, H., Buchbinder, A., Aghoghovbia, M., Hourcade-Potelleret, F., 2018. Clinical pharmacokinetic and pharmacodynamic overview of nilotinib, a selective tyrosine kinase inhibitor. *J. Clin. Pharmacol.* 58 (12), 1533–1540.
- Trevaskis, N.L., Hu, L., Caliph, S.M., Han, S., Porter, C.J., 2015. The mesenteric lymph duct cannulated rat model: application to the assessment of intestinal lymphatic drug transport. *J. Visualized Exp.: JoVE* 97.
- Trevaskis, N.L., Lee, G., Escott, A., Phang, K.L., Hong, J., Cao, E., Katneni, K., Charman, S.A., Han, S., Charman, W.N., Phillips, A.R.J., Windsor, J.A., Porter, C.J. H., 2020. Intestinal Lymph Flow, and Lipid and Drug Transport Scale Allometrically From Pre-clinical Species to Humans. *Front. Physiol.* 11, 458.
- Wolf, A., Couttet, P., Dong, M., Grenet, O., Heron, M., Junker, U., Ledieu, D., Mahl, A., Marrer, E., Persohn, E., Pognan, F., Zhou, W., Tsao, J., Roman, D., 2011. Preclinical evaluation of potential nilotinib cardiotoxicity. *Leuk. Res.* 35 (5), 631–637.
- Wu, Y., Jin, Q., Chen, Y., Li, H., Deng, C., Sun, Z., Li, Y., Wang, B., Li, H., Wu, C., 2020. Bioinspired β -glucan microcapsules deliver FK506 to lymph nodes for treatment of cardiac allograft acute rejection. *Biomater. Sci.* 8 (19), 5282–5292.
- Xia, B., Heimbach, T., He, H., Lin, T.H., 2012. Nilotinib preclinical pharmacokinetics and practical application toward clinical projections of oral absorption and systemic availability. *Biopharm. Drug Disposition* 33 (9), 536–549.
- Xie, Y., Hu, X., He, H., Xia, F., Ma, Y., Qi, J., Dong, X., Zhao, W., Lu, Y., Wu, W., 2016. Tracking translocation of glucan microparticles targeting M cells: implications for oral drug delivery. *J. Mater. Chem. B* 4 (17), 2864–2873.
- Xie, Y., Jiang, S., Xia, F., Hu, X., He, H., Yin, Z., Qi, J., Lu, Y., Wu, W., 2016. Glucan microparticles thickened with thermosensitive gels as potential carriers for oral delivery of insulin. *J. Mater. Chem. B* 4 (22), 4040–4048.
- Young, S., Nitin, N., 2019. Thermal and oxidative stability of curcumin encapsulated in yeast microcarriers. *Food Chem.* 275, 1–7.
- Yu, M., Chen, Z., Guo, W., Wang, J., Feng, Y., Kong, X., Hong, Z., 2015. Specifically targeted delivery of protein to phagocytic macrophages. *Int. J. Nanomed.* 10, 1743.
- Zhang, H., Gu, L., Liu, T., Chiang, K.-Y., Zhou, M., 2014. Inhibition of MDM2 by nilotinib contributes to cytotoxicity in both Philadelphia-positive and negative acute lymphoblastic leukemia. *PLoS One* 9 (6), e100960.
- Zhang, X., Xu, X., Chen, Y., Dou, Y., Zhou, X., Li, L., Li, C., An, H., Tao, H., Hu, H., 2017. Bioinspired yeast microcapsules loaded with self-assembled nanotherapies for targeted treatment of cardiovascular disease. *Mater. Today* 20 (6), 301–313.
- Zhu, S., Yu, R., Qian, G., Deng, L., 2022. A supersaturating drug delivery system to enhance the oral bioavailability of nilotinib. *J. Drug Deliv. Sci. Technol.* 68, 103038.